8-17-2015 12:00 AM

Mercury Removal from Aqueous Solution Using Natural, Synthetic, and Modified Zeolites

Mahshid Attari
The University of Western Ontario

Supervisor
Dr. Sohrab Rohani
The University of Western Ontario

Graduate Program in Chemical and Biochemical Engineering
A thesis submitted in partial fulfillment of the requirements for the degree in Master of Engineering Science

MERCURY REMOVAL FROM AQUEOUS SOLUTION USING NATURAL, SYNTHETIC, AND MODIFIED ZEOLITES

(Thesis format: Integrated Article)

by

Mahshid Attari

Graduate Program in Chemical and Biochemical Engineering

A thesis submitted in partial fulfillment
of the requirements for the degree of Master of Engineering Science

The School of Graduate and Postdoctoral Studies
The University of Western Ontario
London, Ontario, Canada

Abstract

Mercury has been recognized as one of the most hazardous heavy metals. The discharge of effluents containing mercury in soil, sediments and water can inflict an irreversible harm to the environment and human health. In this work, zeolitized coal fly ash as well as gold and gold-iron modified zeolites were successfully employed for mercury removal from a typical industrial wastewater. X-ray diffraction (XRD), thermo-gravimetrical analyses (TGA), surface area measurement (BET), and scanning electron microscopy (SEM-EDX) were utilized to explore the characteristics of the raw and modified zeolites. A pseudo-second-order kinetic model was identified to best represent the kinetic data for mercury adsorption on all examined adsorbents. The adsorption mechanism of mercury on examined zeolite was found to be a multi steps process and the rate-limiting step was mainly surface adsorption.The isothermal adsorption data conformed to the Langmuir and the Freundlich models. Based on kinetic and isothermal results, both chemisorption and physisorption were effective during adsorption process.

Keywords

Mercury, adsorption, coal fly ash, zeolite LTA, clinoptilolite, activated carbon, isotherm, kinetics.

Co-Authorship Statement

This thesis is an integration of two articles. Chapter two was written based on a manuscript submitted to Chemosphere journal. The submission was made in June 2015, entitled: Mercury Removal from Aqueous Solution by Zeolitized Coal Fly Ash: Equilibrium and Kinetic Studies. This paper was written in collaboration with Dr. Sohrab Rohani, Dr. Hossein Kazemian, and Salman Bukhari. My contributions, as the first author, include: literature survey, idea generation, and data collection and management, as well as data analysis and preparation of the first draft. The material for Synthesis of zeolite LTA from CFA was prepared by Salman Bukhari. The rest of the authors significantly contributed to critical review of the manuscript.

Chapter three is a research article in preparation for submission. The manuscript was entitled: Mercury Removal from Industrial Wastewater Using Gold/Iron- Modified Natural and Synthetic Zeolites. This manuscript was co-authored by Dr. Sohrab Rohani and Dr. Hossein Kazemian who both supervised the whole project and reviewed the paper drafts.

Acknowledgments

I would like to thank Dr. Sohrab Rohani with whom I have had the great honor of working for over the past year. His hard work and ability to accomplish so many goals as a scientist and a mentor have been a true inspiration to me.

I am extremely grateful to Dr. Hossein Kazemian for his help and encouragement in my research projects. I feel truly honored to have worked with and learned from him.

I am grateful to all my colleagues at Zeolite and Nanomaterial lab at Western University for their support and the constructive conversations regarding my research projects. Although always very supportive, their honest critiques inspired me to always push an extra step and helped me achieve my goals. I would like to particularly thank Dr. Charlie Wu, Dr. Behin, Dr Alizadeh, Shohreh Almasi, Jinfan Li, and Salman Bukhari for all their time and efforts throughout my research project at Western University.

I would also like to sincerely thank my parents, Mr. Houshang Attari and Ms. Nayyer Attari, who instilled in me a love for learning and an appreciation of education. Their love and support have always provided a strong platform from which I pursed my dreams.

Finally, I would like to thank my husband and best friend, Mehdi Delrobaei, for his unending belief in me and his wholehearted willingness to support my dream.

Table of Contents

List of Tables

List of Figures

List of Appendices

List of Abbreviations

WHO ..... The world health organization

EPA ..... US environmental protection agency

GEF ..... Global environment facility

MCL ..... Maximum contaminant level

WQS ..... Water quality standards

AC ..... Activated carbon

CFA ..... Coal fly ash

LTA ..... Zeolite A

Au/Fe-LTA ..... Gold/Iron modified zeolite A

Brm ..... Bromley natural clinoptilolite

Au-Brm ..... Gold modified Bromley natural clinoptilolite

XRD ..... X-ray diffraction analysis

XRF ..... X-ray fluorescence spectroscopy

ICP-AES ..... Inductively coupled plasma-atomic emission spectroscopy

IUPAC ..... The International Union of Pure and Applied Chemistry

CVAFS ..... Cold Vapor Fluorescence Spectroscopy

BET ..... Burnauer- Emmett-Teller surface area measurment

SEM-EDX ... Scanning Electron Microscopy coupled with energy dispersive X-ray analysis

TGA ..... Thermo-gravimetric analysis

Chapter 1

1 Introduction

1.1 Motivation

Mercury (Hg) is a naturally occurring toxic heavy metal with significant environmental and ecological concern. The US environmental protection agency (EPA) and the world health organization (WHO) list Hg and its compounds as toxic pollutants. In aquatic ecosystems, inorganic mercury transform to methylmercury through biochemical reactions. Methylmercury is known to undergo bioaccumulation and bio magnification which can be passed along the food chain to human.

Besides natural sources such as volcanoes, it enters the environment anthropogenically from sources including ore mining and smelting, coal-fired power plants, battery manufacturing and pharmaceutical industry [1], [2]. In 2012, around 25% of Canada national mercury emissions came from fuel (mainly coal) consumed for electricity and heating. However waste sources including wastewater treatment plants are responsible for the highest share of Hg release to water contributing 57% of the total Hg released to water in 2012. The second highest proportion of aquatic mercury belonged to pulp, paper and paperboard mills representing 25% of the total in the same year [3], [4].

Minamata, in Japan is well-known for the first public health disaster inducing by mercury toxicity. Large amounts of methylmercury discharged from a chemical factory to Minamata Bay during 1950s. Various neurological damage as well as irritability, paralysis insanity and loss of sight were reported as the main toxicological effects of mercury in local people who consumed contaminated aquatic products [5].

Currently the Hg release to the environment continues worldwide. According to WHO and the global environment facility (GEF) 1960 metric tons of mercury were emitted globally in 2010. In 2012, Environment Canada reported that Alberta and Ontario were the first provinces with most of mercury water contamination .Among different sources

pulp and paper industries were the main origin of mercury in Ontario wastewater. The daily mercury intake from food for Canadians is considered to be 0.013 mg. It is recognized, however, that higher levels may occur with diets containing a large proportion of fish or seafood. The WHO and EPA has set a maximum guideline concentration (maximum contaminant level (MCL)) of 6 µg/L and 0.2 µg/L respectively for mercury in drinking water since even ppt amount of mercury in water stream may endure transformation to methylmercury leading to bioaccumulation [1], [4]. Traditional technologies including sulphide precipitation, membrane filtration, bio remediation and adsorption/ion exchange have resisted difficulty to meet this increasingly regulation strict for mercury. All this mention the importance of control even the very low amount of mercury motivate the growing number of researches on the field [6], [7].

Zeolites, the crystalline micro porous aluminosilicates, have been used as adsorbent and ion-exchanger for different environmental friendly applications and water treatment[8]. Their strong affinity for many heavy metal cations including mercury makes them a proper sorbent for such materials. Recently extensive studies have been performed to study these cost-effective adsorbents and develop their effectiveness by modifying specific chemical and physical properties. Gold modification of zeolites suggests potential for easier and more efficient removing mercury from contaminated water.

1.2 Literature Review

1.2.1 Mercury

1.2.1.1 Mercury History

Reviewing the history of mercury in human life, it has been used by humans for numerous purpose including artworks and medicines. There are several evidences that mercury has been used through antiquity. Several inventions during the Industrial Revolution, improved the mercury application for products such as detonator, fungicide paints and polyvinyl chloride. At the end of 19th century the poisonous properties of mercury was well known however its application in dental amalgams, pharmaceutical and cosmetic purpose and gold mining continues over decades [9]–[11].

1.2.1.2 Mercury Chemistry

Mercury is a heavy metal with an atomic number of 80, an atomic mass of 200.59, and a density of 13.55 g/cm3. The electron configuration of mercury is [Xe] $4f^{14}5d^{10}6s^{2}$. Mercury is the only metal that is liquid at room temperature (i.e. melting point:-39.8°C). Oxidation states of mercury are including Hg (0) (elemental Hg), Hg (I) (mercurous Hg), and Hg (II) (mercuric Hg) [9].

1.2.1.3 Mercury Speciation

Mercury mainly exists in several forms including elemental (Hg (0)), inorganic (Hg(I) and Hg(II)), and organic mercury. The various properties of mercury such as solubility, reactivity, mobility, bioavailability, toxicity, bioaccumulation, and bio magnification are influenced by its chemical form. The most solubility in water belongs to Hg (II) salts. As a result such forms of mercury salts are highly mobile and toxic. Since inorganic mercury has high affinity for selenium, sulphur and gold, these elements play an important role to control merury toxicity [12].

Organic mercury (i.e. mehylmercury) includes compounds in which mercury is bonded to a structure containing carbon atoms with a covalent band. Organic mercury can react with important biological complexes and pass through living membranes. The global cycle of mercury happens between atmosphere, water, land and sediment. It also is capable to pass through the food chain. In aquatic environment the primarily forms of mercury species are Hg (II) complexes and Organic mercury (i.e. mono methylmercury cation and dimethylmercury). For the purpose of this research the inorganic aqueous mercury will be considered [1], [9].

1.2.1.4 Mercury Forms in Aqueous Environment

In water Hg (II) cations are surrounded with negative dipoles face of water molecules which breaks the hydrogen bonds. The new built hydration shell have the same sign as the inside mercury ion. This new orientation is able to weaken the hydrogen bonding network between water molecules and result in the mercury cation acting as a polyprotic

acid. In the absence of complexing ligands, the speciation of mercury is basically based on hydrolysis. At a low pH Hg(II) surrounded with 6 water molecules forming a hexaqua ion ($Hg(H2O)_6^{2+}$) with equal Hg-O bond lengths, however at higher pH up to two protons can be released from this hydration sphere making the $Hg(OH)_2$ the dominant inorganic species [9].

$$Hg^{2+} + H_2O \rightleftarrows Hg\,OH^+ + H^+ \qquad K_1 = 10^{-3.4} = [H^+][Hg\,OH^+]/[Hg^{2+}]$$

$$Hg\,OH^+ + H_2O \rightleftarrows Hg\,(OH)_2 + H^+ \qquad K_2 = 10^{-2.7} = [H^+][Hg(OH)_2]/[Hg\,OH^+]$$

$$Hg^{2+} + 2H_2O \rightleftarrows Hg\,(OH)_2 + 2H^+ \qquad K_{overall} = 10^{-6.1} = [H^+]_2[Hg(OH)_2]/[Hg\,OH^+]$$

In the presence of various ligands in aqueous solution mercury can complex with them. This association is influenced by type and concentration of Lewis bases present, the redox status and the pH. The adsorption of mercury on the surface of adsorbent is strongly dependent on the resulting inner or outer complexion. Chemicals such as sulphur and chloride can complex with Hg to arrange very stable Hg-Cl and Hg-S complexes even at very low concentrations. Creation of non-adsorbing complexes, competitive adsorption of stable complexes and the change in adsorbent surface charge as a result of ligand presence would strongly alter overall adsorption of mercury in aqueous solution. As stated earlier the mercury speciation is responsible for the degree of its mobility and solubility. For instance Hg-S complexation decreases mercury solubility, while forming Hg-Cl complexes increase their solubility [2], [13], [14].

1.2.1.5 Mercury Health Impacts

The toxico kinetics of mercury (adsorption, distribution, metabolism and excretion) varies with its chemical speciation, the dose and the rate of exposure. The primarily target organ for elemental Hg vapour is lung which can then penetrate to brain through blood-brain barrier. Insomnia, memory loss, cognitive impairment and thyroid effects are some of symptoms of elemental exposure. Mercurous and mercuric salts main exposure happens through diets and their adsorption occur through the gastrointestinal tract. They mainly damage the gut lining and kidney. Stomach ache, vomiting, diarrhea and

loosening of the teeth are some of the symptoms of inorganic mercury exposure. Inorganic mercury can take up by sulphate-reducing bacteria and convert to methylmercury in aquatic ecosystems. Then it moves up through the food chain to top predators such as large fish and otter. These species have the highest tissue level of mercury. Methyl mercury is also rapidly absorbed through gastrointestinal tract and widely distributed throughout the body. Blindness, deafness, speech impairment, headaches, tremor, and loss of coordination or memory are some of the main symptoms of exposure to methylmercury. In addition methylmercury has particularly negative influence on human developing foetus causing several neurological abnormalities. Steadily exposure to methyl mercury could be fatal. The effects of high level methylmercury poisoning and the resulting public health disaster were noted in Miamata Bay, Japan in 1960s and in Iraq in 1971[1], [2], [5], [10], [15], [16].

1.2.1.6 Mercury Emissions and Regulations

The main origin of mercury release to environment is anthropogenic however volcanic activity and weathering of rocks are responsible to less degree. Nowadays coal-fired power plants are the main global source of atmospheric mercury emissions. It is notable that the mercury which release locally can transport long distances through ocean and air currents and allow a global effect. Direct and indirect discharge, atmospheric deposition, surface run-off and leachate from contaminated soil and landfills are the major lanes of anthropogenic Hg sources to water. Mercury releases to water streams mainly throughout coal-fired power plants, chlor-alkali facilities, metal processing plants, offshore oil activities, and pharmaceutical industries. The US environmental protection agency (EPA) and the world health organization (WHO) established the mercury water quality standards (WQS) at 0.2µg/L and 6µg/L in drinking water, respectively. A value of 1.6 microgram per kilogram of body weight per week or 0.23 microgram per kilogram of body weight per day was established as human permissible mercury uptake by Health Canada (based on a recent evaluation by JECFA (joint Food and Agriculture Organization/World Health Organization Expert Committee on Food Additives) and WHO, 2003) [1], [5], [14].

1.2.1.7 Aqueous Mercury Removal Technologies

A number of treatment technologies are available to capture mercury from contaminated solutions including sulphide precipitation, membrane filtration, bio remediation and adsorption/ion exchange. Sulphide precipitation is the most common method for aqueous mercury removal. It mostly applied for treating chlor-alkali industry and coal-fired power plants wastewater. In this method organic and inorganic sulphides are used to form insoluble Hg-sulfide. To remove this insoluble salt additional treatment such as pH adjustment, coagulation, flocculation, gravity settling or filtration should be needed. Mercury re solubility, difficult monitoring of sulphide levels, residence of sulphide in the effluent, are some of the disadvantages of this method. There is an estimation of $1.50/1000 gal for treating chlor-alkali wastewater using sulfide precipitation. This treatment is capable to reduce mercury concentrations to 10-100μg/L. Coagulation/co–precipitation is used as an alternative for the mentioned sulphide precipitation. In this treatment, alum (aluminum sulphate) or iron salts are used as coagulator. This method can reduce the Hg concentration to 5 to 10 μg/L using alum and 0.5 – 12.8 μg/L using iron salts. Membrane filtration is a complexion-ultrafiltration method that mainly applied membrane containing polyethylenimine as polymeric complexing agent. It was reported that 99% of Hg(II) can be removed by this method. Some innovative researches have introduced application of supported liquid membranes containing chemicals such as trictylamine as carrier and coconut oil as diluent. Also application of ultrasound technique combined with biomass or reduction/vaporization was investigated by some researchers[17]–[24].

1.2.2 Adsorption

Adsorption of pollutants over solid surface of an adsorbent is now recognized as one of the most effective, comprehensive and economic methods. Flexibility in design and operation along with high quality treated effluent and possibility of recovering the adsorbent and pollutant itself are some of advantages of this technique. Numerous studies have investigated the efficiency of various adsorbents for mercury removal from wastewater [9].

1.2.2.1 Theory of Adsorption

Adsorption is a surface phenomenon in which adsorbate molecules, atoms or ions attract to unsaturated positions on the surface of adsorbent because of unbalanced molecular forces. After adsorption reach equilibrium the concentration of adsorbate particles on the solid surface of adsorbent would be higher than their concentration in bulk solution. Adsorption could be a chemical or physical process or a combination of both. Van der Waals forces are responsible for physisorption while chemisorption occurs through redistribution of electrons between adsorbent and adsorbate and the following strong chemical bond. Due to the nature of physisorption, it is a weak alterable and not site-specific process. However the main characteristic of chemisorption is forming a unimolecular thickness of the adsorbed phase caused from strong irreversible and site specific chemical bonds [22], [25]–[28]. The adsorption process on porous adsorbent is generally defined with three main stages. First, the adsorbate is transported from bulk solution to the external surface of the adsorbent (film-diffusion or external-diffusion). Next, the adsorbate transport within the pores of the adsorbent (internal diffusion). In this step that is the rate limiting, a small amount of adsorption occurs on the external surface which is called particle diffusion. At final step the adsorbate is adsorbed on the inner surface of the adsorbent pores and capillary spaces. This is the equilibrium step. The interaction between the adsorbate, matrix and surface of adsorbent have effected on these steps and the resulting metal adsorption. Parameters that could influence on adsorption are included pH, temperature and presence of competitive ions of the adsorption matrix; chemical and physical properties of adsorbate such as ionic radius and solubility; and adsorbent surface chemistry and characteristics [7], [29]–[33].

1.2.2.2 Mercury Adsorbents

Among different sorbent materials, activated carbon (AC) has been used as the most dominant adsorbent for removing mercury from industrial effluent. However its application, mainly in large adsorption systems, is limited due to several disadvantages such as high cost and the difficulty in preparation and regeneration process [34], [35]. A growing number of studies in recent years have suggested various low price sorbents.

These materials could potentially substitute AC in water treatment process to remove heavy metals such as mercury. Zeolites are valuable materials with an extensive application as adsorbents and molecular sieves. Various zeolites have been used as a favorable material in environmental applications and wastewater treatments [6], [36]–[41].

1.2.3 Zeolites

Zeolites are crystalline aluminosilicates consisting of molecular-sized pores and channels. These microporouse structures are made of three-dimensional framework of [SiO4]4- and [AlO4]5- tetrahedra, linked by sharing oxygen atoms. Two important factors that influence the pore size of zeolitic material and its adsorption characteristics are the silicon to aluminum ratio and the number of units within a ring [42]–[44]. In addition, the negative charge resulting from the substitution of Si (IV) by Al (III) in the structure is compensated by the hydrated cations from alkaline and alkaline earth groups of the periodic table. This would result in the loosely bonded cations and water molecules in the pores and channels of zeolite structure which gives them the significant characteristics to exchange cations of heavy metal with external medium or/and adsorb cations, anions and organic compounds from the aquatic solution [45].More than 60 types of zeolites occur naturally. Also about 150 types of synthetic zeolites are produced using different precursors of Si and Al including very low cost starting material such as clay minerals, barley and rice husk silica and coal fly ash. Among porous zeolitic materials, natural clinoptilolite and synthetic zeolite LTA exhibit strong affinity for many heavy metal cations including mercury [28], [45]–[52].

1.2.3.1 Natural Zeolite (Clinoptilolite)

Natural clinoptilolite belongs to HEU framework with silicon to aluminum ratio of more than 4.7. Pure natural clinoptilolite has an ideal chemical composition of $|Na_{1.84}K_{1.76}Mg_{0.2}Ca_{1.24}(H_2O)_{21.36}|$ $[Si_{29.84}Al_{6.16}O_{72}]$ [44]. Potential applications of natural clinoptilolite for environmental remediation processes, particularly for water and soil purification, are studied extensively by many researchers [45], [52]. A few studies are

published on the application of natural zeolite for mercury adsorption in aqueous environment. [53] and [54] reported the use of natural zeolite for removal of mercury from aqueous solutions. However they haven't determined the framework type that selected natural zeolites belonged to.

1.2.3.2 Zeolite LTA

Zeolite NaA with LTA (Linde Type A) structure framework has silicon to aluminum ratio of about 1.0, which is considerably lower than clinoptilolite. LTA ideal chemical composition is $|Na_{96}(H_2O)_{216}|$ $[Si_{96}Al_{96}O_{384}]$ [44]. Zeolite A can be synthesized using different starting materials as source of Al and Si [55]–[57]. Some studies indicated that zeolite LTA could effectively remove heavy metals from contaminated wastewater [25], [50]. However to best of author's knowledge, the selectivity of zeolite LTA toward mercury was only determined by [56].

1.2.3.3 Zeolitized Coal Fly Ash

Coal fly ash is a waste obtained from the combustion of coal in power plants. Worldwide production of coal fly ash exceeds million tons per year. Different zeolites can be synthesized using coal fly ash as starting material. Conversion of CFA into zeolites can enhance its adsorption properties towards heavy metals while reducing its leaching problems [46], [50], [58]. A variety of different zeolitic structures (zeolite X, NaP, LSX, N. ZSM-5, faujasite, LTA, etc.) heave been synthesized from CFA using different methods. Among them zeolite A has become one of the most important zeolites in water purification and treatment industry. Zeolites A can be produced from CFA through several methods including hydrothermal conversion, fusion, ultra sound and microwave irradiation [50], [55], [59], [60].

1.2.3.4 Modification of Zeolites

Natural and synthetic zeolites can be modified chemically using impregnation or ion exchange methods. It would be expected that modification of zeolite surface produce an adsorbent with improved properties that is tailored for a specific function. Selecting a

proper modification process and the right metallic ions for any specific heavy metal removal is of great importance since it may affect the mechanism and kinetic of adsorption process [9], [61]. Gold oxide supports have mainly been considered as a catalyst in hydrogenation and oxidation reactions [62]–[67]. However, gold's well-known tendency to amalgamate with mercury allow for its possible application in treating wastewater contaminated by mercury. Even today elemental Hg-Au amalgamation is used widely in artisanal gold mining and gold recovery. Various preparation methods such as deposition-precipitation, impregnation, incipent wetness impregnation and ion-exchange have been developed to generate chemical supports with active gold particles [12], [22].

1.2.3.5 Gold-iron Bimetallic Modification

Distinctive properties of iron oxide species, arise because of its extremely surface modifiability, excellent magnetic properties, great biocompatibility and proper cost [68]–[70]. It was reported that iron oxides in its different forms such as magnetite, goethite and ferrihydrite is capable to adsorb aqueous mercury (II). The process of Hg adsorption onto iron oxide is known to be chemisorption. Iron modified zeolites are mainly used as a support to stabilize gold. Iron cations play a role as active centers for gold adsorption. This may create strong interaction between iron cations and the precursor of gold makes Au stabilization stronger on zeolite surface [71], [72].

1.3 Thesis Hypothesis

1. Zeolitized CFA could be effectively used in removing mercury from industrial wastewater.

2. The modification of natural zeolite with gold would increase the removal efficiency of this zeolite towards Mercury.

3. Gold-iron modification of zeolite LTA would significantly impact the removal efficiency and adsorption capacity of this bi metallic adsorbent.

4. Some parameters such as adsorbent dose, initial pH and contact time would influence adsorption capacity and adsorption mechanism.

1.4 Thesis Statement and Outlines

The main purposes of this research are:

1. To study the capability of zeolitized CFA as a practical mercury adsorbents from water effluent.

2. To modify synthetic zeolite LTA using gold and iron in order to provide the highest removal efficiency.

3. To increase the adsorption performance of natural clinoptilolite zeolite towards mercury using ion exchange gold particles.

4. To characterize the raw and modified zeolites with various techniques including TGA, BET, XRD and SEM-EDX.

5. To regulate which experimental conditions (i.e. pH, contact time, adsorbent dosage) for each zeolitic adsorbent yield the highest removal of aqueous Hg.

6. To determine the kinetic parameters and isothermal parameters for each zeolitic adsorbent in order to predict some of required conditions for a possible continuous adsorption system for each adsorbents.

7. To predict the adsorption mechanism towards aqueous mercury applying intra-particle diffusion equation.

Bibliography

[1] N. E. Selin, “Global Biogeochemical Cycling of Mercury: A Review,” Annu. Rev. Environ. Resour., vol. 34, no. 1, pp. 43–63, Nov. 2009.

[2] A. P. B. Hall, A. M. Hagan, and P. D. Candidate, “Aqueous Phase Mercury Removal : Strategies for a Secure Future Water Supply Critical National Need Idea White Paper.”

[3] “Technical Background Report for the Global Mercury Assessment,” 2013.

[4] M. Mailman, L. Stepnuk, N. Cicek, and R. a D. Bodaly, “Strategies to lower methyl mercury concentrations in hydroelectric reservoirs and lakes: A review.,” Sci. Total Environ., vol. 368, no. 1, pp. 224–35, Sep. 2006.

[5] R. a Bernhoft, “Mercury toxicity and treatment: a review of the literature.,” J. Environ. Public Health, vol. 2012, p. 460508, Jan. 2012.

[6] O. Rodríguez, I. Padilla, H. Tayibi, and A. López-Delgado, “Concerns on liquid mercury and mercury-containing wastes: a review of the treatment technologies for the safe storage.,” J. Environ. Manage., vol. 101, pp. 197–205, Jun. 2012.

[7] S. Sen Gupta and K. G. Bhattacharyya, “Kinetics of adsorption of metal ions on inorganic materials: A review.,” Adv. Colloid Interface Sci., vol. 162, no. 1–2, pp. 39–58, Feb. 2011.

[8] H. Figueiredo and C. Quintelas, “Tailored zeolites for the removal of metal oxyanions: overcoming intrinsic limitations of zeolites.,” J. Hazard. Mater., vol. 274, pp. 287–99, Jun. 2014.

[9] E. K. Faulconer, “Effects of Activated Carbon Surface Chemistry Modification on,” pp. 1–129, 2012.

[10] J. H. Cho, Y. Eom, and T. G. Lee, “Stabilization/solidification of mercury-contaminated waste ash using calcium sodium phosphate (CNP) and magnesium potassium phosphate (MKP) processes.,” J. Hazard. Mater., vol. 278, pp. 474–82, Aug. 2014.

[11] “(i.e., identifying face cream products containing mercury), direct analysis of the products via XRF or TXRF are the fastest and most straightforward methods, as they do not require preparation of standards, involve minimal manipulation of the sample, and ,” 1990.

[12] K. P. Lisha and T. Pradeep, “Towards a practical solution for removing inorganic mercury from drinking water using gold nanoparticles,” Gold Bull., vol. 42, no. 2, pp. 144–152, Jun. 2009.

[13] X. Zhu and S. D. Alexandratos, “Determination of trace levels of mercury in aqueous solutions by inductively coupled plasma atomic emission spectrometry: Elimination of the ‘memory effect,’” Microchem. J., vol. 86, no. 1, pp. 37–41, 2007.

[14] F. Report, “STEP Mercury Removal Technology Demonstration Project STEP Mercury Removal Technology Demonstration Project Final Report,” no. July, 2000.

[15] A. O. Adegbembo, C. Frcd, and P. A. Watson, “Estimated Quantity of Mercury in Amalgam Waste Water Residue Released by Dentists into the Sewerage System in Ontario , Canada,” vol. 70, no. 11, 2004.

[16] “achieving-low-mercury-concentrations-in-chlor-alkali-wastewaters.pdf.” .

[17] G. Z. Kyzas, N. a Travlou, and E. a Deliyanni, “The role of chitosan as nanofiller of graphite oxide for the removal of toxic mercury ions.,” Colloids Surf. B. Biointerfaces, vol. 113, pp. 467–76, Jan. 2014.

[18] J. Kulkarni, “Studies and Research on Mercury Removal from Water : A Review Abstract :,” no. 2, pp. 221–225, 2015.

[19] B. Tawabini, S. Al-Khaldi, M. Atieh, and M. Khaled, “Removal of mercury from water by multi-walled carbon nanotubes.,” Water Sci. Technol., vol. 61, no. 3, pp. 591–8, Jan. 2010.

[20] J. Liu, K. T. Valsaraj, I. Devai, and R. D. DeLaune, “Immobilization of aqueous Hg(II) by mackinawite (FeS).,” J. Hazard. Mater., vol. 157, no. 2–3, pp. 432–40, Sep. 2008.

[21] K. J. Lee and T. G. Lee, “A review of international trends in mercury management and available options for permanent or long-term mercury storage.,” J. Hazard. Mater., vol. 241–242, pp. 1–13, Nov. 2012.

[22] E. K. Faulconer, N. V. H. von Reitzenstein, and D. W. Mazyck, “Optimization of magnetic powdered activated carbon for aqueous Hg(II) removal and magnetic recovery.,” J. Hazard. Mater., vol. 199–200, pp. 9–14, Jan. 2012.

[23] A. Gupta, S. R. Vidyarthi, and N. Sankararamakrishnan, “Thiol functionalized sugarcane bagasse—A low cost adsorbent for mercury remediation from compact fluorescent bulbs and contaminated water streams,” J. Environ. Chem. Eng., vol. 2, no. 3, pp. 1378–1385, Sep. 2014.

[24] D. S. Han, M. Orillano, A. Khodary, Y. Duan, B. Batchelor, and A. Abdel-Wahab, “Reactive iron sulfide (FeS)-supported ultrafiltration for removal of mercury (Hg(II)) from water.,” Water Res., vol. 53, pp. 310–21, Apr. 2014.

[25] S. Malamis and E. Katsou, “A review on zinc and nickel adsorption on natural and modified zeolite, bentonite and vermiculite: examination of process parameters, kinetics and isotherms.,” J. Hazard. Mater., vol. 252–253, pp. 428–61, May 2013.

[26] H. K. Boparai, M. Joseph, and D. M. O’Carroll, “Kinetics and thermodynamics of cadmium ion removal by adsorption onto nano zerovalent iron particles,” J. Hazard. Mater., vol. 186, no. 1, pp. 458–465, 2011.

[27] K. State and E. State, “Langmuir , Freundlich , Temkin and Dubinin – Radushkevich Isotherms Studies of Equilibrium Sorption of Zn 2 + Unto Phosphoric Acid Modified Rice Husk,” IOSR J. Appl. Chem., vol. 3, no. 1, pp. 38–45, 2012.

[28] H. S. Ibrahim, T. S. Jamil, and E. Z. Hegazy, “Application of zeolite prepared from Egyptian kaolin for the removal of heavy metals: II. Isotherm models.,” J. Hazard. Mater., vol. 182, no. 1–3, pp. 842–7, Oct. 2010.

[29] F. Raji and M. Pakizeh, “Kinetic and thermodynamic studies of Hg(II) adsorption onto MCM-41 modified by ZnCl2,” Appl. Surf. Sci., vol. 301, pp. 568–575, 2014.

[30] D. Robati, “Pseudo-second-order kinetic equations for modeling adsorption systems for removal of lead ions using multi-walled carbon nanotube,” J. Nanostructure Chem., vol. 3, no. 1, p. 55, 2013.

[31] G. Hodaifa, J. M. Ochando-Pulido, S. Ben Driss Alami, S. Rodriguez-Vives, and a. Martinez-Ferez, “Kinetic and thermodynamic parameters of iron adsorption onto olive stones,” Ind. Crops Prod., vol. 49, pp. 526–534, 2013.

[32] K. P. Raven, A. Jain, and R. H. Loeppert, “Arsenite and Arsenate Adsorption on Ferrihydrite: Kinetics, Equilibrium, and Adsorption Envelopes,” Environ. Sci. Technol., vol. 32, no. 3, pp. 344–349, Feb. 1998.

[33] V. K. Jha, M. Matsuda, and M. Miyake, “Sorption properties of the activated carbon-zeolite composite prepared from coal fly ash for Ni(2+), Cu(2+), Cd(2+) and Pb(2+).,” J. Hazard. Mater., vol. 160, no. 1, pp. 148–53, Dec. 2008.

[34] F. Di Natale, A. Erto, A. Lancia, and D. Musmarra, “Mercury adsorption on granular activated carbon in aqueous solutions containing nitrates and chlorides,” J. Hazard. Mater., vol. 192, no. 3, pp. 1842–1850, 2015.

[35] P. Hadi, M.-H. To, C.-W. Hui, C. S. K. Lin, and G. McKay, “Aqueous mercury adsorption by activated carbons.,” Water Res., vol. 73, pp. 37–55, Apr. 2015.

[36] A. Delebarre, “Removal of mercury in aqueous solution by fluidized bed plant fly ash q,” vol. 82, pp. 153–159, 2003.

[37] F.-S. Zhang, J. O. Nriagu, and H. Itoh, “Mercury removal from water using activated carbons derived from organic sewage sludge.,” Water Res., vol. 39, no. 2–3, pp. 389–95, 2005.

[38] J. V. Nabais, P. J. M. Carrott, M. M. L. R. Carrott, M. Belchior, D. Boavida, T. Diall, and I. Gulyurtlu, “Mercury removal from aqueous solution and flue gas by adsorption on activated carbon fibres,” Appl. Surf. Sci., vol. 252, no. 17, pp. 6046–6052, Jun. 2006.

[39] M. Liu, L.-A. Hou, B. Xi, Y. Zhao, and X. Xia, “Synthesis, characterization, and mercury adsorption properties of hybrid mesoporous aluminosilicate sieve prepared with fly ash.,” Appl. Surf. Sci., vol. 273, no. 100, pp. 706–716, May 2013.

[40] D. M. Manohar, K. A. Krishnan, and T. S. Anirudhan, “Removal of mercury (II) from aqueous solutions and chlor-alkali industry wastewater using,” vol. 36, pp. 1609–1619, 2002.

[41] K. Kadirvelu, M. Kavipriya, C. Karthika, N. Vennilamani, and S. Pattabhi, “Mercury (II) adsorption by activated carbon made from sago waste,” Carbon N. Y., vol. 42, no. 4, pp. 745–752, Jan. 2004.

[42] A. S. T. Chiang and K. Chao, “Membranes and ® lms of zeolite and zeolite-like materials,” vol. 62, 2001.

[43] J. A. Kaduk and J. Faber, “CRYSTAL STRUCTURE OF ZEOLITE Y AS A FUNCTION OF ION EXCHANGE,” vol. 12, no. 2, 1995.

[44] M. M. J. Treacy and J. B. Higgins, Collection of simulated XRD powder patterns for zeolites. Amsterdam, The Netherlands: Elsevier, 2007.

[45] S. Wang and Y. Peng, “Natural zeolites as effective adsorbents in water and wastewater treatment,” Chem. Eng. J., vol. 156, no. 1, pp. 11–24, Jan. 2010.

[46] S. S. Bukhari, J. Behin, H. Kazemian, and S. Rohani, “Conversion of coal fly ash to zeolite utilizing microwave and ultrasound energies: A review,” Fuel, vol. 140, pp. 250–266, Jan. 2015.

[47] M. N. Sepehr, M. Zarrabi, H. Kazemian, A. Amrane, K. Yaghmaian, and H. R. Ghaffari, “Removal of hardness agents, calcium and magnesium, by natural and alkaline modified pumice stones in single and binary systems,” Appl. Surf. Sci., vol. 274, pp. 295–305, Jun. 2013.

[48] H. Kazemian, H. Zakeri, and M. S. Rabbani, “Cs and Sr removal from solution using potassium nickel hexacyanoferrate impregnated zeolites</p> </p>,” J. Radioanal. Nucl. Chem., vol. 268, no. 2, pp. 231–236, May 2006.

[49] S. S. Bukhari, J. Behin, H. Kazemian, and S. Rohani, “A comparative study using direct hydrothermal and indirect fusion methods to produce zeolites from coal fly ash utilizing single-mode microwave energy,” J. Mater. Sci., vol. 49, no. 24, pp. 8261–8271, 2014.

[50] K. S. Hui, C. Y. H. Chao, and S. C. Kot, “Removal of mixed heavy metal ions in wastewater by zeolite 4A and residual products from recycled coal fly ash.,” J. Hazard. Mater., vol. 127, no. 1–3, pp. 89–101, Dec. 2005.

[51] E. Katsou, S. Malamis, M. Tzanoudaki, K. J. Haralambous, and M. Loizidou, “Regeneration of natural zeolite polluted by lead and zinc in wastewater treatment systems,” J. Hazard. Mater., vol. 189, no. 3, pp. 773–786, 2011.

[52] N. G. Turan and O. Ozgonenel, “The Design and Implementation of Adsorptive Removal of Cu (II) from Leachate Using ANFIS,” vol. 2013, 2013.

[53] M. Trgo, J. Perić, N. V. Medvidović, M. Ugrina, I. Nuić, M. Macherzynsky, Ł. Uruski, and J. Golas, “MERCURY IONS CAPTURE BY NATURAL AND IRON-MODIFIED ZEOLITE - INFLUENCE OF SOLID / LIQUID RATIO,” pp. 36–39.

[54] a. Chojnacki, K. Chojnacka, J. Hoffmann, and H. Górecki, “The application of natural zeolites for mercury removal: from laboratory tests to industrial scale,” Miner. Eng., vol. 17, no. 7–8, pp. 933–937, Jul. 2004.

[55] J. Behin, S. S. Bukhari, V. Dehnavi, H. Kazemian, and S. Rohani, “Using Coal Fly Ash and Wastewater for Microwave Synthesis of LTA Zeolite,” Chem. Eng. Technol., vol. 37, no. 9, pp. 1532–1540, Sep. 2014.

[56] S. N. Azizi, A. R. Dehnavi, and A. Joorabdoozha, “Synthesis and characterization of LTA nanozeolite using barley husk silica: Mercury removal from standard and real solutions,” Mater. Res. Bull., vol. 48, no. 5, pp. 1753–1759, May 2013.

[57] E. Hums, N. M. Musyoka, H. Baser, A. Inayat, and W. Schwieger, “In-situ ultrasound study of the kinetics of formation of zeolites Na–A and Na–X from coal fly ash,” Ultrasonics, vol. 54, no. 2, pp. 537–543, Feb. 2014.

[58] T.-C. Hsu, C.-C. Yu, and C.-M. Yeh, “Adsorption of Cu2+ from water using raw and modified coal fly ashes,” Fuel, vol. 87, no. 7, pp. 1355–1359, Jun. 2008.

[59] A. Alastuey, E. Herna, X. Querol, N. Moreno, J. C. Uman, F. Plana, and A. Lo, “Synthesis of zeolites from coal fly ash : an overview,” vol. 50, pp. 413–423, 2002.

[60] V. K. Jha, M. Nagae, M. Matsuda, and M. Miyake, “Zeolite formation from coal fly ash and heavy metal ion removal characteristics of thus-obtained Zeolite X in multi-metal systems.,” J. Environ. Manage., vol. 90, no. 8, pp. 2507–14, Jun. 2009.

[61] R. J. White, R. Luque, V. L. Budarin, J. H. Clark, and D. J. Macquarrie, “Supported metal nanoparticles on porous materials . Methods and applications,” no. September 2008, pp. 481–494, 2009.

[62] C. Cellier, S. Lambert, E. M. Gaigneaux, C. Poleunis, V. Ruaux, P. Eloy, C. Lahousse, P. Bertrand, J. P. Pirard, and P. Grange, “Investigation of the preparation and activity of gold catalysts in the total oxidation of n-hexane,” Appl. Catal. B Environ., vol. 70, no. 1–4, pp. 406–416, 2007.

[63] a. Simakov, I. Tuzovskaya, a. Pestryakov, N. Bogdanchikova, V. Gurin, M. Avalos, and M. H. Farías, “On the nature of active gold species in zeolites in CO oxidation,” Appl. Catal. A Gen., vol. 331, pp. 121–128, Jan. 2007.

[64] J. C. Fierro-gonzalez, Y. Hao, and B. C. Gates, “Gold Nanoclusters Entrapped in the r -Cages of Y Zeolites : Structural Characterization by X-ray Absorption Spectroscopy,” pp. 6645–6651, 2007.

[65] C. Baatz, N. Decker, and U. Pruse, “New innovative gold catalysts prepared by an improved incipient wetness method,” J. Catal., vol. 258, no. 1, pp. 165–169, Aug. 2008.

[66] C. Baatz and U. Pruse, “Preparation of gold catalysts for glucose oxidation by incipient wetness,” J. Catal., vol. 249, no. 1, pp. 34–40, Jul. 2007.

[67] a. Simakov, I. Tuzovskaya, N. Bogdanchikova, a. Pestryakov, M. Avalos, M. H. Farias, and E. Smolentseva, “Influence of sodium on activation of gold species in Y–zeolites,” Catal. Commun., vol. 9, no. 6, pp. 1277–1281, Mar. 2008.

[68] J. Groen, a Bruckner, E. Berrier, L. Maldonado, J. Moulijn, and J. Perezramirez, “Iron site modification upon alkaline treatment of Fe-ZSM-5 zeolites—Opportunities for improved N2O decomposition activity,” J. Catal., vol. 243, no. 1, pp. 212–216, Oct. 2006.

[69] M. J. Jiménez-Cedillo, M. T. Olguín, C. Fall, and a. Colín, “Adsorption capacity of iron- or iron–manganese-modified zeolite-rich tuffs for As(III) and As(V) water pollutants,” Appl. Clay Sci., vol. 54, no. 3–4, pp. 206–216, Dec. 2011.

[70] P. Xu, G. M. Zeng, D. L. Huang, C. L. Feng, S. Hu, M. H. Zhao, C. Lai, Z. Wei, C. Huang, G. X. Xie, and Z. F. Liu, “Use of iron oxide nanomaterials in wastewater treatment: a review.,” Sci. Total Environ., vol. 424, pp. 1–10, May 2012.

[71] N. Bogdanchikova, a. Simakov, E. Smolentseva, a. Pestryakov, M. H. Farias, J. a. Diaz, a. Tompos, and M. Avalos, “Stabilization of catalytically active gold species in Fe-modified zeolites,” Appl. Surf. Sci., vol. 254, no. 13, pp. 4075–4083, Apr. 2008.

[72] I. Sobczak, H. Pawlowski, J. Chmielewski, and M. Ziolek, “Gold and gold-iron modified zeolites--towards the adsorptive deodourisation.,” J. Hazard. Mater., vol. 179, no. 1–3, pp. 444–52, Jul. 2010.

Chapter 2

2 Mercury Removal from Aqueous Solution by Zeolitized Coal Fly Ash: Equilibrium and Kinetic Studies

2.1 Introduction

Mercury is recognized as one of the most hazardous heavy metals. The discharge of effluents containing mercury in soil, sediments and water can inflict an irreversible harm to the environment. The main sources of mercury emissions besides the natural origins such as volcanic activities are the process of ore mining, fossil fuels burning, and industrial production processes such as the pharmaceutical industry and battery manufacturing.

Mercury high toxicity is mainly related to the capacity of inorganic mercury to convert to its organic form, methyl mercury and its bioaccumulation in the aquatic species that are in top of the food chain for lots of species including humans. Various neurological damage as well as irritability, paralysis, insanity and loss of sight were reported as the main toxicological effects of mercury in its different forms. Because of this high toxicity of mercury the US Environmental Protection Agency (EPA) specifies the maximum contaminant level (MCL) of Hg at very low level of 0.2 ppb (0.2 µg/L). This has been a great motivation for the growing number of researches on treatment of wastewater towards mercury [1]–[6].

There are different mercury removal technologies such as sulfide precipitation, coagulation, co-precipitation and reverse osmosis. Although all these techniques are effective to some degrees, most of them have disadvantages such as high cost, operational difficulties, complicated industrial setup and large toxic irreversible sludge [7]–[9].

Adsorption has been the simplest, adaptable, well established, and widely used technique for the removal of heavy metals including mercury. In most cases adsorption is not very

expensive and doesn’t need very advanced technologies. Among different sorbent materials, activated carbon (AC) has been the predominantly adsorbent for removing mercury from industrial effluent for decades. However its application, mainly in large adsorption systems, is limited due to its high cost and the difficulty in preparation and regeneration process [10]–[12].

A growing number of studies in recent years have suggested various low price sorbents. These materials could potentially substitute AC in water treatment process to remove heavy metals. Some examples of such adsorbents are including coal fly ash (CFA), naturally occurring zeolites and synthetic zeolites from very low cost starting material containing Si and Al such as clay minerals (kaolin, illite, bentonite, etc.), barley husk silica, rice husk, and fly ash from different sources[13]–[19].

Coal fly ash is a waste obtained from the combustion of coal in power plants. Worldwide production of coal fly ash exceeds million tons per year. Today the increasing production of CFA is a great concern due to its fine structure and toxic elements [20], [21]. Less than half of the produced CFA is recycled and used as a building materials, filler in cement and concrete, making wallboards, soil amendment , acid mine drainage control and also as an additive to stabilize waste [22]. Also coal fly ash has been effectively used for flue gas cleaning, and removing toxic metals, dyes and organic pollutants from industrial wastewater. Different heavy metals such as zinc, lead, nickel, copper, chromium and mercury have been efficiently removed from industrial effluents using coal fly ash [23]–[27].

Many studies have shown that unburned carbon present in fly ash is the key particle that is responsible to capture mercury in coal-fired power plants [23]. This can be the main reason for the effective influence of CFA to remove mercury ions in liquid medium. However, in aquatic solution its application is more complicated since the other heavy metals and toxic species trapped in the CFA structure can be released to the liquid solution during the adsorption process. So while removing mercury from the effluent, other toxic heavy metals such as As and Cr can be released to the medium. Moreover raw CFA, still displays a relatively low adsorption capacity compared to other adsorbents

[28]. During the last few years, some researchers have found that modification of CFA can enhance its adsorption properties while reducing its leaching problems. To do this two main methods have been suggested. First, is to extract and separate unburned carbon from CFA using methods such as gravity separation, electrostatic technologies, and froth flotation; to produce an activated carbon-like porous structure with a much lower BET surface area (around 25-58 m2/g) compared to other synthesized activated carbon [23], [29], [30].

The second method involves conversion of CFA into zeolites that has been shown to enhance mercury removal [25], [28], [31]. Zeolites are valuable materials with an extensive application as adsorbents, ion exchangers and molecular sieves. Various zeolites have been used as a promising material in environmental cleaning process and wastewater treatments [18], [19]. They are microporous aluminosilicates, made of a 3D framework of $[SiO4]^{4-}$ and $[AlO4]^{5-}$ tetrahedra, linked by sharing oxygen atoms. Their special structure dictates lots of pores and cavities. The silicon to aluminum ratio and the number of units within a ring are important factors that influence the pore size of zeolitic material and hence its adsorption characteristics [32]–[34].

Generally, the negative charge resulting from the substitution of Si (IV) by Al (III) in the structure is compensated by the hydrated cations from alkaline and alkaline earth groups of the periodic table. This would result in the loosely bonded cations and water molecules in the pores and channels of zeolite structure which gives them the significant characteristics to exchange cations of heavy metal with external medium or/and adsorb cations, anions and organic compounds from the aquatic solution [35].

A variety of different zeolitic structures (zeolite X, NaP, LSX, N. ZSM, faujasite, LTA, etc.) heave been synthesized from CFA using different methods [28], [36], [37]. Among them zeolite A (with chemical formula Na12Al12Si12O48.37) has become one of the most important zeolites in water purification and treatment industry. Zeolites A can be produced from CFA through several methods including hydrothermal conversion, fusion, ultra sound and microwave irradiation [21], [31], [36].

The aim of present work was an extensive study of a synthesized zeolite LTA from coal fly ash (using microwave irradiation as synthetic method) and its applicability in mercury removal.

Also we investigated the removal performance of Hg(II) ions on the synthesized CFA-ZA and compared its removal efficiency with the parent CFA and also activated carbon as a bench mark. The parameters considered in this study included initial concentration of Hg (II) solution, adsorbents dosage, contact time and initial pH value. Furthermore the Langmuir, Freundlich and Tempkin models were employed to analyze adsorption isotherms. Kinetics of mercury adsorption on CFA-ZA was investigated using first-order, second-order and Elovich models to better understand the adsorption mechanism.

Characterization of all tested adsorbents was performed using scanning electron microscopy (SEM), X-ray powder diffraction (XRD), thermal gravimetric analysis (TGA) and surface area measurement (BET).

2.2 Materials and Methods

2.2.1 Synthesis of Zeolite LTA from CFA

Class F coal fly ash (CaO content <20%) [38] procured from coal fired power plant (OPG, Nanticoke, ON) was zeolitized with the assistance of microwave irradiation. The aluminosilicates were extracted at elevated temperature with caustic soda followed by crystallization. The precursor slurry solution was prepared by adding CFA in 3 M NaOH solution (CFA/solvent weight ratio of 1/5). This slurry was digested at 70°C and 1 rpm for 12 hours in an end-over-end oven to extract the aluminum and silicon contents from CFA. Sodium aluminate was added to the solution to adjust molar batch composition of Na_2O:1 Al_2O_3:1.780 SiO_2:192 H_2O, then aged for two hours at room temperature. The aged samples were irradiated for 10 min with a multimode kitchen microwave under total reflux at atmospheric pressure.

2.2.2 Characterization

The synthesized samples were dried overnight and subjected to X-ray diffraction (XRD) analysis. Rigaku–Miniflex powder diffractometer (Japan) was used to collect XRD data of the raw CFA sample and the synthesized zeolites using CuKα (λ for Kα = 1.54059 Å) over the range of $5°<2\theta<40°$ with step width of 0.02°. The obtained crystalline phase was identified using the standard peaks in literature [39]. The peak areas of the products were determined by "peak fitting" algorithm in the MDI-Jade v 7.5 software (Livermore, California). The chemical composition of the sorbents was evaluated by means of X-ray fluorescence spectroscopy (XRF) utilizing PANalytical PW2400 Wavelength Dispersive. The textural properties of the raw CFA and CFA-ZA were studied by means of Scanning Electron Microscope (SEM) JSM 600F, Joel Japan, operating at 10 keV of acceleration voltage and coupled with energy dispersive X-ray analysis (EDAX).

In the SEM analysis, the samples were coated with a thin layer of gold and mounted on a copper stab using a double-stick tape. For BET (Micrometrics ASAP 2010) surface area measurement, known amounts of samples (e.g. 100 mg) were loaded into the BET sample tube and degassed under vacuum (10–5 Tor) at 150° C for about 12 hours. Inductively coupled plasma-atomic emission spectroscopy (ICP-AES) was used to measure the elemental concentration of mercury inside the various examined solution [40]. The model of ICP-AES was Perkin Elmer Optima-3000 DV System. Hg-196.164 nm wavelength was measured for intensity. The net intensity was calculated through peak area integration minus the backgrounds using ICP expert software (version: v 4.0).

To measure the leaching resistance of the coal fly ash and produced zeolite, mercury concentration in the supernatant liquid obtained by soaking the sample in de-ionized water at constant pH [41] was measured by ICP-AES. The pH values of the aqueous solutions were measured by an Eco Met pH/ TEMP meter (P25, Beckman, China).

2.2.3 Batch Adsorption Studies

In order to conduct the adsorption tests, a wastewater sample from BC mine provided by Kontec Ecology Systems Inc. (Burlington, ON) was used as a medium to make simulated

solutions with higher concentration of mercury. The simulated wastewater with initial concentration of 10, 50 and 100 mg/L of mercury was prepared from 1000 µg/ml AAS standard solution containing mercury chloride salt (Alfa Aesar, Ward Hill, MA, USA). All adsorption experiments were carried out in an end-over-end shaker and oven with continuous shaking at 500 rpm. At room temperature 10 ml of prepared solution were added to precise amount of 0.5 g of each adsorbent including CFA, CFA-ZA and AC. We used this volume of Hg (II) solution to better organize the adsorption experiment. Samples were taken from the batch container after 24 hours and filtered through 0.45 µm syringe filters (Fischer Scientific, Ottawa, ON, Canada). Then the filtered samples were measured to determine Hg (II) concentration by ICP-AES (see section 2.2). In all adsorption experiments, a sample of simulated mercury wastewater solution underwent the same condition without having any absorbent (as a control sample) to eliminate the effect of adsorption on the container walls. The accuracy, reliability and reproductively of the mercury measurement were determined by analyzing in triplicate. Only the averages for each individual measurement were reported in the given graphs. Error bars represent the standard deviations. An adsorption calibration curve was constructed including a blank and five or more standards. The instrumental settings of the manufacturer were followed.

To study the effect of adsorbents/solution mass ratio (from 5 to 100 g/L) on the Hg(II) removal efficiency , various doses of CFA-ZA, raw CFA and AC were applied to 10 ml of 10 mg/L mercury solution. The CFA-ZA adsorption isotherms were obtained adding 2.5 to 1 g of adsorbent to 10 ml of 10 g/L Hg (II) solution. The contact times were fixed at 24 hours.

The 0.5 g of CFA, CFA-ZA, and AC were left in contact with 10 ml of 10 ppm mercury solution at initial pH value of 2.5±0.25. Samples were withdrawn at different time intervals from 5 min to 24 h to determine the optimum contact time to reach equilibrium. For the CFA-ZA, the experiments were repeated with 0.1 and 1 g adsorbent dosage.

Effect of pH on mercury ions sorption was only investigated for zeolitic sample. To do this, 0.5 g of CFA-ZA was dispersed into 10 ml solutions containing 10 mg/L of Hg (II).

The pH value of 10 ppm Hg (II) solution was about 2.5± 0.25. So the initial pH values were adjusted to obtain higher pH values using NaOH 1M and NaOH 2.5 M. The examined pH range was from 2.5 to 10. The batch tests were conducted at room temperature with continuous stirring at 500 rpm for 24 h.

All samples were stored in a refrigerator prior to ICP-AES analysis in order to avoid oxidation of mercury and change in solution concentration and pH. The removal efficiency of each adsorbent was calculated using Eq. (1). C_0 and C_e are the initial and equilibrium concentration of the adsorbate respectively (mg/L).

$$\text{Removal efficiency (\%)} = 100\ (C_0-C_e)/C_0 \quad (1)$$

Most researches in the field have reported mercury removal percent to show the efficiency of their examined sorbents. Obviously this parameter could not be a tangible adsorption capacity since the removal percentage is a totally relative term varying by adsorbent dosage and initial mercury concentration [11].

In order to obtain a more realistic value for sorption capacity, the amount of mercury ions adsorbed per unit mass of each adsorbent was evaluated using the following equation:

$$q_e = (C_0-C_e).V/\ m \quad (2)$$

The q_e is in (mg/g) and expresses the mercury ions adsorbed per gram of adsorbents, V is the test solution volume (L), m is the weight of sorbent (g) and C_0 and C_e are as initial and equilibrium concentrations.

2.2.4 Theory of Adsorption Kinetics

In order to further investigate the adsorption mechanism of the studied adsorbents for removing mercury, the rate of adsorption should be modeled by proper reaction models. In the present study, three kinetic models including a pseudo-first-order, a pseudo-second-order and the Elovich model along with intra-particle diffusion model were

examined with the kinetic data obtained from the batch mode experiments for 3 different initial adsorbent concentrations of prepared CFA-ZA.

2.2.4.1 The Pseudo-first-order Model (Lagergren equation)

The Lagergren equation is probably the most widely used equation that describes the rate of adsorption of a solute from a liquid-phase system. The Lagergren equation has mostly been written as follows:

$$\ln (q_e - q_t) = \ln q_e - k_1 t \quad (3)$$

Where k_1(min-1) is the kinetic coefficient of the pseudo-first-order reaction and q_e and q_t are the amount of sorbents adsorbed at equilibrium and at time t, respectively [42]. If the first-order kinetics is applicable, the plot of ln (q_e-q_t) against t in the above equation should give a linear relationship. Comparison of q_e obtained from the plot and the experimental value of q_e determines the validity of first-order model assumption [7], [43].

2.2.4.2 Pseudo-second-order Model

The second order kinetic model may be expressed on the basis of following linear equation:

$$t/q_t = 1/(k_2 q_e^2) + (1/q_e).t \quad (4)$$

where k_2 is the second order rate constant (g/mg.min) and q_e and q_t are the equilibrium and temporal concentrations. If the second-order kinetics is applicable, the plot of experimental values of t/q_t against t should give a linear relationship [42], [44].

2.2.4.3 The Elovich Kinetic Model

The Elovich model can be described according to the following equation:

$$dq_t/d_t = \alpha \exp (- \beta q_t) \quad (5)$$

Integration of the Elovich with boundary conditions $q_t = q_t$ at t and $q_t = 0$ at t = 0 and assuming $\alpha \beta t >> 1$, leads to the following linear equation:

$$q_t = \beta \ln(\alpha\beta) + \beta \ln(t) \quad (6)$$

Where α is the initial adsorption rate (g/(mg.min)) and β represents the desorption rate (mg/(g.min)) and is related to the number of sites available for adsorption [45], [43], [7].

Although the Elovich kinetic Model was first established for the gas adsorption on solid sorbents, recently it has also been used effectively for describing the adsorption of different materials from aqueous solutions. It describes activated adsorption and assumes an energetically heterogeneous solid surface of sorbent. Which means kinetic of adsorption is not affected by interaction between the adsorbed particles [7], [46]. If this equation applies, the linear plot of q_t vs ln t should have an R^2 value close to 1.

2.2.4.4 Intra Particle Diffusion

The intra particle diffusion can be expressed according to the Weber and Morris equation as follows:

$$q_t = k_i.t^{0.5} \quad (7)$$

In particular occasions, the intra particle diffusion controls the rate of adsorption. This means that the diffusion of the adsorbate ions into the pore of sorbent should also be considered [47]. If this equation applies, the linear plots of q_t vs $t^{0.5}$ should pass through the origin. The k_i is the rate coefficient which can be obtained from the slope of the linear plot [7].

2.2.5 Modeling of the Adsorption Isotherms

Isotherms yield the sorbent capacity for adsorption of specific pollution such as heavy metals at equilibrium. They may also provide information on the surface properties and affinity of the adsorbent to reach its highest capacity. Adsorption isotherms are presented graphically or by an equation ;connect the exact amount of adsorbed metal on the solid

sorbent with the concentration of metal in the solution at equilibrium time and certain temperature[47] .

The International Union of Pure and Applied Chemistry (IUPAC) classify adsorption isotherms into six categories [48]. The most predominantly models are type 1 isotherm also known as Langmuir isotherms. Freundlich and Tempkin models are the other well-known mathematical models that can be used to describe data of adsorption isotherms. In the present work these models were employed to analyze adsorption mechanism of CFA-ZA towards mercury.

2.2.5.1 Langmuir Model

The Langmuir isotherm is a mechanistic model, built based on multiple assumptions. Some of which are: (1) all the active sites on the sorbents have equal energies, (2) there is no interaction between adsorbed molecules, (3) the adsorption is localized and restricted, and (4) it is a heterogeneous catalytic reaction (i.e., the surface reaction is the limiting reaction step) [42]. As a result, this model can define those essential interactions that occur between the metal ions in the solution and the charged surface [47]. The Langmuir equation is given as:

$$q_e = q_m K_L C_e/(1+K_L C_e) \quad (8)$$

And its linear form is as follows:

$$C_e/q_e = 1/(q_m K_L) + C_e/q_m \quad (9)$$

Where q_e is the amount of solute adsorbed per unit weight of adsorbent (mg/g), C_e is the solute (metal) concentration at equilibrium (mg/L), q_m is the monolayer adsorption capacity (mg/g) and K_L is the model constant related to the free energy adsorption. The value of model parameters q_m and K_L can be calculated from the linear plots of C_e/q_e versus C_e [42], [49].

2.2.5.2 Freundlich Model

Freundlich isotherm is an empirical model. This equation is simply a mathematical relationship between the liquid phase and the solid phase equilibrium concentration. It represents the sorption on a heterogeneous surface through a multilayer adsorption mechanism. This equation may be written as follows:

$$q_e = K_F C_e \, 1/n_f \quad (10)$$

The linearized form of the Freundlich equation is

$$\text{Ln } q_e = \ln K_F + (1/n_f) \ln C_e \quad (11)$$

Where q_e is the amount of solute adsorbed per unit weight of adsorbent (mg/g), C_e is the solute (metal) concentration at equilibrium (mg/L), and K_F is the model constant indicative of the relative adsorption capacity of the adsorbent (mg/g (mg/L)n) and $1/n_f$ represents the intensity of the adsorption . By plotting ln q_e vs ln C_e the model parameters can be determined [47], [50], [51].

2.2.5.3 Temkin Model

The following equation describes the linear form of Temkin adsorption isotherm

$$q_e = k_1 \ln K_2 + k_1 \ln C_e \quad (12)$$

where k_1 (l/g) is associated with heat of adsorption and k_2 (dimensionless) is Temkin constant and can be obtained from the linear plot of ln(C_e) vs q_e. This isotherm takes into account the adsorbent–adsorbate interactions and assumes that heat of adsorption (function of temperature) of all molecules in the layer would decrease linearly rather than logarithmic with the surface coverage. This model also characterized by the uniform distribution of the binding energy (up to some maximum binding energy) during adsorption mechanism.

2.3 Results and Discussion

2.3.1 Wastewater Analysis

A wastewater sample from a mine (British Columbia, Canada) provided by Kontec Ecology Systems Inc (Burlington, ON, Canada) was tested using ICP-AES to determine the amount of mercury and other heavy metals as well as other competitive elements such as Na an CA (Table 2-1). The sample then kept in refrigerator according to the standard protocol [52] to minimize evaporation and composition changes. Given the fact that the amount of mercury of this specific waste sample was lower than the allowed level, the sample spiked with some mercury to make a simulated wastewater sample. By using this wastewater as diluent (solvent) to make simulated waste, the effect of the very complex matrix was eliminated. Concentrations of Ag, As, Be, Cd, Co, Hg, Mo, Pb, Sb, Se, Sn and Ti were determined to be lower than 0.01 mg/L. Since the detection limit of ICP-AES for mercury was 0.01 ppm a Tekran 2600 Cold Vapor Fluorescence Spectroscopy (CVAFS) using in vessel purge system (Dual stage gold pre concentration, EPA 1631) and Tek-MDS-2 software package was used to measure mercury concentration. CVAF is one of the most reliable and precise instrumental techniques to measure mercury at very low concentration (i.e. ppt levels and lower). The values for total mercury unfiltered and filtered were determined to be 4.45 and 0.235 ppt (ng/L), respectively.

Table 2-1: Elemental analysis of the mine in BC Mine wastewater measured using ICP-AES technique

Trace Metals	**Ag, As, Be, Cd, Co, Hg, Mo, Pb, Sb, Se, Sn,**	**Zn, V, Ti, P, Cr, Cu, Ba**	**Al, Mn**	**Ni**	**P**	**Sr**	**Fe**	**B**	**Si**	**Ca**	**Mg**	**K**	**Na**

	Ti,												
Conc. (mg/L)	< 0.01	**0.02**	**0.03**	**0.06**	**0.25**	**0.7**	**0.55**	**3.4**	**12.17**	**43.65**	**107.96**	**222.45**	**610.43**

2.3.2 Physical and chemical Characteristics of the Raw and Zeolitized CFA

2.3.2.1 XRD Diffraction Patterns

The XRD analysis of the CFA used for zeolite preparation and the CFA-ZA itself are shown in Figure 2-1A. The standard peaks were obtained from the literature [39]. Quartz (SiO_2) and Mullite ($Al_6Si_2O_{13}$) were identified as the main crystalline constituents of the raw CFA. Also the XRD pattern of zeolitized CFA illustrates the single phase and high crystalline zeolite A. The main characteristic peaks of CFA-ZA appear at 2θ ranging from 5 ° to 24° and can be assigned to (110) face of the cubic structure of zeolite A [25]. The XRD pattern of AC is illustrated in Figure 2-1B. The broad C (002) diffraction peak (2 θ = 15 - 30º) can be attributed to the amorphous carbon structure. The weak and broad

C (101) diffraction peak (2θ = 40 -50º) is due to the axis of the graphite structure diffraction peak (2θ = 40 - 50º) [48] (Figure 2-1B).

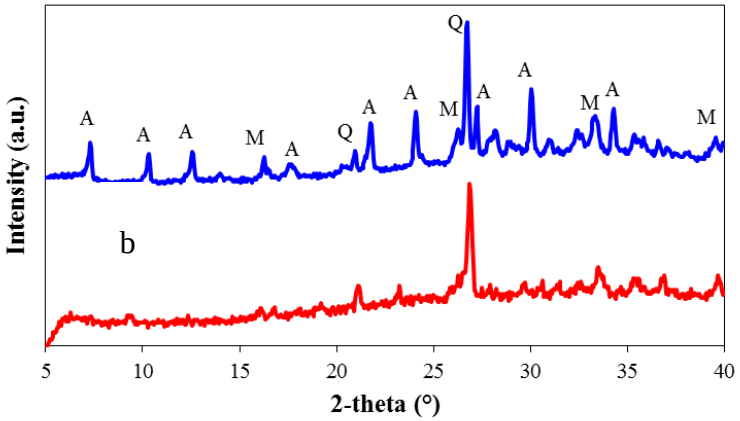

Figure 2-1 A: XRD of precursor Coal Fly Ash (b) and synthesized Zeolite LTA (a).

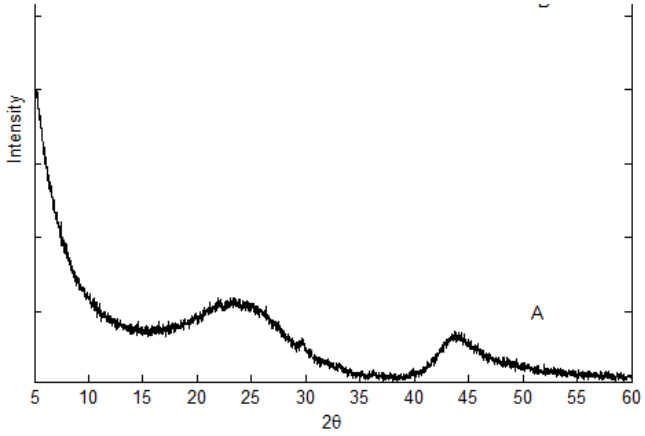

Figure 2-1 B: XRD Pattern of AC sample used in this study

2.3.2.2 XRF Results

The quantitative chemical analysis by XRF show 33.96 % SiO_2, 16.49% Al_2O_3, and a SiO_2/Al_2O_3 ratio of 2.06 for raw CFA, which makes it a good precursor to synthesize low silica LTA type zeolite.

2.3.2.3 SEM Results

Morphological analysis of raw CFA and CFA-ZA performed by SEM is shown in Figure 2-2. The CFA consists of smooth spheres (0.04 - 50 µm, with a mean diameter of 10.02 µm). The cooling of molten products after the combustion of clay compounds in the original coal forms these particles [31]. It can be seen in Figure 2-2 (b) that the produced CFA-ZA is formed as cubes on the surface of CFA particles [21], [53]. The particle size of synthesized zeolite A was in the range of 0.5 - 2 µm with an average diameter of 1.7 µm.

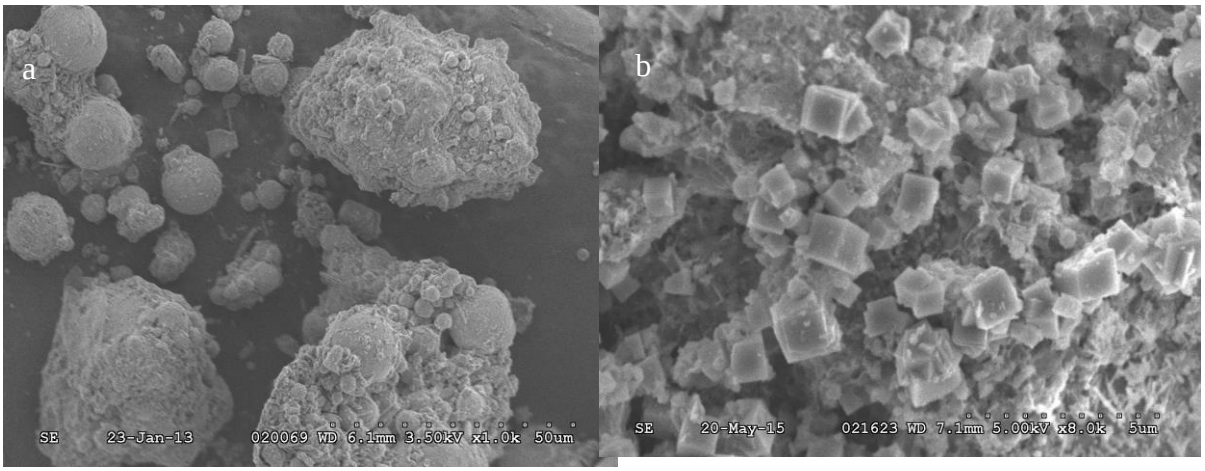

Figure 2-2: SEM micrographs of: (a) CFA and (b) synthesized CFA-ZA.

Table 2-2: Chemical analysis of the CFA sample measured using XRF technique.

Major Oxides	CFA Weight percentage (%)
SiO_2	33.96
TiO_2	1.16
Al_2O_3	16.49
Fe_2O_3	4.65

MnO	0.02
MgO	2.72
CaO	11.28
K_2O	0.87
Na_2O	0.84
P_2O_5	0.59
Cr_2O_3	0.04
BaO	0.31
SrO	0.19
L.O.I.	26.05
Total	99.17
SiO_2/Al_2O_3	2.06

2.3.2.4 BET Results

In a previous paper [54] the result obtained for the BET surface area of CFA-ZA synthesized from raw CFA by microwave irradiation were established and reported. The BET surface area of CFA-ZA was 63.71m^2/g which shows a dramatic improvement over the BET surface area of 15.47 m^2/g for raw CFA.

2.3.2.5 CEC Results

The cation exchange capacity (CEC) of synthesized CFA-ZA was found to be 2.43 meq/g. This was a remarkable improvement over the CEC of raw CFA which was 0.3 meq/g [21]. The CEC values are comparable to the zeolite synthesized with pure

chemical precursors (3.13 meq/g)[54], which indicates that the CFA-ZA has a great potential to be used as an adsorbent in different environmental remediation processes.

2.3.2.6 Leaching Test

As mentioned in the introduction, CFA contains some toxic compounds and elements, apart from mercury, that could potentially be transferred to the surrounding liquid phase. Zeolitization of CFA reduces the probability of leaching these toxic heavy metals and elements to the solution in an adsorption system [25]. As a result, developing a leaching test is necessary for using CFA-ZA as an adsorbent. The toxic properties of CFA and CFA-ZA samples were examined using a standard leaching test [41].The results of elemental analysis showed that the zeolitization of CFA was successfully immobilize different toxic elements including heavy metals such as As and Cr in CFA-ZA framework (Table 2-3).

Table 2-3: ICP results from leach test of the CFA [38] and zeolite produced from microwave radiation method.

Element	CFA (mg/L)	CFA-ZA (mg/L)
Al	1.450	5.01
As	0.03390	< 0.01
B	4.317	0.04
Ba	1.965	0.21
Ca	448.96	60.96
Cu	0.06876	< 0.01
Cr	0.1505	< 0.01

Fe	0.3936	0.05753
Mn	0.01544	< 0.01
Ni	0.05112	< 0.01
Pb	0.2700	< 0.01
V	0.02411	0.0125

2.3.2.7 TGA

Thermo-gravimetric analysis (TGA) curve of the CFA and its zeolitized counterpart are illustrated in Figure 2-3. The samples were subjected to TGA test without special pre-treatment. The CFA showed a weight loss of 6.1 %, in which most of the weight loss occurs at 105 ºC. This gentle slope weight variations and the trend of heat flow changes are a particular behavior of CFA and attributed to the reversible adsorption of atmospheric moisture on external surface and macro pore of CFA. TGA curve for CFA-ZA had 15 % weight loss while a point of inflection at approximately 170 ºC. This weight loss indicates that the water content in this sample is higher than CFA sample confirming the obtained BET micro pore surface area. It could be attributed to evaporation of adsorbed water molecules on the porous structure of the synthesized zeolite.

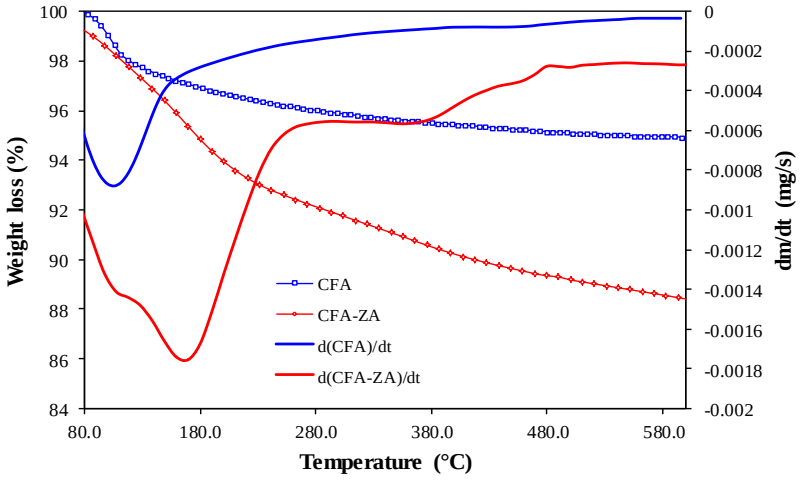

Figure 2-3: Thermo-gravimetric analysis of raw CFA and CFA-ZA (heating rate 10ºC/min, under N_2 atmosphere).

2.3.3 Optimization of Adsorption Parameters

There are various physiochemical parameters influencing the sorbent's adsorption capacity, adsorption mechanism and system's kinetics during the heavy metal uptake from the solution. These factors include the initial metal concentration in solution, competitive cations and liquid medium, ionic strength, solution pH, sorbent type and its grain size, mineral pretreatment, temperature and agitation speed [47]. In this study the effect of contact time, the initial concentration of adsorbent and initial pH of solution was investigated towards mercury adsorption onto CFA-ZA.

2.3.3.1 Effect of Contact Time on Adsorption

Optimizing the contact time is necessary in order to determine adsorption equilibrium during the isotherm assay. Fifty g/L dose of CFA-ZA and AC were applied to 10 mg/L mercury solution for 1 to 24 hours. Based on this study it was determined that all adsorbents reached to equilibrium approximately after 3 hours.

In the case of CFA-ZA adsorbent with 50 g/L and 100 g/L concentration, the initial adsorption rate was so rapid and over 86% and 88% mercury were removed just after 5

minutes of contact. For 50 g/L sample, the adsorption rate was slower, reaching equilibrium at 120 minute. With a CFA-ZA concentration of 100 g/L, the equilibrium was reached just after 30 minutes. For CFA-ZA with 10 g/L concentration over 53% of Hg (II) were removed during the first 5 minute of contact. The removal efficiency then gradually increased to reach the highest value after 120 minute (Figure 2-4).

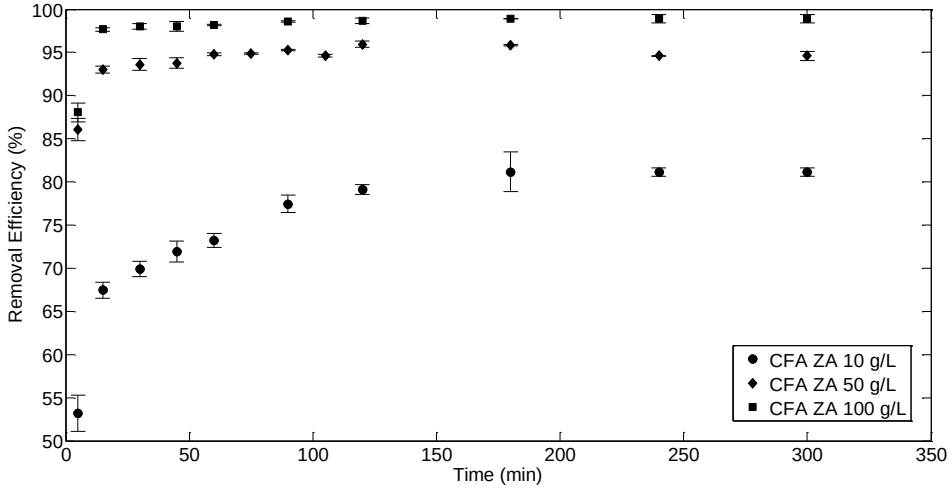

Figure 2-4: Removal efficiency of CFA-ZA towards Hg(II) as a function of time (experimental conditions: Hg(II) 10 mg/L, Adsorbent 10 g/L, 50 g/L and 100 g/L, pH≈2.5 at room temperature).

The amount of Hg (II) adsorbed onto activated carbon (50 g/L) reached to its highest value of over 98% just after 5 min of contact, however beyond this time the removal efficiency slightly decreased until reaching to an equilibrium value of 94% after 120 minutes. It is noticeable from Figure 2-7 that the final equilibrium efficiency of CFA-ZA and AC with the same concentration (50 g/L) is similar indicating the comparable adsorption performance of zeolitized CFA with AC (Figure 2-5).

The changes in adsorption capacity of examined adsorbents as a function of time are illustrated in Figure 2-6. As it was expected the adsorption capacity of CFA-ZA with 10 g/L concentration gradually increases as time progresses; however this rise in adsorption capacity is much smaller for adsorbents at higher concentrations. This may be due to the presence of larger amounts of adsorbents in the liquid medium resulting in more particle

agglomerate and less adsorption capacity [48]. These results confirmed the experimental data from other studies [7], [51], [55]–[57].

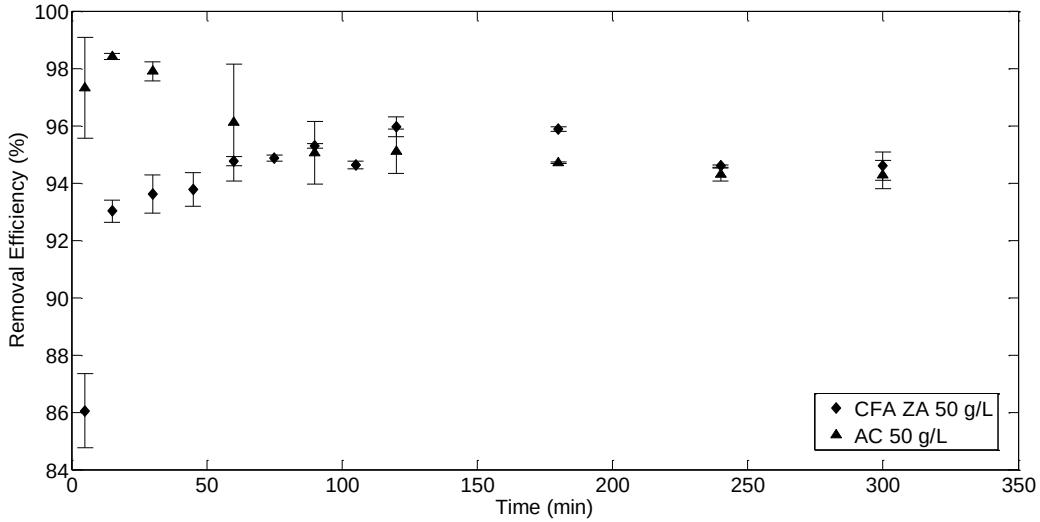

Figure 2-5: Removal efficiency of CFA-ZA and AC towards Hg (II) as a function of time (experimental conditions: Hg(II) 10 mg/L, Adsorbent 50 g/L, pH≈2.5 at room temperature).

The adsorption capacity and the removal efficiency of AC slightly decreased with time (Figures 5 and 6). Essentially in an aqueous solution always there is a competitive adsorption between metal ions and H_2O for the available adsorption sites on the adsorbents surface [58]. Since equilibrium with water proceeds slower, as the system approached to equilibrium a decrease in adsorption capacity was observed.

The solution pH varying as a function of time was investigated for CFA-ZA adsorbents (Figure 2-7). Before CFA-ZAs addition, the aqueous solution pH averaged 2.5 with the percentage change in the pH of over 90 % in the first 5 min of contact. The pH values of CFA-ZA (10 g/L), CFA-ZA (50 g/L), CFA-ZA (100 g/L) were 9.44, 10.59 and11.07, respectively, just after 5 min of first contact. However, for the same adsorbents beyond 120 min, the solutions pH stabilized to an average of 10, 11 and 11.70, respectively.

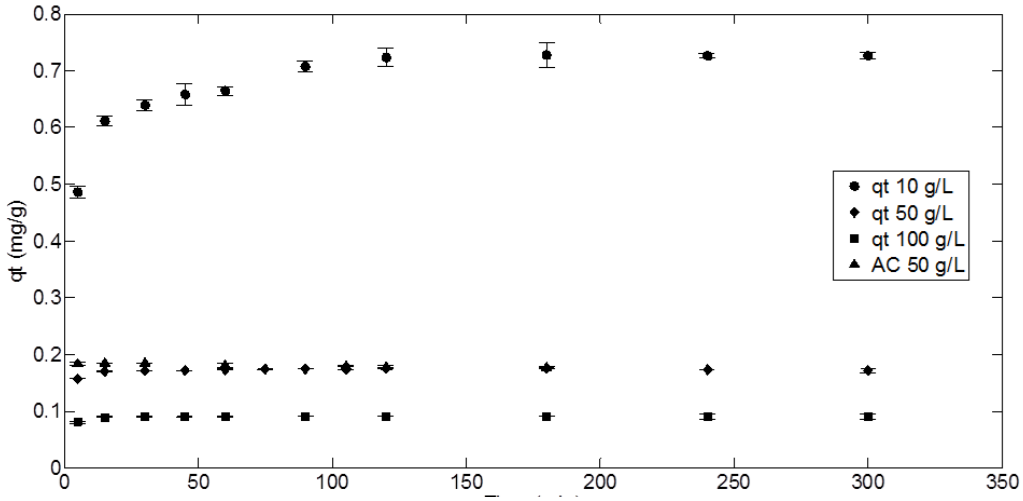

Figure 2-6: Adsorption capacity of CFA-ZA and AC towards Hg(II) as a function of time (experimental conditions: Hg(II) 10 mg/L, Adsorbent 10 g/L ,50 g/L and 100 g/L for CFA-ZA and 50 g/L for AC, pH≈2.5 at room temperature).

For activated carbon the solution pH reached to 7.98 in 60 min after first contact. Beyond this time the pH stabilized to an average of 7.5.

2.3.3.2 Effects of Adsorbent Dose

The grain size (specific surface area) of adsorbent and mainly its mass determine the accessibility and availability of active sites on the surface of the adsorbent. Obviously when the adsorbent to metal solution ratio (solid to liquid ratio) increases, more active sites are available for adsorption in the same solution volume. It is expected that an increase in adsorbent mass at a constant pH and adsorbate concentration, increases the removal efficiency [7], [59]. However in such cases the amount of metal adsorbed per unit of the adsorbent mass decreases.

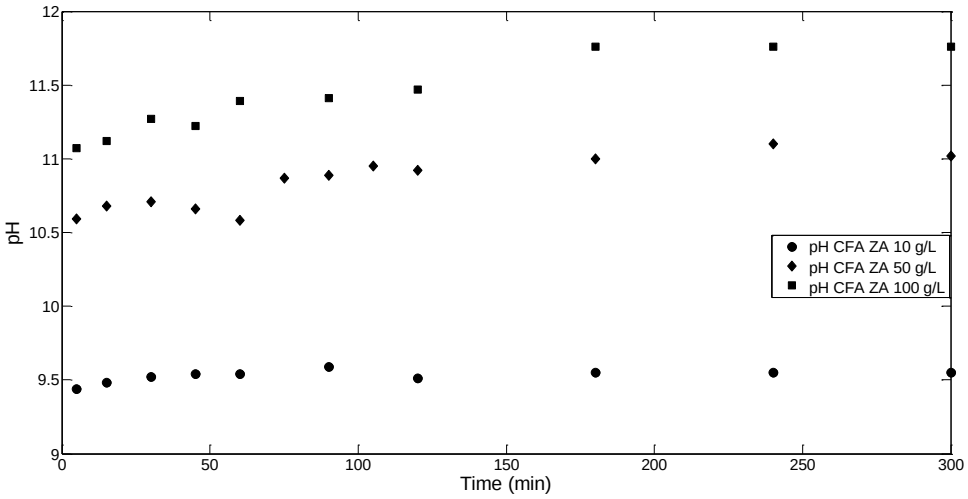

Figure 2-7: Chang in pH of Hg(II) solution as a function of time (experimental conditions: Hg(II) 10 mg/L, Adsorbent 10 g/L ,50 g/L and 100 g/L for CFA-ZA, initial pH≈2.5 at room temperature).

In the present study the effect of the dose of CFA-ZA on Hg (II) adsorption was investigated by varying the adsorbent dose from 1 g/L to 100 g/L on a 10 g/L initial concentration of mercury at room temperature and constant pH. To compare the effect of adsorbent dose on removal efficiency of synthesized CFA-ZA, the parent CFA, and AC experiments were conducted at 5,10,50,80 and 100 g/L mass of mentioned adsorbents.

It can be seen from Figure 2-8 that removal efficiency improved by increasing the adsorbent mass for all examined adsorbents. For CFA-ZA the removal efficiency gradually increased from 65% for 0.01g to the maximum value of 98 % for 0.8 g dose of adsorbent (equal to 1 g/L and 80 g/L, respectively) and flattened thereafter. Considering averaged initial pH value of 2.5 for mercury solution, it was observed that the final pH of solution increased by adding only 0.01 g of CFA-ZA (Figure 2-9). Although increasing the adsorbent mass from 0.25 to 1 g has a small effect on the final pH of solution.

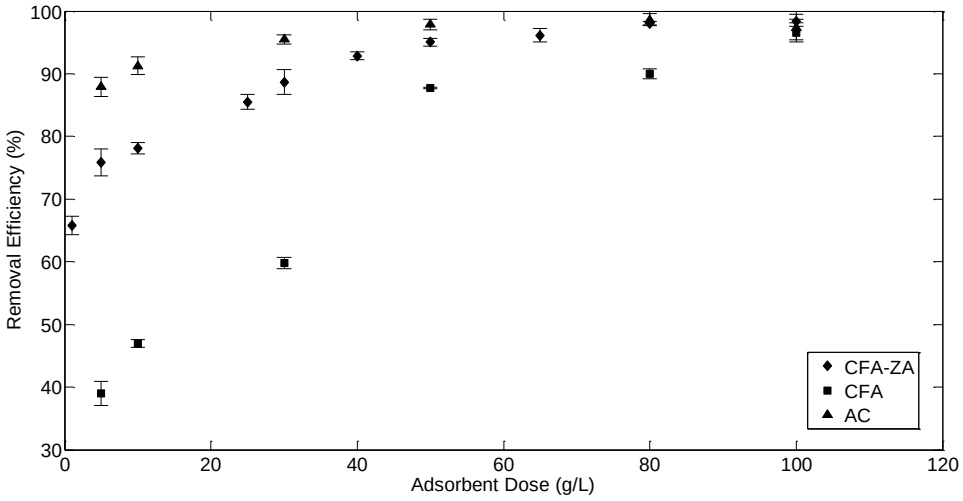

Figure 2-8: Removal efficiency as a function of adsorbent dose (experimental conditions: Hg(II) 10 mg/L, Adsorbent CFA-ZA, raw CFA and AC, initial pH≈2.5 at room temperature).

Increasing the dose of AC from 5 g/L (with 87% removal) to 80 g/L also led to a maximum mercury removal of 98% (see Figure 2-8). Adding 0.05 g of AC had a small effect on the final solution pH increasing it from 2.5 to a value of 3.3. However with larger dose of AC the final pH of solution reached to an average of 7.5.

While similar adsorption trends were observed for AC and CFA-ZA, the effect of adsorbent mass on removal efficiency was more significant for raw CFA (see Figure 2-8). Percentage mercury removal increased from 39% to nearly 96 % when the adsorbent dose increased from 0.05 g to 1 g for raw CFA. However the pH values of the final solution didn't change considerably with increased mass of adsorbent.

Figure 2-10 illustrates the changes in removal efficiency of CFA-ZA as a function of adsorbent mass compared to the mercury adsorption capacity. While the removal efficiency of CFA-ZA increases by increasing adsorbent load, mercury adsorption capacity is shown to have a steady decrease. As it will be discussed later in section 3.3.2, the decrease in adsorption capacity is related to the unavailability of mercury ions in liquid phase per adsorbent site which leads to a decrease in the available active sites on the surface of adsorbent [11], [47].

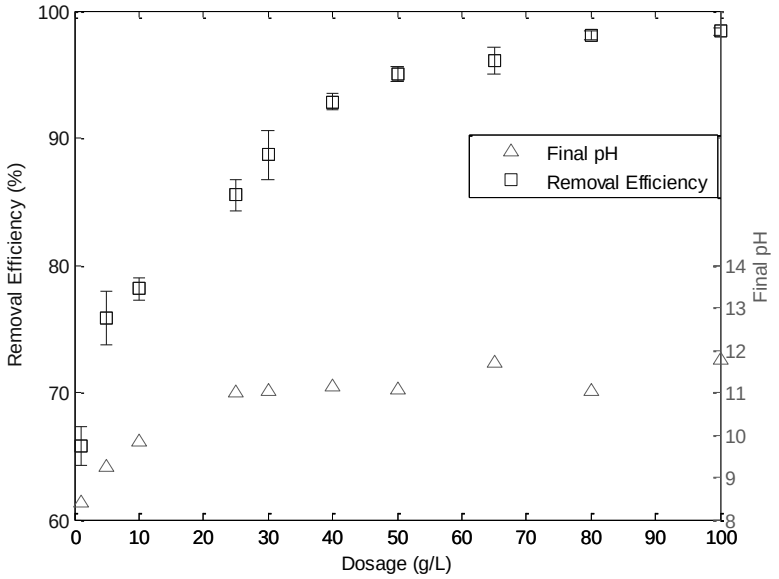

Figure 2-9: Removal efficiency as a function of adsorbent dose and final pH of mercury solution (experimental conditions: Hg(II) 10 mg/L, Adsorbent CFA-ZA, initial pH≈2.5 at room temperature).

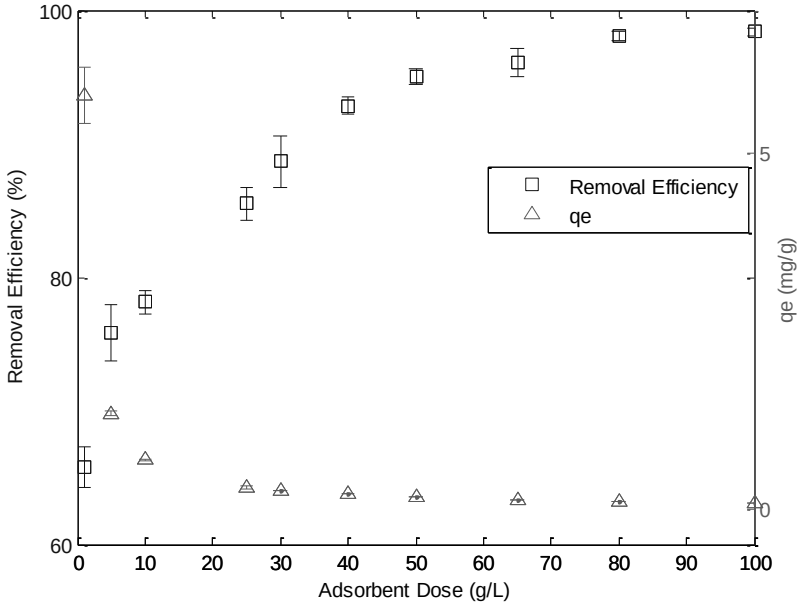

Figure 2-10: Removal efficiency and adsorption capacity as a function of adsorbent dose (experimental conditions: Hg(II) 10 mg/L, Adsorbent CFA-ZA, initial pH≈2.5 at room temperature).

Generally an increase in the sorbent concentration increases the available surface area and number of binding sites for the same solution volume. However an increase in the adsorbent aggregation decreases the available active sites. These interactions affect the adsorption capacity in two ways: first by creating an electrostatic interference such as electrical surface charges on the agglomerated particles that diminish attraction between mercury ions and adsorbent surface. Second, by causing desorption of mercury ions from the surface of adsorbent. Moreover in low sorbent concentration the mercury ions have the chance to enter into inner parts of adsorbent particles. This results in a decrease in the diffusion path length of the adsorbent [7], [11], [31], [47], [56]. Several studies have reported the same impact of concentration on adsorption capacity and heavy metal removal efficiency of various heavy metals [7], [9], [59]–[61].

2.3.3.3 Effect of pH on Adsorption

It has been well recognized that adsorption of heavy metals is a highly pH dependent process. To study the influence of initial pH of the solution on adsorption mechanism, 0.5 g of CFA-ZA was dispersed into 10 ml solutions containing 10 mg/L of mercury. The pH value of 10 ppm mercury solution was about 2.5± 0.25. The initial pH values were adjusted to 4, 6, 7, 8.5 and 10 using NaOH solutions with 1 M and 10 % concentration. It can be seen from Figure 2-11 that when the initial pH increases from 4 to 7 of mercury adsorption by CFA-ZA increases slightly. However, the changes in both removal efficiency and adsorption capacity of CFA-ZA are not significant with different initial contact pH.

Totally, at various pH different mercury speciation exhibit in the solution which are dissimilar in their charges and ability to adsorb on the sorbent. In this study the mercury speciation in various conditions was determined by the speciation program Visual MINTEQ 3.1. Accordingly the mercury speciation in the main matrix condition used for all batch experiments (Mercury solution with 10 mg/L concentration and averaged initial pH of 2.5) was predicted to be 85.68% Hg^{2+}, 9.44% $HgOH^{+}$ and 4.87% $Hg(OH)_2$.While other species of H^{+}, Hg_2OH^{3+}, $Hg_3(OH)_3^{3+}$ and OH^{-} are presented in very low concentration. For systems with a pH value of 5 $Hg(OH)_2$ is the primarily species (i.e.

>99%). Therefore when the system reaches the maximum solubility, most likely this species is removed from the aqueous solution by preferential precipitation on the surface of the adsorbent, which can be considered as the dominant mechanism for mercury adsorption. However the precipitated mercury species on the surface of the adsorbent could be later adsorbed by means of other physicochemical mechanism [11], [13], [62], [63].

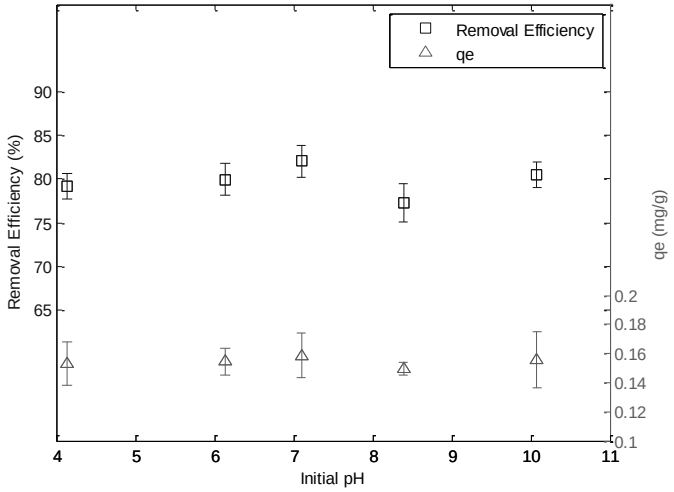

Figure 2-11: Removal efficiency and adsorption capacity as a function of initial pH of Hg(II) solution (experimental conditions: Hg(II) 10 mg/L, Adsorbent CFA-ZA 0.5 g, pH varies at ≈ 4, 6, 7, 8.5 and 10at room temperature).

On other hand, in an acidic environment the performance of most adsorbents reduces due to the presence of protons that competes with mercury ions for the available adsorption sites [11]. However, as it is indicated in Figures 7, 9 and 12 upon addition of only 0.5 g of CFA-ZA the pH value of the solution reached at an equilibrium value of 11.43. These results are mainly notable when compared with AC. [48] reported that as pH increases from pH 2 to pH 10 , mercury adsorption on AC decreases. It can be concluded that the initial pH of the mercury solution does not have a significant influence on the adsorption performance of CFA-ZA since the pH would be raised to more than 7 a couple of minutes after first contact.

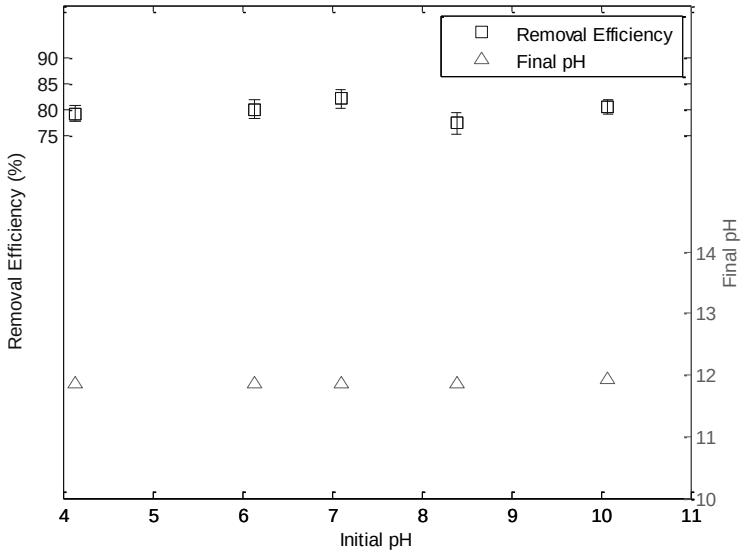

Figure 2-12: Removal efficiency as a function of initial pH and equilibrium pH of Hg(II) solution (experimental conditions: Hg(II) 10 mg/L, Adsorbent CFA-ZA 0.5 g, pH varies at ≈ 4, 6, 7, 8.5 and 10at room temperature).

2.3.4 Adsorption Kinetic Studies

Mechanism of adsorption is largely affected by adsorbate and adsorbent characteristics and their interaction through the contact time. The kinetic study is principally important because it controls the process efficiency [47]. Different kinetic models have been proposed for Hg(II) adsorption on various adsorbents, a pseudo-first-order and a pseudo-second-order for activated carbon [11], [48], a pseudo-second-order for multi walled carbon nanotubes [63], a pseudo-first-order for impregnated fly ash [7], and a pseudo-first-order for natural clinoptilolite [65]. However to the best of our knowledge there is no study on the kinetic parameters of zeolite LTA synthesized from CFA for Hg(II) adsorption. In the present work three kinetic models and one diffusion model were investigated for Hg (II) adsorption by CFA-ZA for three different adsorbent doses. The applicability of all these models was assessed by comparing the R^2 values of their linear plots. The adsorption parameters derived from the application of pseudo-first order, pseudo-second-order and Elovich models along with R^2 (the corresponding regression coefficient) are presented in Table 2-4.

Table 2-4: Calculated kinetic model constants for the adsorption of Hg(II) on CFA-ZA at different adsorbent concentration (Experimental condition: Hg(II) 10 mg/L, Adsorbent CFA-ZA 10g/ L, 50 g/L and 100 g/L, pH at ≈ 2.5 at room temperature).

Adsorbent Dose g/L	**Pseudo-first-order**			**Pseudo-second-order**				**Elovich**		
	K (min^{-1})	q_e	R^2	K_2 (g/mg*min)	R^2	q_e (mg/g) Experimental	q_e (mg/g) Calculated	A (g/mg*min)	B=1/b (g/mg)	R^2
10	0.0343	0.2816	0.936	54	0.9994	0.726	0.7431	60.70	16.447	0.9374
50	0.0276	0.00814	0.7049	56.37	0.99999	0.1740	0.1742	NC	NC	0.7413
100	0.0229	0.00322	0.6832	59.32	1	0.0905	0.090	NC	NC	0.6024

NC: Not Calculated because of very low R^2 value

Lagergren model is a pseudo-first-order model which is widely used. It involves plotting $\ln(q_e-q_t)$ vs t [42], [64]. In Table 2-4, $\ln(q_e-q_t)$ calculated from the kinetic data of Figure 2-6. The data are plotted vs time (Appendix A, Figure S1). Based on data given in Table 2-4, R^2 values are very low for higher concentration of adsorbents indicating poor relationships between the parameters. For the sample with 10 g/L concentration the R^2 is high with a value of 0.936 showing it can be closely matched the experimental results. Pseudo-first-order rate constants for these samples were calculated from the slope of the plot.

These results confirm the general assumption of pseudo-first order kinetic model considering initial concentration of the species involved in the adsorption process (both adsorbate and adsorbent) as essential factors influencing the K constant value and the rate of adsorption process[7].

For the evaluation of the pseudo-second-order equation, t/q_t values were plotted against time (min) based on Eq. (4). Kinetic constant q_e and K were calculated from the slope and intercept of this plot (Figure 2-13). There is a strong linear relationship between experimental data and the pseudo-second order model as it illustrated in Figure 2-13.

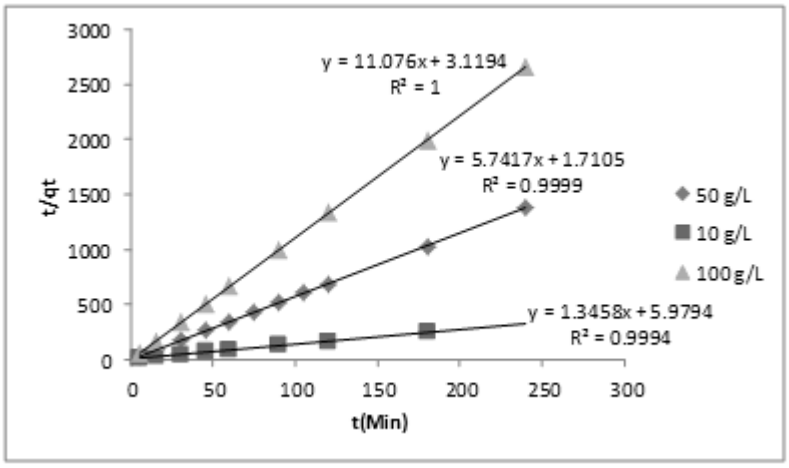

Figure 2-13: Application of the pseudo-second-order model (Eq.(4)) to the experimental data of Figure 8 (experimental conditions: Hg(II) 10 mg/L, Adsorbent CFA-ZA 10g/ L, 50 g/L and 100 g/L, pH ≈ 2.5 at room temperature).

Table 2-4 presents the calculated constants for this model. It is obvious that the data strongly fit the pseudo-second order model with an R^2 value of 1, 0.9999 and 0.9437 for 100g/L, 50 g/L and 10 g/L dose of adsorbent, respectively. As well as the high coefficient of determination value for all adsorbent concentration, the calculated adsorption capacity values obtained from the kinetic model give reasonably very close values compared with experimental adsorption capacity. These observations imply that the Hg (II) sorption on CFA-ZA with different concentration follow the pseudo-second-order sorption rate more closely compared to the pseudo-first-order.

It is well known that a larger adsorption constant K_2, leads to a shorter adsorption time [44], [65], [66].Various studies indicate that the value of K_2 as a time-scaling factor

usually decreases with increasing the initial adsorbate concentration or decreasing adsorbent concentration. So, the higher the initial concentration of adsorbate or the lower the initial concentration of adsorbent, the longer time is required to reach to equilibrium [7], [47], [64], [67].

Also it is strongly suggested that the adsorption is due to chemisorption as assumed with this model, considering the valence forces through sharing or exchange of electrons between active binding sites of sorbent surface and metal ions[43], [68].

As mentioned in section 2.4.3, although Elovich equation has been used to define the adsorption in gas-solid systems, in recent years it has also been applied for modeling liquid medium systems for the adsorption of Cr(VI), Cd(II) and Cu(II) [7], [42] . To examine this model on our experimental data, the plot of q_t vs ln t was developed for 3 different concentrations of adsorbent (Appendix A Figure, S2). Based on regression coefficients, the Elovich model was also successful in describing the kinetics of adsorption by CFA-ZA with the lower concentration of 10 g/L. However, these values were lower for high concentration adsorbents indicating poor fitting of adsorption parameters at 50 and 100 g/L adsorbent concentration.

For CFA-ZA with 10 g/L concentration the data showed stronger fit with the pseudo-second-order kinetic model, with an R^2 value of 0. 9437. However still the other two examined models provided relatively good R^2 values, 0.936 and 0.937, respectively.

2.3.5 Adsorption Rate-controlling Mechanism

To interpret more specifically the experimental data, it is necessary to apply a diffusion model in addition to the well-known kinetic models. Generally there are 3 main steps in the adsorption of a metal species by a porous adsorbent:

(1) The adsorbate transport to the external surface of the adsorbent (film-diffusion);

(2) The adsorbate transport within the pores of the adsorbent (although a small amount of adsorption occurs on the external surface which is called particle diffusion)

(3) The adsorbate is adsorbed on the external surface of the adsorbent

Obviously the slowest of these transport steps would determine the overall rate of adsorption [47], [42], [7], [53] .The intra particle diffusion model is based on the theory proposed by Weber and Moris and is represented by:

$$q_t = k_d\, t^{1/2} + \theta \qquad (13)$$

where K_d (mg/g.min$^{1/2}$) is the intra particle diffusion rate constant and θ (mg/g) is a constant related to the thickness of boundary layer [42], [59], [69]. Applying this model, one can determine the rate-controlling mechanism of the adsorption processes.

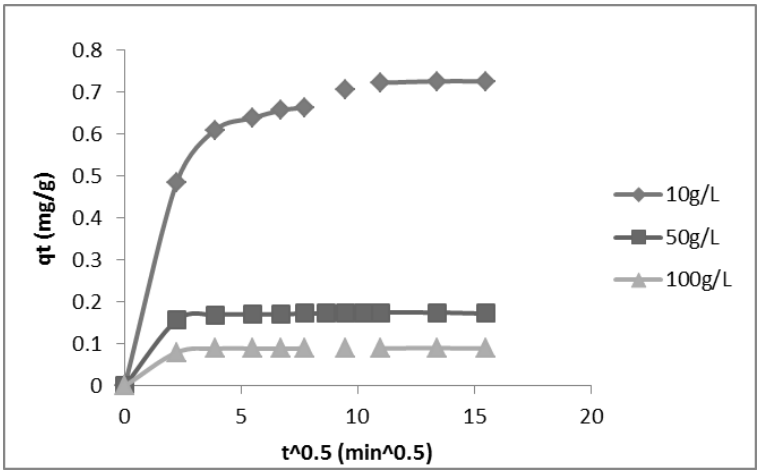

Figure 2-14: Test of the intra particle diffusion model (Eq.(4)) to the experimental data of Figure 6. (Experimental conditions: Hg(II) 10 mg/L, Adsorbent CFA-ZA 100 g/L , pH ≈ 2.5 at room temperature).

Intra particle diffusion parameters were obtained by plotting q_t vs $t^{0.5}$. If the plot from experimental data gives a straight line then the sorption process is only controlled by intra-particle diffusion. In our case, the plot of q_t vs $t^{0.5}$ is not linear for CFA-ZA with various concentration therefore intra particle diffusion is not the sole rate-limiting step. As it is illustrated in Figure 2-14, multiple rate-limiting steps might take place in this system hence multi linear plots were observed for the adsorbents with 10, 50 and 100 g/L concentration indicating two different diffusion steps and two distinct controlling stages in the sorption process (Figures 14).

Initially, of the rate of metal removal from the solution is higher. This higher rate corresponds to the external surface adsorption or boundary layer effect [59], [70]. In the second portion which may be called the intra particle diffusion or pore diffusion step, the adsorption gradually increases since equilibrium had almost been reached. The slope of the second linear part of this plot was used to determine the rate parameter of pore diffusion stage which is the rate limiting step of the process. The calculated parameters for intra particle diffusion are presented in Table 2-5. All these results suggest that the sample with lower concentration of 10 g/L demonstrated immediate uptake of Hg(II) at a much higher capacity than the CFA-ZA samples with higher concentration. For various concentrations of CFA-ZA, the adsorption process is controlled by external mass transfer followed by intra-particle diffusion mass transfer.

Table 2-5: Calculated intra particle diffusion constants for the adsorption of Hg(II) on CFA-ZA at different adsorbent concentration (Experimental condition: Hg(II) 10 mg/L, Adsorbent CFA-ZA 10 g/L, 50 g/L and 100 g/L, pH at ≈ 2.5 at room temperature).

Adsorbent Dose g/L	**K_i (mg/g.min$^{1/2}$)**	**θ**	**R^2**
CFA-ZA-10	0.0238	0.4834	0.8622
CFA-ZA-50	0.008	0.1668	0.9719
CFA-ZA-100	0.0001	0.0889	0.9626

2.3.6 Adsorption Isotherms

Isotherm analysis is beneficial in estimating the capacity of the adsorbents for adsorption of specific chemicals and may be performed in two ways, introducing a constant and specific amount of adsorbent to a series of solution with various initial concentrations of Hg(II), or applying varying weights of dried adsorbent to a constant volume of Hg(II) solution [58]. It is also necessary to identify beforehand the equilibrium contact time. For the present study the latter method was applied. 0.25 to 1 g of CFA-ZA were introduced

to 10 ml Hg (II) solution with 10 ppm initial concentration. Figure 2-15 illustrates the non-linear relationship of Hg (II) concentration in the solution with metal concentration at room temperature. Results were analyzed using Langmuir, Freundlich and Temkin models. The fitted parameters are listed in Table 2-6.

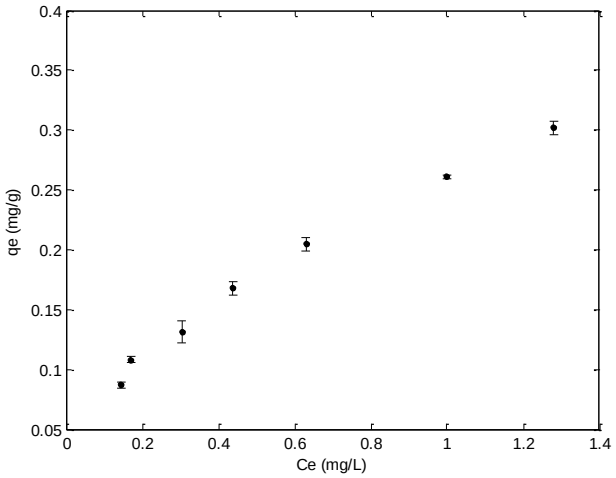

Figure 2-15: Nonlinearized relationship between C_e and q_e for adsorption of Hg (II) onto CFA-ZA(experimental conditions: Hg(II) 10 mg/L, Adsorbent CFA-ZA dose in the range of 0.1, 0.2, 0.3 ,0.5 0.65,0.8,1 g , pH ≈ 2.5 at room temperature).

Table 2-6: Calculated Langmuir, Freundlich and Temkin parameters for the adsorption of Hg(II) on CFA-ZA at a range of different adsorbent dose from 0.1 g to 1 g (Experimental condition: Hg(II) 10 mg/L, equilibrium time 24 h, pH at ≈ 2.5 at room temperature).

CFA-ZA	Freundlich				Langmuir				Tempkin		
Dose g/L											
10,25,30 40,50,65 80,100	K_f(mg/g)(mg/L)^n	$1/n_f$	n_f	R^2	q_m(mg/g)	K_L(l/mg)	R_L	R^2	K_1(L/g)	K_2	R^2
	0.2622	0.5448	1.8355	0.9913	0.4416	1.5122	0.0697	0.9627	0.0938	15.974	0.9664

Based on data analysis, both Freundlich and Langmuir isotherms can describe adequately the adsorption isotherm of Hg (II) onto CFA-ZA. However the best fitting results

belonged to Freundlich model with R^2 value of 0.9913. This good fitting of the experimental data to Freundlich model (plotting ln C_e vs ln q_e) implied that physisorption mechanism was occurring in the adsorption system [42], [48].

The Langmuir model represents monolayer adsorption on specific homogenous sites. While the main assumption for Freundlich model is physical adsorption on heterogeneous surfaces with a heterogeneous energy distribution. It also describes reversible adsorption which is not restricted to the formation of monolayer [42]. Consequently the assumption of multilayer adsorption is well fitted with the obtained experimental data in the studied temperature and adsorbent concentration**.**

The value of 1/n parameter obtained from applying Freundlich linearized equation to the experimental results (Figure 2-16) is 0.5448 which is between 0 and 1, indicating the heterogeneity of the CFA-ZA surface and the affinity of Hg(II) ions for it, which also indicate that the adsorption of Hg (II) by CFA-ZA is favorable [47].

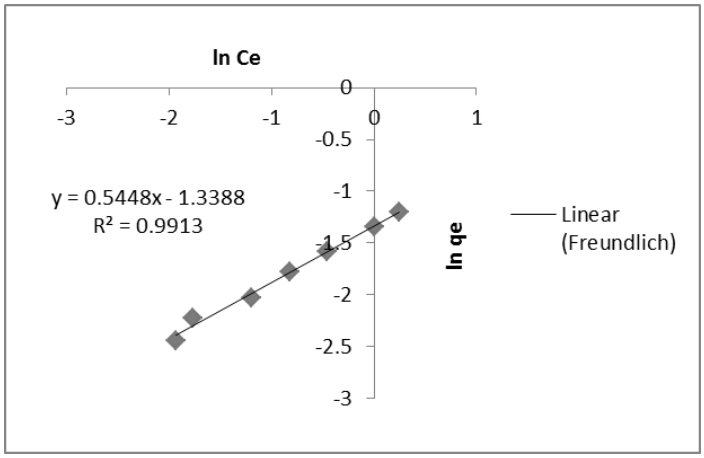

Figure 2-16: Freundlich isotherm for adsorption of Hg (II) onto CFA-ZA (experimental conditions: Hg(II) 10 mg/L, Adsorbent CFA-ZA dose in the range of 0.1, 0.2, 0.3 ,0.5 0.65,0.8,1 g , pH ≈ 2.5 at room temperature).

As mentioned before Langmuir model describes adsorption on a strongly homogeneous surface (obviously does not occur for a synthesized zeolite from coal fly ash with a complex matrix) [71]). Parameters of Langmuir model were obtained by plotting C_e/q_e vs C_e (Appendix A, Figure S3). As it can be seen from Table 2-6, a smaller R^2 value for Langmuir linear plot compared with Freundlich (0.9627 vs 0.9913) was obtained indicating that chemisorption is not the sole mechanism in the adsorption system. However, from the results of kinetic studies one can conclude that both physisorption and chemisorption should be considered in the adsorption mechanism of mercury on CFA-ZA with stronger role belonging to physisorption.

The R_L is a dimensionless equilibrium constant is given as:

$$R_L=1/ (1+bC_0) \quad (14)$$

Where C_0 is the initial concentration and b is the Langmuir constant. R_L between 0 and 1 indicates favorable adsorption while $R_L>1$ indicates unfavorable adsorption, $R_L=1$ is linear and Irreversible adsorption is suggested for $R_L = 0$ [48]. As it can be seen from Table 2-6 the calculated R_L value is 0.0697 which suggests favorable adsorption mechanism.

Equation (12) describes Temkin adsorption isotherm. The Temkin constant can be obtained from the linear plot of $\ln(C_e)$ vs q_e (Appendix A, Figure S4). Values of Temkin constants and the corresponding regression coefficient are presented in Table 2-6. Generally the Temkin isothermal model is based on the assumption that the adsorption is characterized by a uniform distribution of the binding energies; up to some maximum binding energy [62] It also assumes that the interaction between adsorbate and adsorbent has strong influence on adsorption heat [42]. The regression coefficient obtained from plotting experimental results ($\ln(C_e)$ vs q_e) (Appendix A Figure, S4) has a value of 0.9664, indicating that Temkin model is able to describe the adsorption of mercury onto CFA-ZA to some extent.

2.4 Conclusion

Zeolite LTA synthesized from coal fly ash was successfully applied for mercury adsorption from an aquatic solution. Applying a leaching test on the obtained zeolite showed its capability to immobilize toxic heavy metals by trapping them in its matrix. From the batch experimental results of adsorption, it was concluded that mercury can be effectively removed by CFA-ZA from aqueous solution. It was revealed that the removal efficiency of CFA-ZA is comparable with that of activated carbon at the same adsorbent concentration and experimental condition.

Adsorbent concentration had a strong influence on the adsorption performance of CFA-ZA. The removal efficiency increased by increasing adsorbent dose, however, the adsorption capacity decreased due to the physical blockage of some of the adsorption sites. It was observed that the removal efficiency of CFA-ZA didn't change significantly with solution pH.

Adsorption kinetics was found to be well predicted by a pseudo-second-order kinetic model. The examined rate controlling model indicated that a multi stage mechanism of adsorption took place. Freundlich isothermal model explained the adsorption isotherms better as compared to Langmuir model. However, considering results obtained from kinetics and isothermal studies, it can be suggested that both physisorption and chemisorption took place in the adsorption mechanism with the main role belonging to the physisorption of mercury ions on the surface of coal fly ash zeolite LTA.

Bibliography

[1] N. E. Selin, “Global Biogeochemical Cycling of Mercury: A Review,” Annu. Rev. Environ. Resour., vol. 34, no. 1, pp. 43–63, Nov. 2009.

[2] J. Kulkarni, “Studies and Research on Mercury Removal from Water : A Review Abstract :,” no. 2, pp. 221–225, 2015.

[3] D. M. Manohar, K. A. Krishnan, and T. S. Anirudhan, “Removal of mercury (II) from aqueous solutions and chlor-alkali industry wastewater using,” vol. 36, pp. 1609–1619, 2002.

[4] K. J. Lee and T. G. Lee, “A review of international trends in mercury management and available options for permanent or long-term mercury storage.,” J. Hazard. Mater., vol. 241–242, pp. 1–13, Nov. 2012.

[5] “Technical Background Report for the Global Mercury Assessment,” 2013.

[6] R. a Bernhoft, “Mercury toxicity and treatment: a review of the literature.,” J. Environ. Public Health, vol. 2012, p. 460508, Jan. 2012.

[7] S. Sen Gupta and K. G. Bhattacharyya, “Kinetics of adsorption of metal ions on inorganic materials: A review.,” Adv. Colloid Interface Sci., vol. 162, no. 1–2, pp. 39–58, Feb. 2011.

[8] S. Babel and T. A. Kurniawan, “Low-cost adsorbents for heavy metals uptake from contaminated water : a review,” vol. 97, pp. 219–243, 2003.

[9] T. A. Kurniawan, G. Y. S. Chan, W. Lo, and S. Babel, “Comparisons of low-cost adsorbents for treating wastewaters laden with heavy metals.,” Sci. Total Environ., vol. 366, no. 2–3, pp. 409–26, Aug. 2006.

[10] A. K. Sen and A. K. De, “ADSORPTION OF MERCURY (I1) BY COAL FLY ASH,” vol. 21, no. 8, pp. 885–888, 1987.

[11] P. Hadi, M.-H. To, C.-W. Hui, C. S. K. Lin, and G. McKay, “Aqueous mercury adsorption by activated carbons.,” Water Res., vol. 73, pp. 37–55, Apr. 2015.

[12] F. Di Natale, a Lancia, a Molino, M. Di Natale, D. Karatza, and D. Musmarra, “Capture of mercury ions by natural and industrial materials.,” J. Hazard. Mater., vol. 132, no. 2–3, pp. 220–5, May 2006.

[13] S. N. Azizi, A. R. Dehnavi, and A. Joorabdoozha, “Synthesis and characterization of LTA nanozeolite using barley husk silica: Mercury removal from standard and real solutions,” Mater. Res. Bull., vol. 48, no. 5, pp. 1753–1759, May 2013.

[14] C. Sullivan, M. Tyrer, C. R. Cheeseman, and N. J. D. Graham, “Disposal of water treatment wastes containing arsenic - a review.,” Sci. Total Environ., vol. 408, no. 8, pp. 1770–8, Mar. 2010.

[15] J. Cai, B. Shen, Z. Li, J. Chen, and C. He, “Removal of elemental mercury by clays impregnated with KI and KBr,” Chem. Eng. J., vol. 241, no. March 2005, pp. 19–27, Apr. 2014.

[16] H. S. Ibrahim, T. S. Jamil, and E. Z. Hegazy, “Application of zeolite prepared from Egyptian kaolin for the removal of heavy metals: II. Isotherm models.,” J. Hazard. Mater., vol. 182, no. 1–3, pp. 842–7, Oct. 2010.

[17] X. Ren, Z. Zhang, H. Luo, B. Hu, Z. Dang, C. Yang, and L. Li, “Adsorption of arsenic on modified montmorillonite,” Appl. Clay Sci., vol. 97–98, pp. 17–23, Aug. 2014.

[18] H. Kazemian, H. Zakeri, and M. S. Rabbani, “Cs and Sr removal from solution using potassium nickel hexacyanoferrate impregnated zeolites</p> </p>,” J. Radioanal. Nucl. Chem., vol. 268, no. 2, pp. 231–236, May 2006.

[19] M. N. Sepehr, M. Zarrabi, H. Kazemian, A. Amrane, K. Yaghmaian, and H. R. Ghaffari, “Removal of hardness agents, calcium and magnesium, by natural and alkaline modified pumice stones in single and binary systems,” Appl. Surf. Sci., vol. 274, pp. 295–305, Jun. 2013.

[20] V. Somerset, L. Petrik, and E. Iwuoha, “Alkaline hydrothermal conversion of fly ash precipitates into zeolites 3: the removal of mercury and lead ions from wastewater.,” J. Environ. Manage., vol. 87, no. 1, pp. 125–31, Apr. 2008.

[21] S. S. Bukhari, J. Behin, H. Kazemian, and S. Rohani, “A comparative study using direct hydrothermal and indirect fusion methods to produce zeolites from coal fly ash utilizing single-mode microwave energy,” J. Mater. Sci., vol. 49, no. 24, pp. 8261–8271, Aug. 2014.

[22] K. Schroeder, M. Schoffstall, and A. Kim, “Adsorption of Mercury onto Fly Ash,” 2003.

[23] J. Li and M. M. Maroto-Valer, “Computational and experimental studies of mercury adsorption on unburned carbon present in fly ash,” Carbon N. Y., vol. 50, no. 5, pp. 1913–1924, Apr. 2012.

[24] W. Xu, H. Wang, T. Zhu, J. Kuang, and P. Jing, “Mercury removal from coal combustion flue gas by modified fly ash,” J. Environ. Sci., vol. 25, no. 2, pp. 393–398, Feb. 2013.

[25] C. Wang, J. Li, X. Sun, L. Wang, and X. Sun, “Evaluation of zeolites synthesized from fly ash as potential adsorbents for wastewater containing heavy metals,” J. Environ. Sci., vol. 21, no. 1, pp. 127–136, Jan. 2009.

[26] a. D. Papandreou, C. J. Stournaras, D. Panias, and I. Paspaliaris, “Adsorption of Pb(II), Zn(II) and Cr(III) on coal fly ash porous pellets,” Miner. Eng., vol. 24, no. 13, pp. 1495–1501, Oct. 2011.

[27] T.-C. Hsu, C.-C. Yu, and C.-M. Yeh, “Adsorption of Cu2+ from water using raw and modified coal fly ashes,” Fuel, vol. 87, no. 7, pp. 1355–1359, Jun. 2008.

[28] V. K. Jha, M. Nagae, M. Matsuda, and M. Miyake, “Zeolite formation from coal fly ash and heavy metal ion removal characteristics of thus-obtained Zeolite X in multi-metal systems.,” J. Environ. Manage., vol. 90, no. 8, pp. 2507–14, Jun. 2009.

[29] G. E. Dunham, R. a. DeWall, and C. L. Senior, “Fixed-bed studies of the interactions between mercury and coal combustion fly ash,” Fuel Process. Technol., vol. 82, no. 2–3, pp. 197–213, Aug. 2003.

[30] P. Abad-Valle, M. a. Lopez-Anton, M. Diaz-Somoano, and M. R. Martinez-Tarazona, “The role of unburned carbon concentrates from fly ashes in the oxidation and retention of mercury,” Chem. Eng. J., vol. 174, no. 1, pp. 86–92, Oct. 2011.

[31] K. S. Hui, C. Y. H. Chao, and S. C. Kot, “Removal of mixed heavy metal ions in wastewater by zeolite 4A and residual products from recycled coal fly ash.,” J. Hazard. Mater., vol. 127, no. 1–3, pp. 89–101, Dec. 2005.

[32] A. S. T. Chiang and K. Chao, “Membranes and ® lms of zeolite and zeolite-like materials,” vol. 62, 2001.

[33] J. A. Kaduk and J. Faber, “CRYSTAL STRUCTURE OF ZEOLITE Y AS A FUNCTION OF ION EXCHANGE,” vol. 12, no. 2, 1995.

[34] M. M. J. Treacy, “Collection of Simulated XRD Powder Patterns for Zeolites Editors :,” 2001.

[35] S. Wang and Y. Peng, “Natural zeolites as effective adsorbents in water and wastewater treatment,” Chem. Eng. J., vol. 156, no. 1, pp. 11–24, Jan. 2010.

[36] A. Alastuey, E. Herna, X. Querol, N. Moreno, J. C. Uman, F. Plana, and A. Lo, “Synthesis of zeolites from coal fly ash : an overview,” vol. 50, pp. 413–423, 2002.

[37] J. Behin, S. S. Bukhari, V. Dehnavi, H. Kazemian, and S. Rohani, “Using Coal Fly Ash and Wastewater for Microwave Synthesis of LTA Zeolite,” Chem. Eng. Technol., vol. 37, no. 9, pp. 1532–1540, Sep. 2014.

[38] S. S. Bukhari, J. Behin, H. Kazemian, and S. Rohani, “Conversion of coal fly ash to zeolite utilizing microwave and ultrasound energies: A review,” Fuel, vol. 140, pp. 250–266, Jan. 2015.

[39] M. M. J. Treacy and J. B. Higgins, Collection of simulated XRD powder patterns for zeolites. Amsterdam, The Netherlands: Elsevier, 2007.

[40] X. Zhu and S. D. Alexandratos, “Determination of trace levels of mercury in aqueous solutions by inductively coupled plasma atomic emission spectrometry : Elimination of the ‘ memory effect ,’” vol. 86, pp. 37–41, 2007.

[41] A. Baba and A. Kaya, “Leaching characteristics of fly ash from thermal power plants of soma and tunçbilek, turkey,” pp. 171–181, 2004.

[42] R. Arasteh, M. Masoumi, a. M. Rashidi, L. Moradi, V. Samimi, and S. T. Mostafavi, “Adsorption of 2-nitrophenol by multi-wall carbon nanotubes from aqueous solutions,” Appl. Surf. Sci., vol. 256, no. 14, pp. 4447–4455, May 2010.

[43] F. Raji and M. Pakizeh, “Kinetic and thermodynamic studies of Hg(II) adsorption onto MCM-41 modified by ZnCl2,” Appl. Surf. Sci., vol. 301, pp. 568–575, May 2014.

[44] D. Robati, “Pseudo-second-order kinetic equations for modeling adsorption systems for removal of lead ions using multi-walled carbon nanotube,” J. Nanostructure Chem., vol. 3, no. 1, p. 55, 2013.

[45] K. P. Raven, A. Jain, and R. H. Loeppert, “Arsenite and Arsenate Adsorption on Ferrihydrite: Kinetics, Equilibrium, and Adsorption Envelopes,” Environ. Sci. Technol., vol. 32, no. 3, pp. 344–349, Feb. 1998.

[46] C. Wang, J. Li, L. Wang, X. Sun, and J. Huang, “Adsorption of Dye from Wastewater by Zeolites Synthesized from Fly Ash: Kinetic and Equilibrium Studies,” Chinese J. Chem. Eng., vol. 17, no. 3, pp. 513–521, Jun. 2009.

[47] S. Malamis and E. Katsou, “A review on zinc and nickel adsorption on natural and modified zeolite, bentonite and vermiculite: examination of process parameters, kinetics and isotherms.,” J. Hazard. Mater., vol. 252–253, pp. 428–61, May 2013.

[48] E. K. Faulconer, N. V. H. von Reitzenstein, and D. W. Mazyck, “Optimization of magnetic powdered activated carbon for aqueous Hg(II) removal and magnetic recovery.,” J. Hazard. Mater., vol. 199–200, pp. 9–14, Jan. 2012.

[49] R. Barzamini, C. Falamaki, and R. Mahmoudi, “Adsorption of ethyl, iso-propyl, n-butyl and iso-butyl mercaptans on AgX zeolite: Equilibrium and kinetic study,” Fuel, vol. 130, pp. 46–53, Aug. 2014.

[50] a. Deepatana and M. Valix, “Comparative adsorption isotherms and modeling of nickel and cobalt citrate complexes onto chelating resins,” Desalination, vol. 218, no. 1–3, pp. 334–342, Jan. 2008.

[51] J. U. K. Oubagaranadin, N. Sathyamurthy, and Z. V. P. Murthy, “Evaluation of Fuller’s earth for the adsorption of mercury from aqueous solutions: a comparative study with activated carbon.,” J. Hazard. Mater., vol. 142, no. 1–2, pp. 165–74, Apr. 2007.

[52] J. T. Martin, T.D., Brockhoff, C.A., Creed, “DETERMINATION OF METALS AND TRACE ELEMENTS IN WATER AND WASTES OFFICE OF RESEARCH AND DEVELOPMENT EPA Method 200.7,” Usepa, vol. 4, pp. 1–58, 1994.

[53] E. Hums, N. M. Musyoka, H. Baser, A. Inayat, and W. Schwieger, “In-situ ultrasound study of the kinetics of formation of zeolites Na–A and Na–X from coal fly ash,” Ultrasonics, vol. 54, no. 2, pp. 537–543, Feb. 2014.

[54] S. S. Bukhari, J. Behin, H. Kazemian, and S. Rohani, “Synthesis of zeolite Na-A using single mode microwave irradiation at atmospheric pressure: The effect of microwave power,” Can. J. Chem. Eng., p. n/a–n/a, Mar. 2015.

[55] M. Trgo, J. Perić, N. V. Medvidović, M. Ugrina, I. Nuić, M. Macherzynsky, Ł. Uruski, and J. Golas, “MERCURY IONS CAPTURE BY NATURAL AND IRON-MODIFIED ZEOLITE - INFLUENCE OF SOLID / LIQUID RATIO,” pp. 36–39.

[56] M. Liu, L.-A. Hou, B. Xi, Y. Zhao, and X. Xia, “Synthesis, characterization, and mercury adsorption properties of hybrid mesoporous aluminosilicate sieve prepared with fly ash.,” Appl. Surf. Sci., vol. 273, no. 100, pp. 706–716, May 2013.

[57] A. Delebarre, “Removal of mercury in aqueous solution by fluidized bed plant fly ash q,” vol. 82, pp. 153–159, 2003.

[58] E. K. Faulconer, “EFFECTS OF ACTIVATED CARBON SURFACE CHEMISTRY MODIFICATION ON,” pp. 1–129, 2012.

[59] D. Mohan and C. U. Pittman, “Arsenic removal from water/wastewater using adsorbents--A critical review.,” J. Hazard. Mater., vol. 142, no. 1–2, pp. 1–53, Apr. 2007.

[60] S. Ahmed, S. Chughtai, and M. A. Keane, “The removal of cadmium and lead from aqueous solution by ion exchange with Na-Y zeolite,” vol. 13, pp. 57–64, 1998.

[61] G. Lv, Z. Li, W.-T. Jiang, C. Ackley, N. Fenske, and N. Demarco, “Removal of Cr(VI) from water using Fe(II)-modified natural zeolite,” Chem. Eng. Res. Des., vol. 92, no. 2, pp. 384–390, Feb. 2014.

[62] M. J. Jiménez-Cedillo, M. T. Olguín, C. Fall, and a. Colín, “Adsorption capacity of iron- or iron–manganese-modified zeolite-rich tuffs for As(III) and As(V) water pollutants,” Appl. Clay Sci., vol. 54, no. 3–4, pp. 206–216, Dec. 2011.

[63] B. Tawabini, S. Al-Khaldi, M. Atieh, and M. Khaled, “Removal of mercury from water by multi-walled carbon nanotubes.,” Water Sci. Technol., vol. 61, no. 3, pp. 591–8, Jan. 2010.

[64] D. S. Han, M. Orillano, A. Khodary, Y. Duan, B. Batchelor, and A. Abdel-Wahab, “Reactive iron sulfide (FeS)-supported ultrafiltration for removal of mercury (Hg(II)) from water.,” Water Res., vol. 53, pp. 310–21, Apr. 2014.

[65] S. A. Jafari and S. Cheraghi, “Mercury removal from aqueous solution by dried biomass of indigenous Vibrio parahaemolyticus PG02: Kinetic, equilibrium, and thermodynamic studies,” Int. Biodeterior. Biodegradation, vol. 92, pp. 12–19, Aug. 2014.

[66] D. K. Mondal, B. K. Nandi, and M. K. Purkait, “Removal of mercury (II) from aqueous solution using bamboo leaf powder: Equilibrium, thermodynamic and kinetic studies,” J. Environ. Chem. Eng., vol. 1, no. 4, pp. 891–898, Dec. 2013.

[67] a. Chojnacki, K. Chojnacka, J. Hoffmann, and H. Górecki, “The application of natural zeolites for mercury removal: from laboratory tests to industrial scale,” Miner. Eng., vol. 17, no. 7–8, pp. 933–937, Jul. 2004.

[68] F. Raji and M. Pakizeh, “Study of Hg(II) species removal from aqueous solution using hybrid ZnCl2-MCM-41 adsorbent,” Appl. Surf. Sci., vol. 282, pp. 415–424, 2013.

[69] J. Farrell and D. Mishra, “Mechanisms for Arsenic Removal by Ferric Hydroxide Adsorbents.”

[70] E. Katsou, S. Malamis, M. Tzanoudaki, K. J. Haralambous, and M. Loizidou, “Regeneration of natural zeolite polluted by lead and zinc in wastewater treatment systems,” J. Hazard. Mater., vol. 189, no. 3, pp. 773–786, 2011.

[71] M. J. Jiménez-Cedillo, M. T. Olguín, C. Fall, and a. Colín, “Adsorption capacity of iron- or iron–manganese-modified zeolite-rich tuffs for As(III) and As(V) water pollutants,” Appl. Clay Sci., vol. 54, no. 3–4, pp. 206–216, Dec. 2011.

Chapter 3

3 Mercury Removal from Industrial Wastewater Using Gold/Iron- Modified Natural and Synthetic Zeolites

3.1 Introduction

Mercury is a toxic heavy metal of significant environmental and ecological concern. Besides the natural origin of mercury such as volcanic activities, it has been released to the environment mainly through the human activities including ore mining and smelting, combustion of fossil fuels, pharmaceutical industry and battery manufacturing in the last decades[1]. Mercury is included in both the US environmental protection agency (EPA) and the world health organization (WHO) priority list of pollutants categorized as a human carcinogen, mutagen and teratogen. Mercury is known to undergo bioaccumulation and can be passed along the food chain to human. Mercury may largely affect brain, nerves and immune systems. The WHO and EPA have set a maximum guideline concentration of 6 µg/L and 0.2 µg/L for mercury in drinking water, respectively. Given the above mentioned facts, the removal of mercury from contaminated water and wastewaters is a major priority before discharge to the environment [2]–[4].

A number of treatment technologies are available to capture mercury from contaminated solutions including sulphide precipitation, membrane filtration, bio remediation and adsorption/ion exchange.

Adsorption of mercury by various solid materials is known as an efficient method for treatment of contaminated wastewater effluent [5], [6]. Extensive studies have been done to develop cost-effective adsorbents for mercury removal. Various adsorbents such as clays, zeolites, agricultural waste biomass, fly ash and activated carbon have been tested for this purpose [7].

Activated carbon is the most dominant adsorbent used for removing of mercury, with several drawbacks such as high cost and the difficulty in preparation and regeneration process [8], [9].

Zeolites are crystalline aluminosilicates with three-dimensional structure consisting of molecular-sized pores and channels. More than 60 types of zeolites occur naturally and more than 150 types of synthetic zeolites are manufactured using different precursors of Si and Al. Natural and synthetic zeolites with various framework topologies and their modified forms have been used as adsorbent, ion-exchanger, molecular sieve, heterogeneous catalysis for different environmental friendly applications. For instance, adsorption efficiency of different zeolites for removing heavy metal cations such as cadmium, lead, nickel, and manganese [10]–[14] , anionic species such as chromate and arsenate [15], [16], and organic pollutants [17], [18] have been studied. Some of porous zeolitic materials such as natural clinoptilolite and synthetic zeolite LTA exhibit strong affinity for many heavy metal cations including mercury [13], [19]–[22].

Natural clinoptilolite belongs to HEU framework with silicon to aluminum ratio of more than 4.7. Pure natural clinoptilolite has a chemical composition of $|Na_{1.84}K_{1.76}Mg_{0.2}Ca_{1.24}(H2O)_{21.36}|$ $[Si_{29.84}Al_{6.16}O_{72}]$[23]. Potential applications of natural clinoptilolite for environmental remediation processes, particularly for water and soil purification, are studied extensively by many researchers [13], [21].

Zeolite NaA with LTA (Linde Type A) structure framework has silicon to aluminum ratio of about 1.0, which is considerably lower than clinoptilolite. The ideal chemical composition of LTA is $|Na_{96}(H2O)_{216}|$ $[Si_{96}Al_{96}O_{384}]$ [23], [24]. Zeolite A can be synthesized using different starting materials as source of Al and Si [12], [22], [25], [26]. Some studies indicated that zeolite LTA could effectively remove heavy metals from contaminated wastewater [22].

A few studies are published on the application of zeolite LTA and clinoptilolite for mercury adsorption. [27] and [28] reported the use of natural zeolite for removal of mercury from aqueous solutions and the selectivity of zeolite LTA toward mercury was determined by [26]. To the best of the authors' knowledge, however, there are limited

technical data on thermodynamic and kinetics of mercury adsorption on these zeolites. Moreover, we could not find any published reports on the effect of the zeolite modification process on mercury removal.

Selecting a proper modification process for any specific heavy metal removal is of great importance [29]. Modification process for developing effective adsorbents of mercury removal, should be studied carefully in terms of selection of the right metallic cations, because it may affect the mechanism and kinetic of adsorption process [30].

The sole part of this study is about enhancing the adsorption of a natural clinoptilolite and a synthetic zeolite 4A and their modified forms for removal of Hg(II) from a modeled wastewater solution. Given the fact that gold has a great tendency to amalgamate with mercury [31], modification of the adsorbents with gold was considered. .

Because of unique properties of iron oxide species, such as extreme surface modifiability, excellent magnetic properties, great biocompatibility and low cost [32]–[34], use of these compounds for heavy metal removal applications has been extensively studied by many researchers all around the world.

In the case of bimetallic modification, iron modified zeolites is used as a support to stabilize gold. Iron cations play a role as active centers for gold adsorption. This may create strong interaction between iron cations and the gold precursor which makes Au stabilization stronger on zeolite surface [35], [36]. The results revealed that the adsorption capacity and selectivity of the modified zeolite for Hg (II) were increased

The removal efficiency of Hg (II) ions on the gold/iron modified zeolite LTA and gold modified natural clinoptilolite were studied and compared tin comparison to the parent zeolites. Initial concentration of Hg (II) solution, adsorbents dosage and contact time were studied. As part of equilibrium studies, Langmuir, Freundlich and Tempkin isothermal models were used to fit the experimental data. Furthermore, first-order, second-order and Elovich kinetics models were performed to study the kinetic of Hg (II) adsorption on the examined adsorbents.

3.2 Experimental

3.2.1 Modification of the Zeolites

Synthetic zeolite 4A in the form of powder (Si/Al = 1.01, PR China) and natural clinoptilolite (Si/Al= 5.2, Bromley, BC, Canada) and their modified forms were used. The clinoptilolite sample was pulverized and sieved to particle size < 250 µm. To remove soluble impurities, both zeolites were washed several times with distillated water and then dried at 250 °C and stored inside a desiccator.

3.2.1.1 Gold Modification

Gold was incorporated into the zeolites following an ion exchange procedure (S. Jafari et al. 2009; J. H. Chen et al. 2005; Sobczak et al. 2010a). A gold solution of $8*10^{-4}$ M was prepared using gold (III) chloride trihydrate ($HAuCl_4.3\ H_2O$; (Au_2Cl_6), Au 49.5 %, Sigma Aldrich, USA). The final pH of the solution was adjusted to 6 using a 2.5 M solution of NaOH. Eight g of each zeolite was added to 1000 ml of the prepared solution, and stirred at 80 °C for 18 hours. The gold modified samples filtered using a o.45 µm cellulose filter, then washed with deionized water and dried at 150°C.

3.2.1.2 Gold-iron Modification

Gold/Iron bimetallic modified zeolites prepared by loading iron first and then gold. Zeolite samples were modified with iron by means of an ion exchange procedure (Bogdanchikova et al. 2008; Sobczak et al. 2010a, Menhaje-Bena R, 2004). Ten g zeolite were added to 50 ml of prepared 0.05 M solution of ferric nitrate nonahydrate (Fe (NO3)3. 9 H2O) (Alfa Aesar, USA), and stirred for 6 hours at 40°C. The samples were filtered, washed and dried at 100° C.

Then, gold was loaded on iron-modified zeolite using the incipient wetness impregnation method (Baatz et al. 2008; Sobczak et al. 2010, Kazemian et al. 2013). The required amount of freshly prepared solution of gold (corresponding to 0.1 wt% of Au) was prepared by dissolving sufficient amount of $HAuCl_4.3\ H_2O$ in deionized water. This

solution was added drop wise to the Fe-modified zeolite under constant mixing. The resulting modified adsorbents were dried f at 80 °C for 16h and then calcinated at 350 °C for 3h. All adsorbents including raw and modified samples characterized by means of BET, TGA, XRD and SEM-EDX instrumental analyses.

3.2.2 Characterization

The X-ray diffraction (XRD) analysis (Rigaku–Miniflex powder diffractometer, Japan) was performed using CuKα (λ for Kα = 1.54059 Å) over the range of $5°<2\theta<60°$ with step size of 0.02°. The XRD patterns were compared with those of reference peaks [23]. The areas of the characteristic peaks were determined by "peak fitting" algorithm using the MDI-Jade v 7.5 software (Livermore, California).

The surface morphology of the samples was characterized by Scanning Electron Microscopy coupled with energy dispersive X-ray analysis (SEM-EDX; JSM 600F, Joel Japan, 10 KeV). Elemental mapping of the modified samples was done using SEM-EDX to observe the state of distribution of gold and iron atoms. The chemical composition of the adsorbents was measured by means of X-ray fluorescence spectroscopy (XRF) utilizing a PANalytical PW2400 Wavelength Dispersive.

The specific surface area, pore volume and pore size of all selected zeolites were measured by Burnauer- Emmett-Teller (BET) method using a Micrometrics Accelerated Surface Area and Porosimetry (ASAP) 2010 BET surface area analyzer. Zeolitic samples were degassed for 6 hours at 150°C, before the analysis.

Thermo gravimetric analysis of the samples was performed using a Mettler Toledo TGA/SDTA 851e model (Switzerland) with a Stare software (version 6.1) by heating the sample from ambient temperature up to 1050 °C under the nitrogen purge of 40 ml/min and a heating rate of 10 °C/min. A inductively coupled plasma-atomic emission spectroscopy (ICP-AES) (Perkin Elmer Optima-3000 DV System) was used to measure the elemental concentration of mercury of all waste solutions before and after each adsorption tests [40].

3.2.3 Adsorption of Mercury

One of the objectives of this research was to develop an efficient adsorbent for capturing mercury from a contaminated industrial wastewater of a mineral processing industry. The simulated wastewater with initial concentration of 10 mg/L of mercury was prepared using a 1000 µg/ml AAS standard solution containing mercury chloride salt (Alfa Aesar, Ward Hill, MA, USA). Actual wastewater sample from a mine in British Columbia (provided by Kontec Ecology Systems Inc. Burlington, ON) was used as a medium to see the effect of competing ions. The results of chemical analysis of the actual wastewater can be seen at Table S1 of the Appendix B).

The experiments were carried out in batch mode using translucent polypropylene tubes with sealing cap (Thermo scientific, Nalgene, Oak Ridge, ON, Canada) at room temperature in an end over end shaker oven with constant shaking at 500 rpm (Appendix B, Figure S1). Independent blank experiments (i.e., no sorbent) conducted to eliminate the effect of adsorption on the container walls.

To examine the removal efficiency of adsorbents, 10 ml of the simulated wastewater with different initial concentration of mercury were added to a known amount (0.5 g) of each adsorbent (encoded as “Brm” for natural clinoptilolite; “Au- Brm” for gold-modified natural zeolite , “LTA” for synthetic 4A zeolite and “Au/Fe-LTA” for gold/iron modified zeolite 4A) at room temperature. After 24 h of reaction to reach equilibrium, sample aliquots were collected and filtered using a 0.45 µm syringe filter (Fischer Scientific, Ottawa, ON, Canada), then the mercury concentration was measured by ICP-AES technique.

All of the adsorption experiments were performed in triplicate to ensure the reliability and reproducibility of the mercury measurements results. The pH of solution was measured before and after each adsorption test. An adsorption calibration curve was constructed using five standard solutions. The average for each series of measurements is reported in this paper. Error bars represent the standard deviations.

The removal efficiency of adsorbents can be expressed as:

Removal efficiency (%) = 100 $(C_0-C_e)/C_0$ (1)

where C_0 and C_e are the initial and equilibrium concentration of the adsorbate (i.e. mercury), respectively (mg/L). The amount of mercury ions adsorbed per unit mass of each adsorbent was calculated using the following equation:

$q_e= (C_0-C_e).V/ m$ (2)

where q_e in (mg/g) expresses the mercury ions adsorbed per g of adsorbents, V is the solution volume (ml), m is the mass of sorbent (g) and C_0 and C_e are the initial and equilibrium concentrations (mg/L).

3.2.4 Kinetics and Mechanism of Adsorption

To study the kinetics of Hg (II) adsorption by the zeolites, known amounts of each adsorbents were added to 10 ml of 10 mg/L Hg(II) solution. The solution to adsorbent ratio was 10 in all adsorption tests. Samples were collected at different time intervals from 5 min to 24 h for Hg(II). Lagergren's pseudo first-order kinetics expression, pseudo second-order rate expression and Elovich rate equation were used to examine the adsorption kinetics of Hg (II) ions (Table 3-1). Intra particle diffusion model fits the experimental data to study adsorption mechanisms and determine the rate-limiting step.

3.2.5 Equilibrium Isotherms

Adsorption isotherms were obtained by varying the initial sorbent concentrations (e.g. 1 g/L to 100 g/L for the Brm samples) in 10ml of 10 mg/L solution of mercury. The contact times set at 24 hours. Adsorption of Hg (II) ions by zeolite adsorbents was modeled using three adsorption isotherms models of Langmuir, Freundlich and Temkin (Table 3-2, Appendix B).

Table 3-1: Reaction kinetic models.

Reaction kinetic Models	Non-linear equation	Linear equation	Model parameters	Reference
pseudo-first order	$q_t=q_e\ (1-e^{-k_1 t})$	$\ln (q_e-q_t) = \ln q_e - k_1 t$	q_e, k_1	[42],[41]
pseudo-second order	$q_t= q_e^2 k_2 t/(1+q_e k_2 t)$	$t/q_t =1/(k_2 q_e^2) + (1/q_e)*t$	q_e, k_2	[43], [6],[44]
Elovich model	$q_t= (1/\beta_e)\ln (\alpha\beta_e t+1)$	$q_t=\ln (\alpha\beta_e)/\beta_e+\ln t/\beta_e$	α,β_e	[22], [45]
Diffusion Model	$q_t= k_{id}\ t^{0.5}$		k_{id}	[46], [47]

Table 3-2: Isothermal models.

Reaction Isothermal Models	Non-linear equation	Linear equation	Model parameters	Reference
Langmuir	$q_e = q_m\ K_L C_e/(1+K_L C_e)$	$C_e/q_e = 1/(q_m K_L) + C_e/q_m$	q_e, k_L	[47], [48]
Freundlich	$q_e = K_F\ C_e^{\ 1/n_f}$	$\text{Ln}\ q_e = \ln K_F +(1/n_f) \ln C_e$	q_e, k_f	[48], [49]
Temkin	-	$q_e =k_1 \ln K_2 +k_1 \ln C_e$	K_1,k_2	[50],[48]

3.2.6 Finding the Best Kinetic and Isotherm Models

To assess the best kinetic and isothermal models, the linear coefficient (R^2 values) were determined and compared. In addition, the non-linear Chi-square test was used to measure the differences between the experimental and modeled data for kinetic study using the following equation:

$$X^2 = \sum (q_{e,exp} - q_{e,cal})^2 / q_{e,cal} \qquad (3)$$

Where $q_{e,exp}$ is experimental equilibrium capacity data (Eq 2) and $q_{e,cal}$ is the equilibrium capacity of the selected model. Obviously a smaller value for X^2 suggests higher similarity between experimental and modeled data.

3.3 Results and Discussion

3.3.1 Chemical Composition and Structure of Zeolites

Table S2 in the Appendix B, presents the data on the chemical composition and Si/Al ratio of the raw natural and synthetic zeolites. Considering the XRD pattern and the Si/Al ratio of natural zeolite, which is 5.2, it can be concluded that the samples is natural clinoptilolite zeolite (Treacy and Higgins 2007; Wang and Peng 2010, Charkhi 2010). Loss on ignition (LOI) was found to be 9.33 % by heating the sample at 1050°C for 3 hours in an electrical furnace, that is very close to ~8% weight loss in 100 °C due to water evaporation and ~1% weight loss around 700 °C (studied by thermal analysis technique, section 3.2.3). For the synthetic 4A zeolite, however, the SiO_2 percentage is found to be higher than that for natural zeolite resulting in a Si/Al ratio of 1.01, which is in the range of Si/Al characteristic of zeolite LTA structure (Behin et al. 2014, Bukhari, 2015).

3.3.2 Gold and Iron Species in Zeolites

3.3.2.1 X-ray Diffraction

Figure1illustrates the XRD patterns of parent and modified zeolites. According to the XRD patterns, the main zeolitic phase of raw Bromley correlates to the HEU structure, which can be either heulandite or clinoptilolite [23]. Concerning the chemical composition of the raw natural zeolite sample (Appendix B, Table S2), in which the Si/Al ratio is higher than 4, clinoptilolite can be considered as the major phase of this natural adsorbent.

As expected, the framework crystallinity of the natural clinoptilolite sample remained intact after modification with gold. The diffraction characteristic peaks of metallic gold

could be identified at $2\theta = 38.2^{o}$ from Au (1 1 1) and 44.8^{o} from Au (2 0 0)[37], [38]. Using "peak fitting" algorithm in the MDI-Jade v 7.5 software, a peak was detected at $2\theta = 38.22^{o}$ corresponding to metallic gold (Au^{o}). This peak confirmed the gold incorporation on the zeolite surface.

XRD patterns of the synthetic zeolite before and after modification, which are illustrated in Figure 3-2 indicate that the structure of zeolite LTA remains unchanged after surface modification with gold and iron. Synthetic zeolite LTA has two relatively strong peaks at $2\theta = 38.01^{o}$ and 44.78^{o} [23] very close to the main peaks of gold at $2\theta = 38.2^{o}$ and 44.8^{o} [37], [38]. Considering very small content of gold (less than 1 %.wt), it would be expected that the strong peaks of synthetic zeolite LTA suppress the overlapped gold characteristic peaks. However, using "peak fitting" algorithm in the MDI-Jade v 7.5 software, interestingly one peak was detected at $2\theta = 44.88^{o}$ with 500 value for “area under peak” indicative of Au (2 0 0). Also the calculated “surface area under peak” for $2\theta \approx 38.2^{o}$ showed an increase from 1439 for raw LTA to 3603 for modified one representative Au (111). Both evidences strongly indicate the presence of gold in gold-iron modified zeolite LTA.

Iron exchanged zeolite LTA was used as support for gold introduced. For iron oxides the characteristic peaks are identified at 2θ = 33.2, 35.6, 40.9, 49.5° [33], [51]. XRD of standard structure of zeolite LTA has very similar peaks at 2θ = 33.3, 35.6, 40.1, 49.7°. The “surface area under peak” was calculated for all the target peaks. At 2θ = 33.3 -33.4° the “surface area under the peak” increased from 1408 for raw LTA to 1444 for Au/Fe-LTA which can be allocated to iron. The crystalline structure of iron oxides was not assigned for other peaks. This could be an evidence of good dispersion of iron species (Fe_xO_y) on the internal/external surface of adsorbent [36].

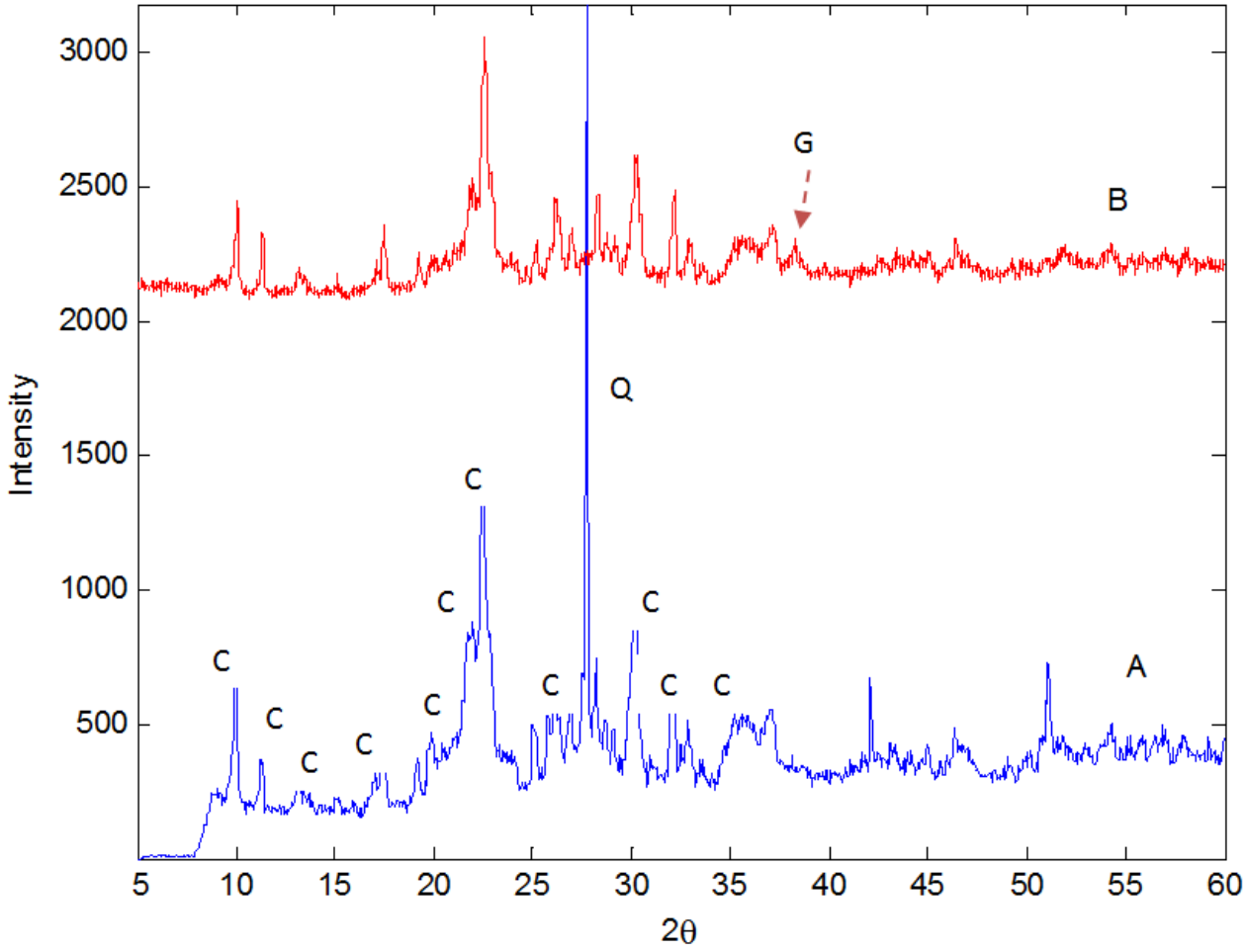

Figure 3-1: XRD of parent of A) Bromley natural clinoptilolite and B) gold modified Bromley (C: Clinoptilolite, Q: Quartz and G: Gold).

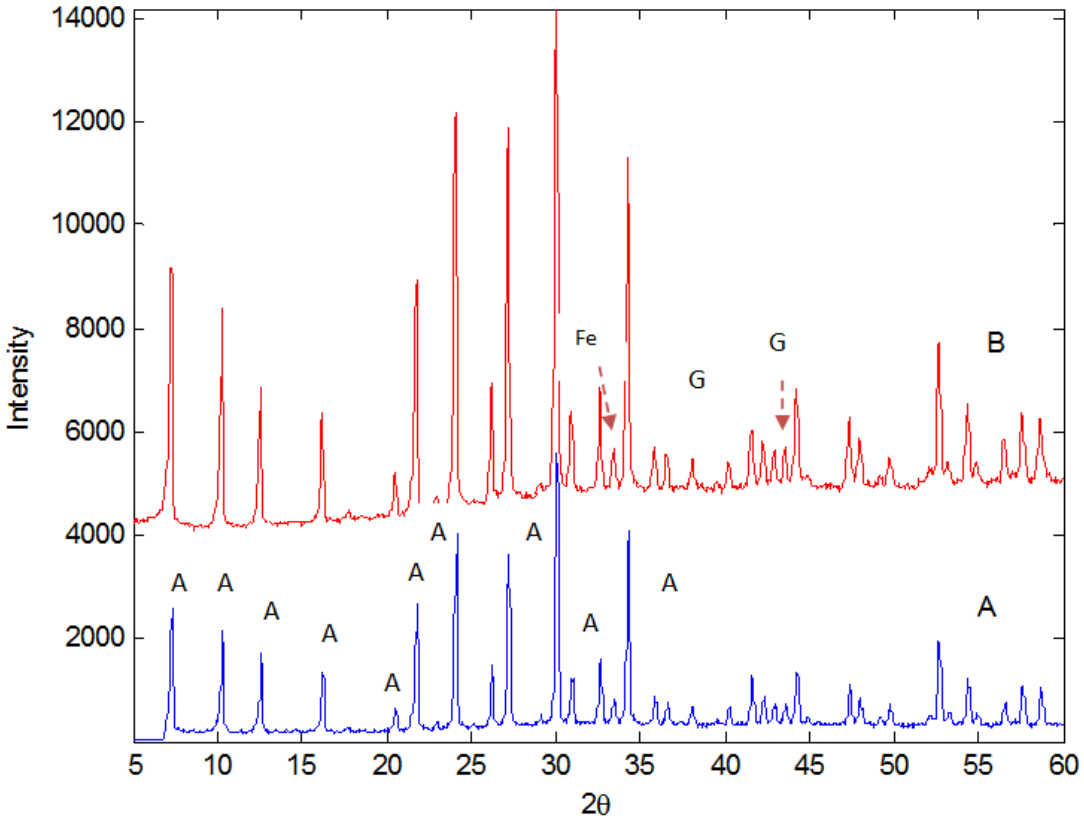

Figure 3-2: XRD of pattern of : A) untreated synthetic zeolite LTA and B) Au/Fe-LTA (Characteristic peaks: A Zeolite LTA, G: Gold and Fe: Iron.

3.3.2.2 SEM-EDX

SEM micrographs of the zeolites are illustrated in Figure 3-3. The crystalline structure of clinoptilolite was clearly visible for the natural zeolite sample. Natural clinoptilolite forms broad flat rectangular faces with angled corners [52] . This “coffin shape” is typical of many species of clinoptilolite (Figure 3-3a).

The cubic structure of zeolite LTA is clearly visible in the SEM image of synthetic zeolite [53], [54]. The SEM results demonstrate the difference in morphology and crystalline structure of two zeolite samples.

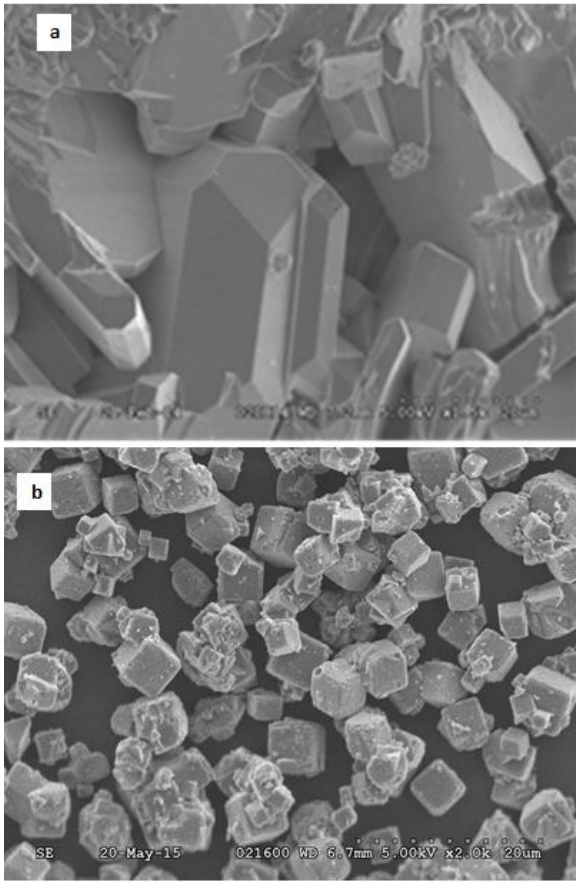

Figure 3-3: SEM micrographs of: (a) zeolite clinoptilolite and (b) zeolite LTA.

A more detailed analysis of the chemical composition of the surface of the modified samples and the presence of iron and gold on the synthetic zeolite and gold on the natural zeolite was conducted via elemental mapping by energy dispersive X-ray (EDX) of the SEM technique, which is illustrated in Figure 3-4. In addition, the composition of modified zeolites was obtained by randomly selecting area on the solid surfaces and analyzing by SEM-EDX (Figure5).

The proper distribution of red dots in Au map for Au-Brm adsorbent (Figure 3-4, a) indicates appropriate dispersing of gold particles on the zeolite surface. However, the places were shown with blue dashed lines indicate the location of the gold more accumulate.

The corresponding elemental mapping for Au/Fe-LTA zeolite presented in (Figure 3-4b, c) reflects stronger homogeneous distribution of gold compared to iron on the entire surface of modified zeolite. Energy dispersive X-ray (EDX) analysis that is conducted to evaluate the presence of gold and iron on the modified samples are shown in Figure 3-5

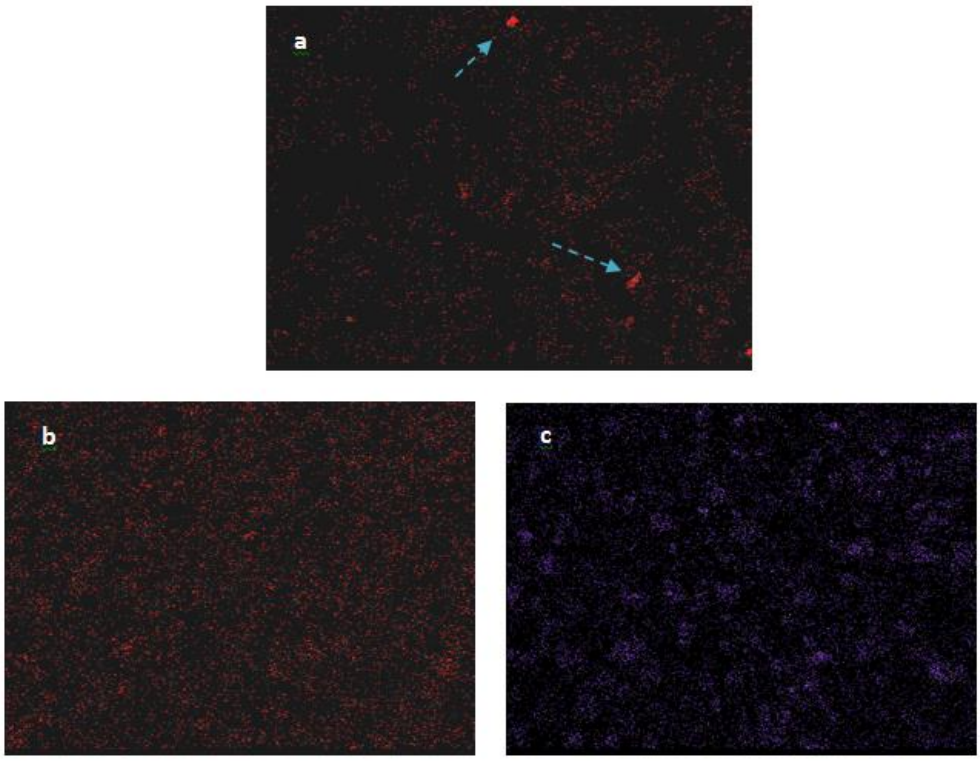

Figure 3-4: SEM–EDX elemental mapping of: a) gold on the gold-modified natural zeolite, b) gold on the Au/Fe-modified synthetic zeolite, c) Iron on the Au/Fe modified synthetic zeolite.

The EDX spectrum of the Au-Brm sample gives the characteristic peaks for Au at 2.20 and 2.60 keV with 1.05 wt% of gold. For Au/Fe-LTA sample the EDX spectrum gives the characteristic peaks of Au at 2.60 keV with 0.51wt% and characteristic peaks of Fe at 6.40 keV with 0.63wt%. The results of elemental mapping by means of EDX confirmed the presence of gold and iron in modified zeolites with homogenous distribution on the surface of zeolites particulates.

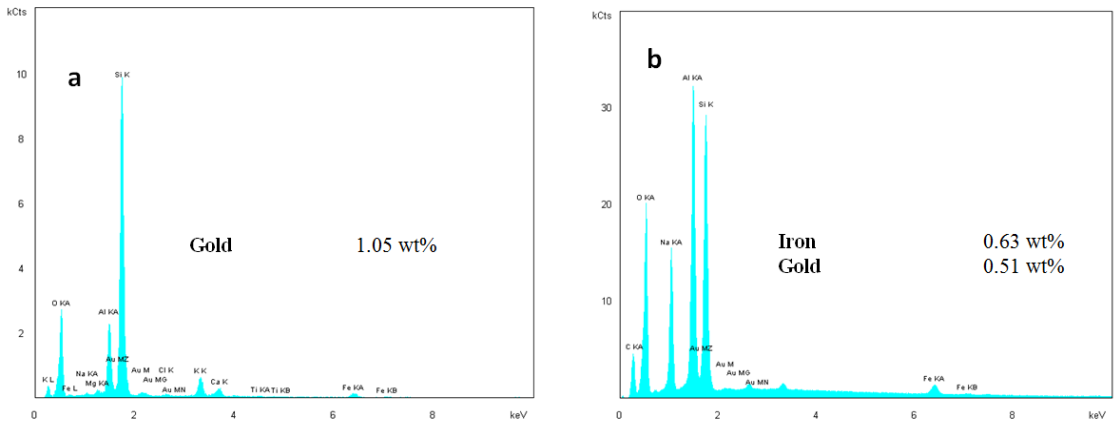

Figure 3-5: Energy dispersive X-ray (EDX) analysis of (a) Au-Brm, and (b) Au/Fe-LTA.

3.3.2.3 TGA

Figure 3-6 displays the thermal profiles of all examined adsorbents in this study. For raw and modified Bromley, the main weight loss occurs around 100°C corresponding to ~ 8-9% of the overall weight loss, which belongs to reversible water content of zeolitic phase of the samples (Figure 3-6a). However, their TGA graph show a small extra peak at ~700°C, that can be attributed to other minerals containing carbonate ion $[CO_3]^{2-}$ (e.g, calcium carbonate). Calcium carbonate decomposes around 700-900°C. It is hard to prove the presence of calcium carbonate via XRD pattern because the main peak of calcium carbonate appears at 2θ = ~29.5°, which overlaps with one of the broad peaks of clinoptilolite (i.e.2θ = ~28-31°). The weight loss of the natural zeolite samples at ~700°C is close to 1-1.5%. These values are comparable with LOI of raw Bromley at 8.22 ^{o}.

The TGA curve of LTA and its modified counterpart are illustrated in Figure 3-6b, in which ~7 % weight loss for LTA occurs at 200 °C. This could be attributed to evaporation of adsorbed water molecules on the macro pores (i.e., capillary water) and external structure of the synthesized zeolite.The overall weight loss of Au/Fe-LTA is increased slightly to ~ 7.5%, which is reasonable due to the modification changes. Given the TGA and LOI data, it can be concluded that the main weight loss of the natural samples is due to water evaporation rather than decomposition of any other component.

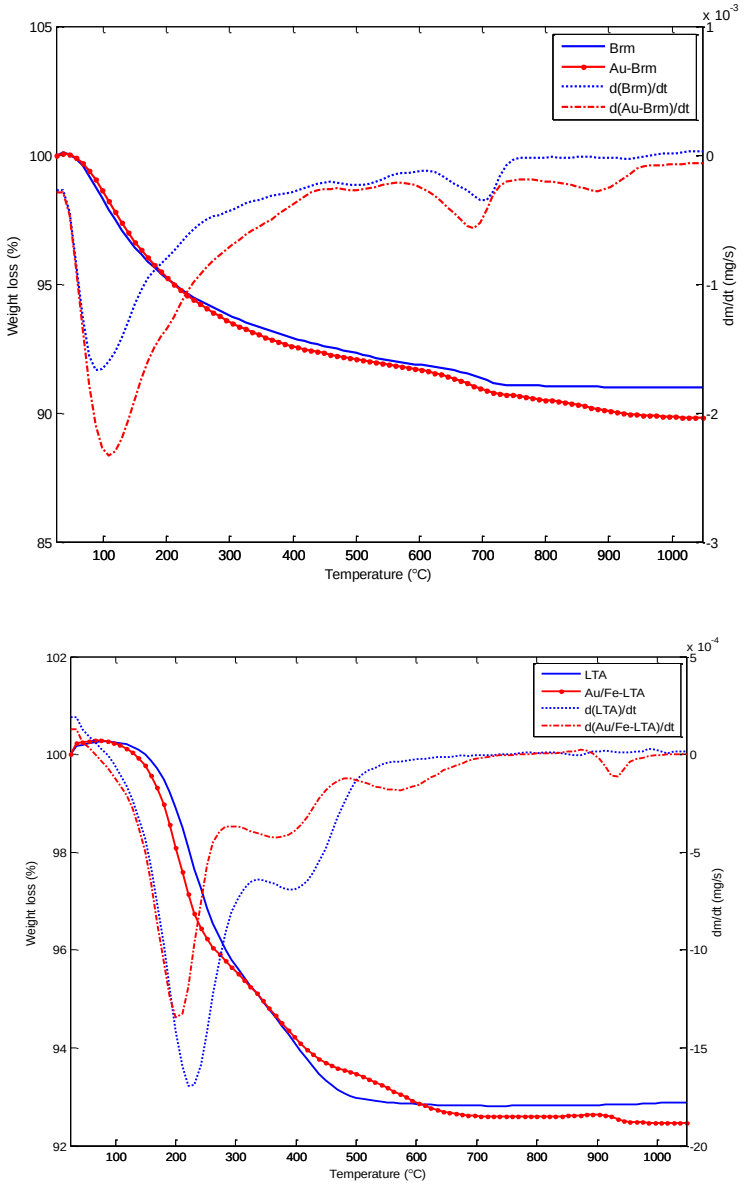

Figure 3-6: Thermo-gravimetric analysis of (a) raw and modified natural zeolite and (b) raw and modified LTA (heating rate 10°C/min, under N_2 atmosphere of 40ml/min).

3.3.2.4 BET

The BET is one of the most reliable techniques to determine some of the important parameters of porous zeolitic materials such as specific surface area, micro pore area and

pore diameter. All of these factors affect zeolite applications as adsorbent and catalysts [55]. Table 3-3 presents the specific surface areas and pore size of all tested adsorbents before and after modification.

The BET surface areas of the Bromley natural zeolite sample and its Au-modified form were 30.51 m^2/g and 15.98 m^2/g, respectively. BET surface area of natural clinoptilolite is in the range 30-40 m^2/g depending on the origin [10]. The decrease of surface area of the Au-modified natural zeolite can be attributed to the loading of gold on the zeolite pores and cavities.

The BET surface areas of modified Au-Fe-LTA showed a dramatic improvement over the BET surface area of parent LTA. According to XRF analysis the synthetic zeolite LTA contains some impurities including 17 % sodium content (Appendix B, Table S2), which can be attributed to the presence of unreacted sodium hydroxide that is used during the synthesis process. It seems the soluble compounds and other impurities that occupy pores and channels of untreated synthetic zeolite are removed during the course of modification and calcination. Therefore, increasing of the surface area of the Au/Fe-LTA modified zeolite is observed.

3.3.3 Mercury Species in Different pH

It is well known that adsorption of heavy metals is a highly pH dependent process and the activity of adsorbent is strongly affected by solution pH [6], [56]. Different species of mercury in aqueous solutions at various pH, which are determined using the Visual MINTEQ 3.1 speciation program, are summarized in Table 3-4. Charges and sizes of various mercury species are different that affect their adsorption by adsorbents.

As it is presented in Table 3-4, for systems with a pH value of 5 and more, $Hg(OH)_2$ is the dominant species (i.e. >99%). At a pH of approximately 2.5 (with 10 mg/L Hg(II) solution) for all of the adsorption tests, the mercury was mainly in the form of Hg^{2+}(i.e. 85.68%) with 9.44% of $HgOH^+$ and 4.87% of $Hg(OH)_2$ and very low level of Hg_2OH^{3+}, $Hg_3(OH)_3{}^{3+}$.

Table 3-3: BET results for all un-modified and modified samples.

Sample name	BET Surface Area m^2/g	Langmuir Surface Area m^2/g	Micropore Area m^2/g	External Surface Area m^2/g	Adsorption Average Pore Diameter (4V/A by BET)Å
Brm	30.5122	42.7850	1.4780	29.0342	78.7402
Au-Brm	15.9849	21.3719	20.7530	-4.7680	112.9207
LTA	8.3276 m^2/g	19.4601	-5.0521	13.3797	51.1094
Au/FE-LTA	24.3423 m^2/g	34.4069	-0.6628	25.0051	59.4229

Table 3-4: Mercury speciation as a function of pH.

Solution pH	concentration (mg/L)	Hg^{2+} (%)	$HgOH^{+}$ (%)	$Hg(OH)_2$. (%)	Other species (Hg_2OH^{3+}, $Hg_3(OH)_3{}^{3+}$)
1.77	100	98.546	1.355	0.099	Very low
1.88	50	97.47	2.262	0.268	Very low
2.5	10	85.68	9.44	4.87	Very low
3	10	50.27	18.64	31.07	Very low
3.5	10	11.52	13.98	74.49	Very low
4	10	1.4	5.49	93.1	Very low
4.5	10	0.75	4.06	95.18	Very low
>=5	10	Very low	Very low	>99	Very low

3.3.4 Effect of Adsorbent Dose

Given the fact that mass of adsorbent determines the availability of active sites, adsorbent dosage affects adsorption process significantly [57]. This means increasing the adsorbent to solution ratio will increase the number of active sites available for adsorption in the same volume of solution. While the removal efficiency will be increased at higher dosage of adsorbent, however, the amount of metal adsorbed per unit mass of adsorbent (i.e., adsorption capacity) decreased [58].

The influence of sorbent dose on Hg(II) adsorption was examined by varying the adsorbent dose of the zeolitic adsorbents at initial mercury concentration of 10 g/L at room temperature and constant initial pH of 2.5.

Figure 3-7A shows that removal efficiency of Au/Fe-LTA slightly improved by increasing the adsorbent dosage indicating that even very small dosage of this adsorbent (i.e., 1 g/L) shows a considerable removal efficiency (i.e. close to 100%) for the tested mercury concentration of 10 ppm. The final pH of solution changed from 4.9 for 0.5 g/L adsorbent dose to 7.6 for 100 g/L adsorbent dose (Figure 3-7B).

As mentioned in section 3.3 for mercury solution with a pH value of 5 and more, $Hg(OH)_2$ is the dominant species at 99%. It can be concluded that increasing the pH, as a result of higher dosage of adsorbent, will change the mercury speciation from cationic Hg^{2+} to $Hg(OH)^{+}$ and $Hg(OH)_2$, which means precipitation will be the dominant removal mechanism at higher pH. For Au/Fe-LTA, however, it seems that changing the pH of the mercury solution as a function of various adsorbent doses did not have a significant influence on the performance of the adsorbent.

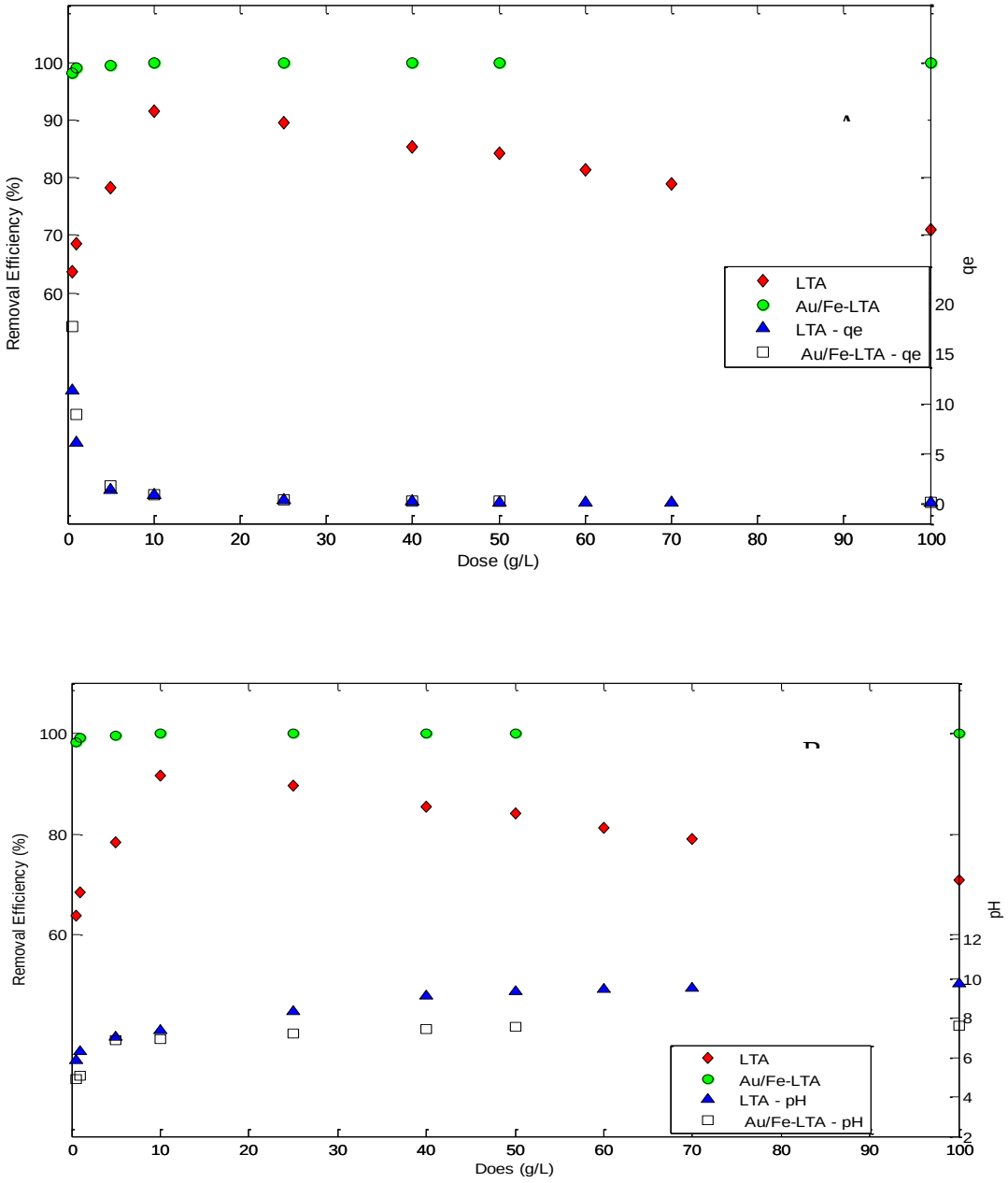

Figure 3-7: (a) Removal efficiency and adsorption capacity as a function of adsorbent dose of LTA and Au/Fe-LTA (experimental conditions: 10 ml Hg(II) 10 mg/L, initial pH≈2.5 at room temperature). (b) Removal efficiency and pH as a function of adsorbent dose of LTA and Au/Fe-LTA (experimental conditions: 10 ml Hg(II) 10 mg/L, initial pH≈2.5 at room temperature).

For LTA the removal efficiency gradually increased from 63% for 5 g/L to the maximum value of 91% for 10 g/L of adsorbent and significantly decreased thereafter. It is well known that the presence of competing ions in wastewater (with higher selectivity for adsorbent compare to heavy metal ions) may suppress adsorption of mercury.

As it is presented in Table S2, large amounts of free sodium ions exist in the structure of zeolite LTA as a result of synthesis process. The sodium ions will be released to the aqueous medium after first contact. Moreover the industrial wastewater which was used as the medium to make the mercury solution is very complex containing various species including sodium ions (Table S1).The complex medium of the wastewater and the interaction of various species contained in wastewater result in formation of stable complexes that are not adsorbed on the adsorbents' surface. It is notable that with coordination number of 6, ionic radius and crystal radius of both Na(I) and Hg(II) are similar with values of 1.16 Å and 1.02 Å, respectively [59]. All this can reduce the metal adsorption by decreasing the soluble metal concentration and/or hinder the metal ions to reach active adsorption sites due to surface complexion or competition ions. Consequently as we expected, the removal efficiency of LTA towards Hg(II) increased as a result of increasing adsorbent dose from 1g/L to 10 g/L. However, after that releasing more sodium ions to the solution suppresses the removal efficiency of zeolite LTA towards Hg(II). Considering averaged initial pH value of 2.5 for mercury solution, it was observed that the final pH of solution increased to 6.3 by adding only 1g/L of adsorbent.

Figure 3-8B shows that removal efficiency of Brm and Au-Brm samples are improved by increasing the adsorbent dosage. The removal efficiency is higher for Au-Brm compared to Brm samples with the same adsorbent dosage. However, this difference is higher at lower adsorbent mass. For instance at the same adsorbent dosage of 1g/L the removal efficiency of Brm is 13% compared to 44 % for Au-Brm, indicating that modification of the natural clinoptilolite with very low amount of gold successfully increased its removal efficiency for Hg(II) even at very low dosage of adsorbent. Also increasing the adsorbent mass for both clinoptilolite adsorbent from 1g/L to 10 g/L has some effect on the final pH of solution and the maximum removal efficiency achieved in higher pH values (Figure 3-8B).

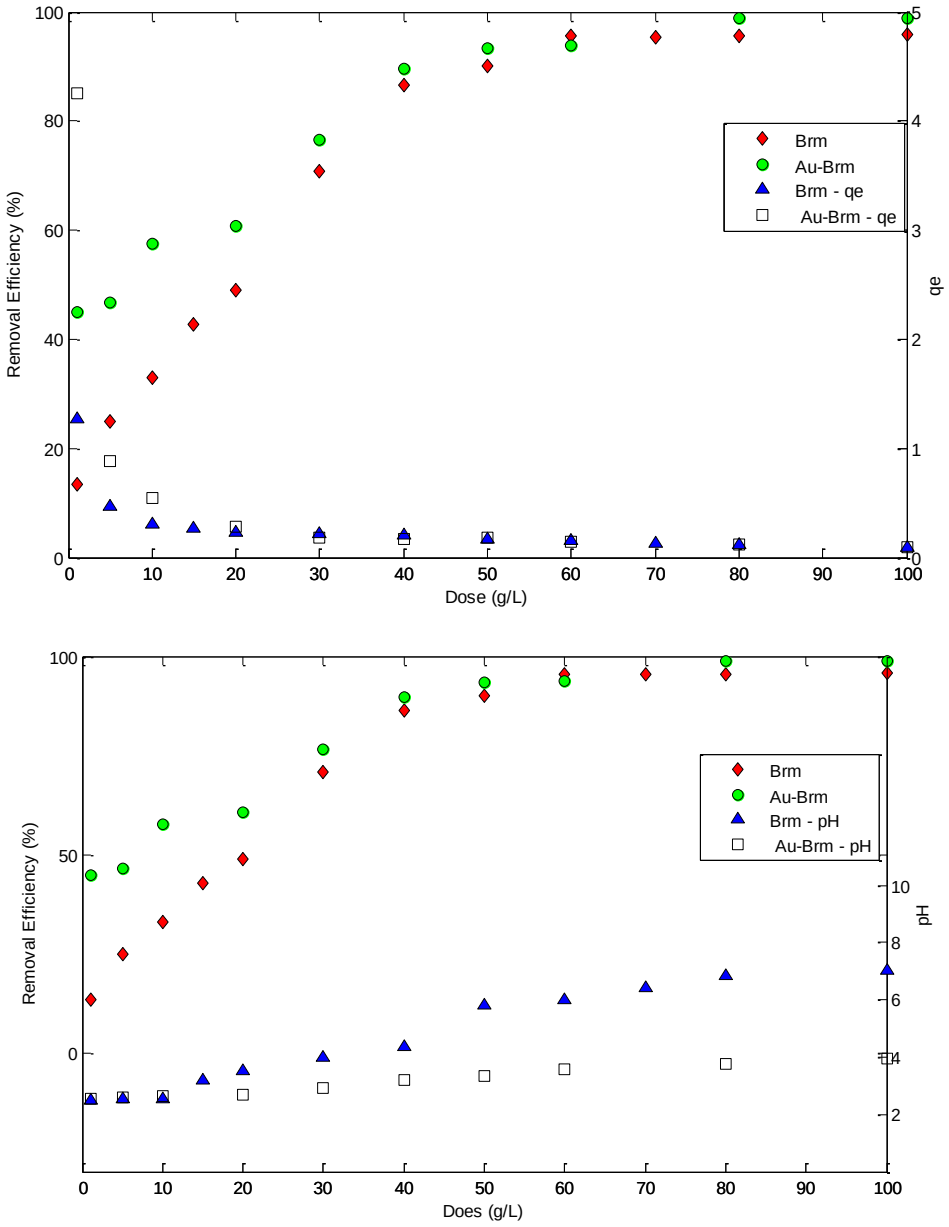

Figure 3-8: (a) Removal efficiency and adsorption capacity as a function of adsorbent dose of Brm and Au-Brm (experimental conditions: 10 ml Hg(II) 10 mg/L, initial pH≈2.5 at room temperature). (b) Removal efficiency and pH as a function of adsorbent dose of Brm and Au-Brm (experimental conditions: 10 ml Hg(II) 10 mg/L, initial pH≈2.5 at room temperature).

It can be concluded that for LTA, Au/Fe-LTA and Brm adsorbents the maximum removal efficiency would be achieved at higher pH. Essentially increasing pH has influence on the final removal efficiency in two opposing ways [9]. Deprotonating and negatively charge of the zeolite surface result in attracting metal ions and increase the adsorption of metal on the surface of adsorbent. Alkaline environment decreases metal solubility and causes metal precipitation which may mask the true metal sorption on adsorbent. Therefore, at pH higher than 4, $Hg(OH)_2$ is the dominant species, which can be removed from the aqueous solution by preferential precipitation on the surface of the adsorbent. However, the precipitated mercury species on the surface of the adsorbent could be later adsorbed by means of other physicochemical mechanism (Faulconer, et al 2012; Malamis and Katsou 2013).

It was observed that for Au-Brm samples, the final pH of solution is acidic for the entire range of the tested dosages. According to Table 4 the primarily species are Hg^{2+}, $(Hg OH)^{+}$ and $Hg (OH)_2$ in the pH range of 2.5 to 4. In such an acidic environment the performance of most adsorbents reduces due to the presence of protons that competes with mercury ions for the available adsorption sites [61]. Consequently, the overall removal efficiency and adsorption capacity of Au-Brm sample in such an acidic solution indicate its high capability as a remarkable adsorbent for mercury. Figures 7A and 8A illustrate the changes in removal efficiency of adsorbents as a function of adsorbent mass compared to the mercury adsorption capacity.

Obviously, the removal efficiency of all adsorbents increases by increasing adsorbent load, while mercury adsorption capacity decreases steadily. In fact, at higher adsorbent dosage, the available surface area increases, while at the same time the accumulation of the adsorbent can decrease the true accessible binding sites. Accordingly, all these phenomena diminish attraction between mercury ions and adsorbent surface might result desorption of mercury ions from the surface of adsorbent. The same phenomena have been reported by several studies [7], [9], [19], [33], [58], [62], [63].

3.3.5 Effect of Contact Time

To determine the equilibrium time for each zeolitic sample, optimized amounts of zeolites (i.e., (70 g/L) for Brm, (50 g/L) for Au-Brm, (10 g/L) for LTA and Au/Fe-LTA) were added to 10 ml of mercury solution (10 mg/L) for 1 to 24 hours (Figure 3-9). Experimental data revealed that LTA and Au/Fe-LTA reached the equilibrium point after 3 hours, however the initial adsorption rate of Au/Fe-LTA was very fast and more than 97% of the mercury was removed from the solution in 5 minutes. For the LTA with the same dosage, however, ~ 80% of Hg (II) was removed during the first 5 minutes of the reaction. The removal efficiency then gradually increased to reach the highest value after 240 minutes as it is illustrated in Figure 3-9b.

The time required to reach sorption equilibrium was ~24 h for Brm and Au-Brm samples (Figure 3-9a). In the case of untreated natural sample (Brm) with 70 g/L the initial adsorption rate was slower, which resulted in a 68% of mercury removal after 15 minutes. While the Au-Brm sample with 50 g/L adsorbent dosage reached a 75% removal efficiency at similar contact time. These results confirmed the experimental data from other studies indicating that natural zeolites need more time to reach equilibrium, which make them inappropriate for application in adsorption in continuous systems. The changes in adsorption capacity of examined adsorbents as a function of time are illustrated in the same Figure 3-9. The adsorption capacity of all samples gradually increases as time progresses; however, the increasing rate of the adsorption capacity is slower for the Brm and Au-Brm samples.

PH change of the solution as a function of time was investigated for all adsorbents (Appendix B, Figure S2). Before adding adsorbents, the pH of Hg (II) aqueous solution was set at 2.5. After 5 min of first contact, the pH values of Brm (70 g/L) , Au-Brm (50 g/L), LTA (10 g/L) and Au/Fe-LTA(10 g/L) reached to 6.11, 3.01, 9.41 and 6.15, respectively, and the solutions pH did not change significantly after that time.

It can be concluded that modification of the natural clinoptilolite and the synthetic zeolite LTA could considerably increase the initial adsorption rate. Such rapid initial adsorption rate is very important especially in continuous adsorption systems.

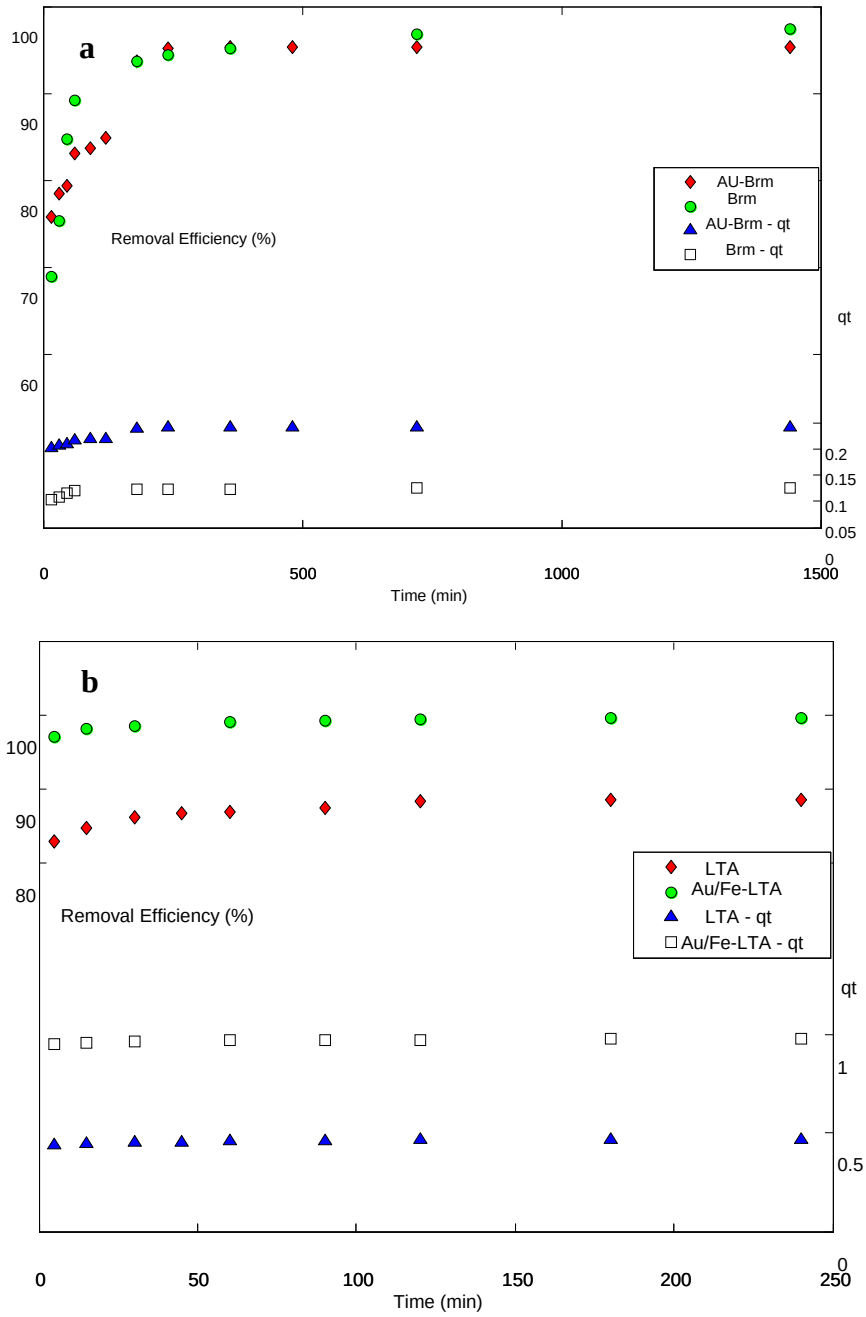

Figure 3-9: Removal efficiency and adsorption capacity of (a) Brm (70 g/L), Au-Brm(50 g/L) and (b) LTA, Au/Fe-LTA (10 g/L) towards Hg(II) as a function of time (experimental conditions: Hg(II) 10 mg/L, initial pH≈2.5 at room temperature).

3.3.6 Adsorption Kinetic

Adsorption reaction models and adsorption diffusion models are mathematical models, which have been proposed to describe experimental data. To evaluate the kinetics of the adsorption process, the pseudo first-order, the pseudo second-order and the Elovich models were tested to interpret the adsorption process. The intra-particle diffusion model were tested to describe the main steps of adsorption of Hg(II) on the examined adsorbents [44], [45]. The obtained parameters of kinetic and diffusion models are summarized in Tables 3-5, 3-6, and 3-7.

The applicability and validity of all these models was assessed by comparing the R^2 values of their linear plots and also applying the Chi-square test (Eq.3) to experimental data (Table 3-5b).

Table 3-5: Calculated kinetic model constants for the adsorption of Hg(II) on Brm, Au-Brm, LTA and Au/Fe-LTA (Experimental condition: Hg(II) 10 mg/L, pH at ≈ 2.5 at room temperature).

Adsorbent	**Pseudo-first-order**			**Pseudo-second-order**				**Elovich**		
	K (min^{-1})	q_e	R^2	K_2 (g/mg.min)	R^2	q_e (mg/g) Experimental	q_e (mg/g) Calculated	A (g/mg.min)	B=1/b (g/mg)	R^2
Brm	0.005	0.012	0.8721	1.6833	1	0.07622	0.0766	67.068	212.765	0.8213
Au-Brm	0.0118	0.038	0.8937	0.6984	0.9999	0.1927	0.1942	1046.07	92.592	0.8693
LTA	0.0354	0.051	0.9203	2.284	1	0.468	0.469	5.65*10E20	123.45	0.9799
Au/Fe-LTA	0.0145	0.022	0.979	2.6287	1	0.979	0.9796	9.22*10E58	149.27	0.9909

Table 3-6: Calculated X2 values for the adsorption of Hg(II) on Brm, Au-Brm, LTA and Au/Fe-LTA(Experimental condition: Hg(II) 10 mg/L, pH at ≈ 2.5 at room temperature).

Adsorbent	X^2 for Pseudo-first-order	X^2 for Pseudo-second-order
Brm	0.34	1.8*10 -6
Au-Brm	0.62	1.15*10 -5
LTA	3.4	2.13*10 -6
Au/Fe-LTA	43.29	3.67*10 -7

3.3.6.1 Pseudo-first Order Kinetic

Lagergen equation also known as pseudo-first order model is the predominantly used sorption rate equations, which is expressed by the following equation:

$$\ln (q_e - q_t) = \ln q_e - k_1 t \quad (4)$$

where $k_1$is the rate constant of the pseudo-first order equation (min^{-1}), q_t and q_e (mg /g) are the amounts of the metal ions adsorbed at time t (min) and at equilibrium, respectively.

The values of $k_1$and q_e can be determined by the slope of linear plots of $\ln(q_e - q_t)$ against t (Appendix B, Figure S3).

The R^2 values for Brm and Au-Brm adsorbents were relatively low indicating poor relationships between the parameters. In addition, there is a poor agreement between the experimental equilibrium adsorption and q_e derived using Eq. (4). This implies that the Hg(II) sorption process by these adsorbents did not follow a pseudo first-order kinetics.

R^2 values for LTA and Au/Fe-LTA are 0.9203 and 0.9713, respectively, which are relatively good (Tables 3-5, 3-6). However, the calculated sorption capacity obtained from first order kinetic model did not fit reasonably the experimental sorption capacity. These results suggest that this equation may not be an appropriate model to described the adsorption of Hg(II) on raw and modified zeolite LTA.

3.3.6.2 Pseudo- second Order Kinetic

The second order kinetic model may be expressed on the basis of following linear equation proposed by Ho in 1995[44], [58]:

$$t/q_t = 1/(k_2\, q_e^2) + (1/q_e).t \qquad (5)$$

where k_2 is the second order rate constant (g/mg.min) and q_e and q_t are the equilibrium and temporal concentrations. If the second-order kinetics is applicable, the plot of experimental values of t/q_t against t should give a linear relationship [47], [64]. Kinetic constant q_e and K were calculated from the slope and intercept of this plot (Figure 3-10, Table 3-2).

The correlation coefficients values; R^2, for the pseudo second order kinetic model fits are 1.00 for LTA, Au-Fe-LTA and Brm and 0.9999 for Au-Brm. Moreover, the calculated equilibrium adsorption capacities derived from pseudo second order equation are in close agreement with those observed experimentally. This suggests that the data strongly fit Eq. 5 and the adsorption of Hg (II) on all adsorbents follow the pseudo-second order rate more closely compared to the pseudo-first-order.

Also it is strongly recommended that the adsorption is resulted by a chemical interaction as assumed in this model, considering the valence forces through sharing or exchange of electrons between active binding sites of sorbent surface and metal ions [45], [65]. Other studies have reported similar trends for adsorption of Hg(II) ions from aqueous solution by other adsorbents.

Table 3-6 presents the X^2 values for all examined models. From Chi-square equation it was concluded that lowest X^2 values for second order equation suggest similarity between data from model and experiment.

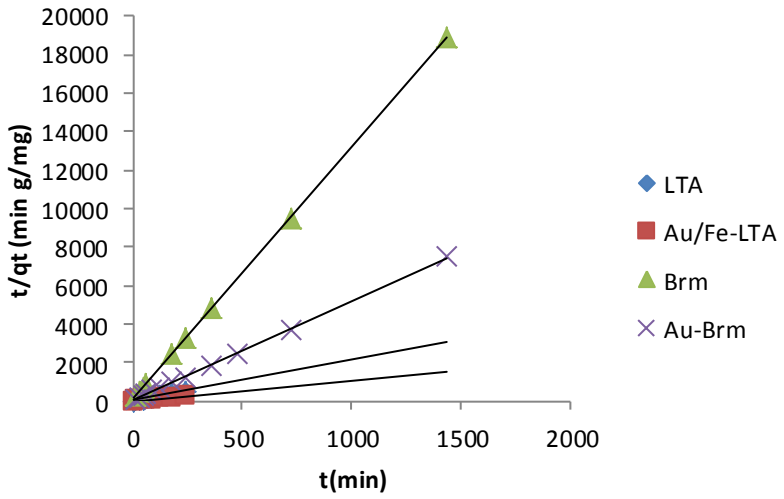

Figure 3-10: Application of the pseudo-second-order model (Eq.(5)) to the experimental data of Figure 8. (experimental conditions: Hg(II) 10 mg/L, Adsorbent Brm, Au-Brmand (b) LTA, Au/Fe-LTA (pH ≈ 2.5 at room temperature).

3.3.6.3 The Elovich Kinetic Model

The Elovich kinetic Model was first established to describe the adsorption of gas on solid systems. Recently, however, it is used for effectively describing the adsorption of pollutants from aqueous solutions. The Elovich model is described by the following equation:

$$dq_t/d_t = \alpha \exp(-\beta q_t) \quad (6)$$

Integration of the Elovich with boundary conditions $q_t = q_t$ at t and $q_t = 0$ at $t = 0$ and assuming $\alpha \beta t >> 1$, leads to the following linear equation:

$$q_t = \beta \ln(\alpha\beta) + \beta \ln(t) \quad (7)$$

Where α is the initial adsorption rate (g/(mg.min)) and β represents the desorption rate (mg/(g.min)) and is related to the number of sites available for adsorption [42], [45], [58].

The Elovich equation constants can be calculated from the slope and intercept of q_t vs. ln(t) plot (Figure S4, Table 3-2).

Based on regression coefficients, the Elovich model is successful in describing the kinetics of adsorption by LTA and Au/Fe LTA adsorbents. It describes activated adsorption for these two adsorbents and assumes an energetically heterogeneous solid surface of sorbent. This means that the kinetics of adsorption is not affected by interaction between the adsorbed particles [58], [66].

However, the R^2 values were very low for Brm and Au-Brm adsorbents indicating poor fitting of adsorption Elovich parameters.

3.3.7 Adsorption Mechanism

The intra-particle diffusion model was applied to the experimental results to find the adsorption rate-controlling mechanism. The adsorption rate of a metal species by a porous adsorbent can be described by the following three steps: (1) the adsorbate is transported from the bulk solution to the external surface of the adsorbent (film or surface diffusion); (2) the adsorbate is transported within the pores and interior of adsorbent particles (intraparticle or pore diffusion; although a small amount of adsorption occurs on the external surface which is called particle diffusion), and finally (3) the adsorbate is adsorbed on the interior sites of the adsorbent.

Obviously the slowest of these transport steps would determine the overall rate of adsorption [22], [47], [58], [67]. Since the third step is very rapid, the overall kinetic of adsorption will be controlled by either film diffusion or intra particle diffusion. The intra particle diffusion model is based on the theory proposed by Weber and Moris and is represented by:

$$q_t = k_d\, t^{0.5} + \theta \qquad (8)$$

where K_d (mg/g.min$^{1/2}$) is the intra particle diffusion rate constant and θ (mg/g) is a constant related to the thickness of boundary layer [47], [57], [68].

If the plot of q_t versus $t^{0.5}$ is linear, then the intra particle diffusion is involved in the adsorption process. In addition, the intra particle diffusion is the sole rate-limiting step if the plot passes through the origin. While a multi linear q_t versus $t^{0.5}$ graph indicates that two or more stages are involved in the adsorption process.

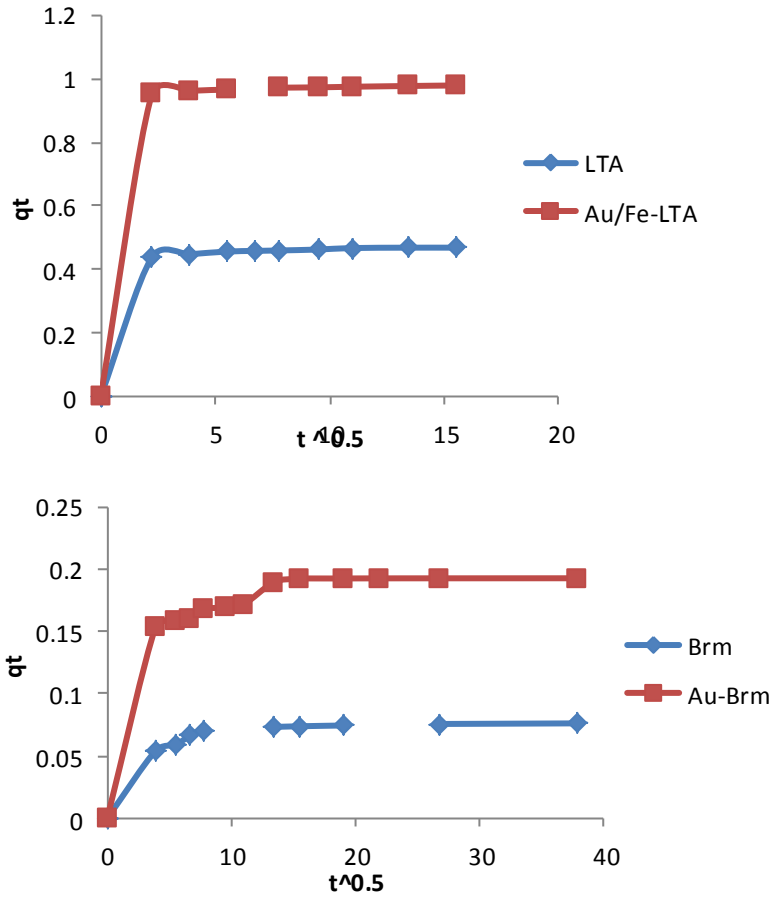

Figure 3-11: Test of the intra particle diffusion model (Eq.(4)) to the experimental data of Figure 8 (experimental conditions: Hg(II) 10 mg/L, Adsorbent Brm , Au-Brm and (b) LTA, Au/Fe-LTA , pH ≈ 2.5 at room temperature).

As it is illustrated in Figure 3-11 the plot of Hg(II) adsorbed amount (q_t) versus square root of time for LTA and Au/Fe-LTA presents a multi linear two steps process. This suggests that adsorption occurred in two phases. Initially, the rate of metal removal from

the solution is very rapid. This higher rate corresponds to the external surface or film diffusion (i.e., boundary layer effect). In the second linear section, the adsorption gradually increases since equilibrium had almost been reached. In this part intraparticle or pore diffusion is the rate limiting.

For Brm and Au-Brm samples, multi-linear plots were observed indicating multiple rate-limiting steps. The initial sharper stage represents surface diffusion, the second linear section represents intra particle or pore diffusion when adsorption is gradually increasing. The last stage is the final equilibrium stage.

The results suggest that (a) LTAs samples demonstrate immediate uptake of Hg(II) at a much higher capacity than Brm and Au-Brm adsorbents. (b) The intra particle diffusion does not seem to be the only rate-limiting step as none of the plots pass through the origin. (c) Two processes (for Brm and Au-Brm) and three processes (LTA and Au/Fe-LTA) are controlling the adsorption rate but in any particular time range only one process is the rate limiting.

Table 3-7 illustrates the rate constant k_i that was calculated from the slope of the second linear stage. In addition, the thickness of the boundary layer is related to the value of intercept θ. Larger intercepts indicate a more important role of surface diffusion as the rate limiting step. Comparing θ values for raw and modified zeolites, suggests that for both Au-Brm and Au/Fe-LTA the surface diffusion is more vital because of the surface modification.

3.3.8 Adsorption Isotherms

An adsorption isotherm defines the fraction of metal molecules that are distributed between liquid and solid phases at equilibrium. They may also provide information on the surface properties and affinity of the adsorbent to reach its highest capacity. To study the isothermal behaviour of adsorbents, varying weights of dried adsorbent were added to a constant volume of 10 mg/L of Hg(II) solution for 24 hours to assure equilibrium. Results were analyzed using Langmuir, Freundlich and Temkin models. The correlation

coefficient used to assess the quality of the fit. The models' parameters are listed in Table 8.

Table 3-7: Calculated intra particle diffusion constants for the adsorption of Hg(II) (Experimental condition: Hg(II) 10 mg/L, Adsorbent Brm, Au-Brm and (b) LTA, Au/Fe-LTA , pH at ≈ 2.5 at room temperature).

Adsorbent Dose g/L	**K_i (mg/g.min$^{1/2}$)**	**θ**	**R^2**
Brm	0.0048	0.033	0.9757
Au-Brm	0.0036	0.1375	0.904
LTA	0.0021	0.4425	0.9193
Au/Fe-LTA	0.0016	0.9573	0.9397

The Langmuir isothermal constants q_m and K are determined from the intercept and slope of a plot C_e/q_e versus C_e for all examined adsorbents. As it is illustrated in Table 7 the Langmuir correlation coefficient values for Hg (II) adsorption onto all adsorbents are relatively high (i.e., $R^2 > 0.95$) indicating good agreement between model parameters and observed behaviour. The Langmuir model represents monolayer adsorption on specific homogenous sites.The mercury adsorption capacity on Au-Brm sample was 0.3115 mg/g which is much higher than the adsorption capacity of other examined adsorbents.

The R_L is a dimensionless equilibrium constant given as:

$$R_L=1/(1+bC_0) \quad (9)$$

Table 3-8: Calculated Langmuir, Freundlich and Temkin parameters for the adsorption of Hg(II) on Brm, Au-Brm and LTA and Au/Fe-LTA (range of

adsorbent dose from 0.05 g to 1 g) - Experimental condition: Hg(II) 10 mg/L, equilibrium time 24 h, pH at ≈ 2.5 at room.

	Freundlich				Langmuir				Tempkin		
Adsorbent	K_f $(mg/g)(mg/L)^n$	n_f	$1/n_f$	R^2	q_m(mg/g)	K_L(l/mg)	R_L	R^2	K_1 (L/g)	K_2	R^2
Brm	**0.1574**	**4.081**	**0.24**	**0.9844**	**0.2335**	**3.741**	**0.0276**	**0.9762**	**0.0362**	**96.987**	**0.9378**
Au-Brm	**0.1780**	**2.1317**	**0.46**	**0.9193**	**0.3115**	**2.2036**	**0.0460**	**0.9785**	**0.0713**	**26.255**	**0.7431**
LTA	**0.2746**	**-0.6311**	**1.58**	**0.9946**	**0.0426**	**-1.0354**	**0.1219**	**0.9587**	**-0.2455**	**0.3417**	**0.9063**
Au/Fe-LTA	**198.34**	**0.7411**	**1.34**	**0.9243**	**0.0087**	**-100.243**	**0.0011**	**0.9837**	**5.1278**	**91.698**	**0.8162**

Where C_0 is the initial concentration and b is the Langmuir constant. R_L between 0 and 1 indicates favourable adsorption, while $R_L>1$ indicates unfavourable adsorption, $R_L=1$ is linear and irreversible adsorption is suggested for $R_L = 0$ [60]. As it can be seen from Table 3-8 the calculated R_L values are between 0 and 1 which suggest favourable adsorption mechanism.

The slope and intercept of plots of log q_e versus log C_e, were used to calculate Freundlich isotherm constants K_F and n. Based on the data, Freundlich model can describe adequately the adsorption isotherm of Hg (II) onto Brm, Au-Brm, LTA and Au/Fe-LTA with R^2 values of 0.9844, 0.9193, 0.9946 and 0. 9243.

It is suggested that K_f is associated with the adsorption capacity and n_f is represented as the adsorption intensity. So the greater values of K_f for Au/Fe-LTA correspond to a greater capacity of the adsorbent. The values of $1/ n_f$ parameter were obtained from applying Freundlich linearized equation to the experimental data are between 0 and 1. The smaller the values of $1/n_f$ the stronger is the adsorption bond. From Table 3-8 the smallest value of $1/ n_f$ belonged to Au-Brm indicating the highest affinity between adsorbate and adsorbent and is suggestive of chemisorption (L-type isotherms).

Linear plots for Temkin adsorption isotherms are developed (Table 3-8), considering uniform distribution of the binding energies; up to some maximum binding energy. It also assumes chemisorption of an adsorbate onto the adsorbent. The good correlation coefficients values for Brm and LTA samples support the findings that the adsorption of Hg (II) onto these adsorbents is a chemisorption process.

3.3.9 Conclusions

Zeolite LTA and natural clinoptilolite can be used as effective adsorbents for removing mercury from contaminated water and wastewater streams. Modifying the natural zeolite with gold and bimetallic modification of zeolite LTA significantly increased mercury adsorption rate, adsorption capacity, and removal efficiency. EDX and XRD analysis confirmed that gold and iron modified the surface of parent zeolites. The pseudo second order kinetic model accurately described the adsorption kinetics. The adsorption mechanism was found to be chemisorption and the rate-limiting step was mainly surface adsorption for all raw and modified samples. Both the Langmuir and Freundlich isotherms showed good agreement with experimental data, indicating both chemisorption and physisorption counterpart in the adsorption process.

Results from this study suggest that both natural clinoptilolite (Bromley, Canada) and the synthetic zeolite LTA are very effective adsorbents for Hg(II) and their modifications with iron and gold successfully increase their efficacy.

Bibliography

[1] “Technical Background Report for the Global Mercury Assessment,” 2013.

[2] J. Kulkarni, “Studies and Research on Mercury Removal from Water : A Review Abstract :,” no. 2, pp. 221–225, 2015.

[3] K. J. Lee and T. G. Lee, “A review of international trends in mercury management and available options for permanent or long-term mercury storage.,” *J. Hazard. Mater.*, vol. 241–242, pp. 1–13, Nov. 2012.

[4] N. E. Selin, “Global Biogeochemical Cycling of Mercury: A Review,” *Annu. Rev. Environ. Resour.*, vol. 34, no. 1, pp. 43–63, Nov. 2009.

[5] T. A. Kurniawan, G. Y. S. Chan, W. Lo, and S. Babel, “Comparisons of low-cost adsorbents for treating wastewaters laden with heavy metals.,” *Sci. Total Environ.*, vol. 366, no. 2–3, pp. 409–26, Aug. 2006.

[6] S. Sen Gupta and K. G. Bhattacharyya, “Kinetics of adsorption of metal ions on inorganic materials: A review.,” *Adv. Colloid Interface Sci.*, vol. 162, no. 1–2, pp. 39–58, Feb. 2011.

[7] S. Babel and T. A. Kurniawan, “Low-cost adsorbents for heavy metals uptake from contaminated water : a review,” vol. 97, pp. 219–243, 2003.

[8] F. Di Natale, A. Erto, A. Lancia, and D. Musmarra, “Mercury adsorption on granular activated carbon in aqueous solutions containing nitrates and chlorides,” *J. Hazard. Mater.*, vol. 192, no. 3, pp. 1842–1850, 2015.

[9] P. Hadi, M.-H. To, C.-W. Hui, C. S. K. Lin, and G. McKay, “Aqueous mercury adsorption by activated carbons.,” *Water Res.*, vol. 73, pp. 37–55, Apr. 2015.

[10] M. N. Sepehr, M. Zarrabi, H. Kazemian, A. Amrane, K. Yaghmaian, and H. R. Ghaffari, “Removal of hardness agents, calcium and magnesium, by natural and alkaline modified pumice stones in single and binary systems,” *Appl. Surf. Sci.*, vol. 274, pp. 295–305, Jun. 2013.

[11] B. R. Albert, A. K. Cheetham, J. A. Stuart, and C. J. Adams, “Investigations on P zeolites : synthesis , characterisation , and structure of highly crystalline low-silica NaP,” vol. 21, pp. 133–142, 1998.

[12] J. Behin, S. S. Bukhari, V. Dehnavi, H. Kazemian, and S. Rohani, “Using Coal Fly Ash and Wastewater for Microwave Synthesis of LTA Zeolite,” *Chem. Eng. Technol.*, vol. 37, no. 9, pp. 1532–1540, Sep. 2014.

[13] S. Wang and Y. Peng, “Natural zeolites as effective adsorbents in water and wastewater treatment,” *Chem. Eng. J.*, vol. 156, no. 1, pp. 11–24, Jan. 2010.

[14] H. Figueiredo and C. Quintelas, “Tailored zeolites for the removal of metal oxyanions: overcoming intrinsic limitations of zeolites.,” *J. Hazard. Mater.*, vol. 274, pp. 287–99, Jun. 2014.

[15] P. L. Smedley and D. G. Kinniburgh, “Chapter 1 . Source and behaviour of arsenic in natural waters Importance of arsenic in drinking water.”

[16] B. Daus, R. Wennrich, and H. Weiss, “Sorption materials for arsenic removal from water : a comparative study,” vol. 38, pp. 2948–2954, 2004.

[17] T. S. Jamil, H. S. Ibrahim, I. H. Abd El-Maksoud, and S. T. El-Wakeel, “Application of zeolite prepared from Egyptian kaolin for removal of heavy metals: I. Optimum conditions,” *Desalination*, vol. 258, no. 1–3, pp. 34–40, Aug. 2010.

[18] A. a. Al-Shammari, S. a. Ali, N. Al-Yassir, A. M. Aitani, K. E. Ogunronbi, K. a. Al-Majnouni, and S. S. Al-Khattaf, “Catalytic cracking of heavy naphtha-range hydrocarbons over different zeolites structures,” *Fuel Process. Technol.*, vol. 122, pp. 12–22, Jun. 2014.

[19] K. S. Hui, C. Y. H. Chao, and S. C. Kot, “Removal of mixed heavy metal ions in wastewater by zeolite 4A and residual products from recycled coal fly ash.,” *J. Hazard. Mater.*, vol. 127, no. 1–3, pp. 89–101, Dec. 2005.

[20] H. S. Ibrahim, T. S. Jamil, and E. Z. Hegazy, “Application of zeolite prepared from Egyptian kaolin for the removal of heavy metals: II. Isotherm models.,” *J. Hazard. Mater.*, vol. 182, no. 1–3, pp. 842–7, Oct. 2010.

[21] N. G. Turan and O. Ozgonenel, “The design and implementation of adsorptive removal of Cu(II) from leachate using ANFIS.,” *ScientificWorldJournal.*, vol. 2013, p. 590267, Jan. 2013.

[22] S. Malamis and E. Katsou, “A review on zinc and nickel adsorption on natural and modified zeolite, bentonite and vermiculite: examination of process parameters, kinetics and isotherms.,” *J. Hazard. Mater.*, vol. 252–253, pp. 428–61, May 2013.

[23] M. M. J. Treacy and J. B. Higgins, *Collection of simulated XRD powder patterns for zeolites*. Amsterdam, The Netherlands: Elsevier, 2007.

[24] H. Van Koningsveld and J. M. Bennett, “Zeolite Structure Determination from X-Ray Diffraction,” vol. 2, pp. 1–29, 1999.

[25] S. S. Bukhari, J. Behin, H. Kazemian, and S. Rohani, “Conversion of coal fly ash to zeolite utilizing microwave and ultrasound energies: A review,” *Fuel*, vol. 140, pp. 250–266, Jan. 2015.

[26] S. N. Azizi, A. R. Dehnavi, and A. Joorabdoozha, “Synthesis and characterization of LTA nanozeolite using barley husk silica: Mercury removal from standard and real solutions,” *Mater. Res. Bull.*, vol. 48, no. 5, pp. 1753–1759, May 2013.

[27] M. Trgo, J. Perić, N. V. Medvidović, M. Ugrina, I. Nuić, M. Macherzynsky, Ł. Uruski, and J. Golas, “MERCURY IONS CAPTURE BY NATURAL AND IRON-MODIFIED ZEOLITE - INFLUENCE OF SOLID / LIQUID RATIO,” pp. 36–39.

[28] a. Chojnacki, K. Chojnacka, J. Hoffmann, and H. Górecki, “The application of natural zeolites for mercury removal: from laboratory tests to industrial scale,” *Miner. Eng.*, vol. 17, no. 7–8, pp. 933–937, Jul. 2004.

[29] J. Groen, a Bruckner, E. Berrier, L. Maldonado, J. Moulijn, and J. Perezramirez, “Iron site modification upon alkaline treatment of Fe-ZSM-5 zeolites—Opportunities for improved N2O decomposition activity,” *J. Catal.*, vol. 243, no. 1, pp. 212–216, Oct. 2006.

[30] R. J. White, R. Luque, V. L. Budarin, J. H. Clark, and D. J. Macquarrie, “Supported metal nanoparticles on porous materials . Methods and applications,” no. September 2008, pp. 481–494, 2009.

[31] K. P. Lisha and T. Pradeep, “Towards a practical solution for removing inorganic mercury from drinking water using gold nanoparticles,” *Gold Bull.*, vol. 42, no. 2, pp. 144–152, Jun. 2009.

[32] J. Groen, a Bruckner, E. Berrier, L. Maldonado, J. Moulijn, and J. Perezramirez, “Iron site modification upon alkaline treatment of Fe-ZSM-5 zeolites—Opportunities for improved N2O decomposition activity,” *J. Catal.*, vol. 243, no. 1, pp. 212–216, Oct. 2006.

[33] M. J. Jiménez-Cedillo, M. T. Olguín, C. Fall, and a. Colín, “Adsorption capacity of iron- or iron–manganese-modified zeolite-rich tuffs for As(III) and As(V) water pollutants,” *Appl. Clay Sci.*, vol. 54, no. 3–4, pp. 206–216, Dec. 2011.

[34] P. Xu, G. M. Zeng, D. L. Huang, C. L. Feng, S. Hu, M. H. Zhao, C. Lai, Z. Wei, C. Huang, G. X. Xie, and Z. F. Liu, “Use of iron oxide nanomaterials in wastewater treatment: a review.,” *Sci. Total Environ.*, vol. 424, pp. 1–10, May 2012.

[35] N. Bogdanchikova, a. Simakov, E. Smolentseva, a. Pestryakov, M. H. Farias, J. a. Diaz, a. Tompos, and M. Avalos, “Stabilization of catalytically active gold species in Fe-modified zeolites,” *Appl. Surf. Sci.*, vol. 254, no. 13, pp. 4075–4083, Apr. 2008.

[36] I. Sobczak, H. Pawlowski, J. Chmielewski, and M. Ziolek, “Gold and gold-iron modified zeolites--towards the adsorptive deodourisation.,” *J. Hazard. Mater.*, vol. 179, no. 1–3, pp. 444–52, Jul. 2010.

[37] J. H. Chen, J. N. Lin, Y. M. Kang, W. Y. Yu, C. N. Kuo, and B. Z. Wan, “Preparation of nano-gold in zeolites for CO oxidation: Effects of structures and number of ion exchange sites of zeolites,” *Appl. Catal. A Gen.*, vol. 291, no. 1–2, pp. 162–169, 2005.

[38] I. Sobczak, H. Pawlowski, J. Chmielewski, and M. Ziolek, “Gold and gold-iron modified zeolites--towards the adsorptive deodourisation.,” *J. Hazard. Mater.*, vol. 179, no. 1–3, pp. 444–52, Jul. 2010.

[39] C. Baatz, N. Decker, and U. Pruse, “New innovative gold catalysts prepared by an improved incipient wetness method,” *J. Catal.*, vol. 258, no. 1, pp. 165–169, Aug. 2008.

[40] X. Zhu and S. D. Alexandratos, “Determination of trace levels of mercury in aqueous solutions by inductively coupled plasma atomic emission spectrometry: Elimination of the ‘memory effect,’” *Microchem. J.*, vol. 86, no. 1, pp. 37–41, 2007.

[41] H. Zheng, D. Liu, Y. Zheng, S. Liang, and Z. Liu, “Sorption isotherm and kinetic modeling of aniline on Cr-bentonite,” *J. Hazard. Mater.*, vol. 167, no. 1–3, pp. 141–147, 2009.

[42] K. P. Raven, A. Jain, and R. H. Loeppert, “Arsenite and Arsenate Adsorption on Ferrihydrite: Kinetics, Equilibrium, and Adsorption Envelopes,” *Environ. Sci. Technol.*, vol. 32, no. 3, pp. 344–349, Feb. 1998.

[43] R. Barzamini, C. Falamaki, and R. Mahmoudi, “Adsorption of ethyl, iso-propyl, n-butyl and iso-butyl mercaptans on AgX zeolite: Equilibrium and kinetic study,” *Fuel*, vol. 130, pp. 46–53, 2014.

[44] D. Robati, “Pseudo-second-order kinetic equations for modeling adsorption systems for removal of lead ions using multi-walled carbon nanotube,” *J. Nanostructure Chem.*, vol. 3, no. 1, p. 55, 2013.

[45] F. Raji and M. Pakizeh, “Kinetic and thermodynamic studies of Hg(II) adsorption onto MCM-41 modified by ZnCl2,” *Appl. Surf. Sci.*, vol. 301, pp. 568–575, May 2014.

[46] H. K. Boparai, M. Joseph, and D. M. O’Carroll, “Kinetics and thermodynamics of cadmium ion removal by adsorption onto nano zerovalent iron particles,” *J. Hazard. Mater.*, vol. 186, no. 1, pp. 458–465, 2011.

[47] R. Arasteh, M. Masoumi, a. M. Rashidi, L. Moradi, V. Samimi, and S. T. Mostafavi, “Adsorption of 2-nitrophenol by multi-wall carbon nanotubes from aqueous solutions,” *Appl. Surf. Sci.*, vol. 256, no. 14, pp. 4447–4455, May 2010.

[48] K. State and E. State, “Langmuir , Freundlich , Temkin and Dubinin – Radushkevich Isotherms Studies of Equilibrium Sorption of Zn 2 + Unto Phosphoric Acid Modified Rice Husk,” *IOSR J. Appl. Chem.*, vol. 3, no. 1, pp. 38–45, 2012.

[49] S. Saha and P. Sarkar, “Arsenic remediation from drinking water by synthesized nano-alumina dispersed in chitosan-grafted polyacrylamide.,” *J. Hazard. Mater.*, vol. 227–228, pp. 68–78, Aug. 2012.

[50] a. Deepatana and M. Valix, “Comparative adsorption isotherms and modeling of nickel and cobalt citrate complexes onto chelating resins,” *Desalination*, vol. 218, no. 1–3, pp. 334–342, Jan. 2008.

[51] R. Han, L. Zou, X. Zhao, Y. Xu, F. Xu, Y. Li, and Y. Wang, “Characterization and properties of iron oxide-coated zeolite as adsorbent for removal of copper(II) from solution in fixed bed column,” *Chem. Eng. J.*, vol. 149, no. 1–3, pp. 123–131, Jul. 2009.

[52] D. C. Bain and B. F. L. Smith, “Chemical analysis,” in *Handbook of determinative methods in clay mineralogy*, Glasgow: Blackie, 1987, pp. 248–274.

[53] S. Yang, M. Lach-hab, I. I. Vaisman, E. Blaisten-Barojas, X. Li, and V. L. Karen, “Framework-Type Determination for Zeolite Structures in the Inorganic Crystal Structure Database,” *J. Phys. Chem. Ref. Data*, vol. 39, no. 3, p. 033102, 2010.

[54] S. S. Bukhari, J. Behin, H. Kazemian, and S. Rohani, “Synthesis of zeolite Na-A using single mode microwave irradiation at atmospheric pressure: The effect of microwave power,” *Can. J. Chem. Eng.*, p. n/a–n/a, Mar. 2015.

[55] A. Corma, M. J. Díaz-Cabañas, J. Martínez-Triguero, F. Rey, and J. Rius, “A large-cavity zeolite with wide pore windows and potential as an oil refining catalyst.,” *Nature*, vol. 418, no. 6897, pp. 514–517, 2002.

[56] a M. Starvin and T. P. Rao, “Removal and recovery of mercury(II) from hazardous wastes using 1-(2-thiazolylazo)-2-naphthol functionalized activated carbon as solid phase extractant.,” *J. Hazard. Mater.*, vol. 113, no. 1–3, pp. 75–9, Sep. 2004.

[57] D. Mohan and C. U. Pittman, “Arsenic removal from water/wastewater using adsorbents--A critical review.,” *J. Hazard. Mater.*, vol. 142, no. 1–2, pp. 1–53, Apr. 2007.

[58] S. Sen Gupta and K. G. Bhattacharyya, “Kinetics of adsorption of metal ions on inorganic materials: A review.,” *Adv. Colloid Interface Sci.*, vol. 162, no. 1–2, pp. 39–58, Feb. 2011.

[59] O. Rodríguez, I. Padilla, H. Tayibi, and A. López-Delgado, “Concerns on liquid mercury and mercury-containing wastes: a review of the treatment technologies for the safe storage.,” *J. Environ. Manage.*, vol. 101, pp. 197–205, Jun. 2012.

[60] E. K. Faulconer, N. V. H. von Reitzenstein, and D. W. Mazyck, “Optimization of magnetic powdered activated carbon for aqueous Hg(II) removal and magnetic recovery.,” *J. Hazard. Mater.*, vol. 199–200, pp. 9–14, Jan. 2012.

[61] E. Katsou, S. Malamis, M. Tzanoudaki, K. J. Haralambous, and M. Loizidou, “Regeneration of natural zeolite polluted by lead and zinc in wastewater treatment systems,” *J. Hazard. Mater.*, vol. 189, no. 3, pp. 773–786, 2011.

[62] M. Liu, L.-A. Hou, B. Xi, Y. Zhao, and X. Xia, “Synthesis, characterization, and mercury adsorption properties of hybrid mesoporous aluminosilicate sieve prepared with fly ash.,” *Appl. Surf. Sci.*, vol. 273, no. 100, pp. 706–716, May 2013.

[63] A. A. Ismaiel, M. K. Aroua, and R. Yusoff, “Palm shell activated carbon impregnated with task-specific ionic-liquids as a novel adsorbent for the removal of mercury from contaminated water,” *Chem. Eng. J.*, vol. 225, pp. 306–314, Jun. 2013.

[64] D. Robati, “Pseudo-second-order kinetic equations for modeling adsorption systems for removal of lead ions using multi-walled carbon nanotube,” *J. Nanostructure Chem.*, vol. 3, no. 1, p. 55, 2013.

[65] F. Raji and M. Pakizeh, “Study of Hg(II) species removal from aqueous solution using hybrid ZnCl2-MCM-41 adsorbent,” *Appl. Surf. Sci.*, vol. 282, pp. 415–424, 2013.

[66] C. Wang, J. Li, L. Wang, X. Sun, and J. Huang, “Adsorption of Dye from Wastewater by Zeolites Synthesized from Fly Ash: Kinetic and Equilibrium Studies,” *Chinese J. Chem. Eng.*, vol. 17, no. 3, pp. 513–521, Jun. 2009.

[67] E. Hums, N. M. Musyoka, H. Baser, A. Inayat, and W. Schwieger, “In-situ ultrasound study of the kinetics of formation of zeolites Na–A and Na–X from coal fly ash,” *Ultrasonics*, vol. 54, no. 2, pp. 537–543, Feb. 2014.

[68] J. Farrell and D. Mishra, “Mechanisms for Arsenic Removal by Ferric Hydroxide Adsorbents.”

Chapter 4

4 Conclusions

4.1 Contributions

The zeolitic adsorbents from natural origin and synthetic source and their modified forms were optimized for removing aquatic mercury from a model wastewater. All examined zeolites including the synthetic zeolite LTA, the gold-iron modified LTA, the natural clinoptilolite sample, the gold modified clinoptilolite and the zeolitized coal fly ash were successful to achieve high removal efficiency towards mercury. Their performances were truly comparable with activated carbon that is the predominant mercury adsorbent at the same adsorbent concentration and experimental condition.

An extended literature review was presented in chapter 1 on mercury history, mercury chemistry and speciation, its properties in aquatic environment, mercury health issues, the current origin of mercury emissions and existing regulations. Also mercury removal technologies including adsorption as well as available zeolitic adsorbents for eliminating mercury in contaminated water were described.

The work presented in Chapter 2 defined the successful application of a sample of zeolite LTA synthesized from coal fly ash in our research group for mercury adsorption. Applying a leaching test on the obtained zeolite showed its capability to immobilize toxic heavy metals by trapping them in its matrix.

Adsorbent concentration had a strong influence on the adsorption performance of CFA-ZA. The removal efficiency increased by increasing adsorbent dose, however, the adsorption capacity decreased due to the physical blockage of some of the adsorption sites. It was observed that the removal efficiency of CFA-ZA didn't change significantly with solution pH. Adsorption kinetics of mercury over CFA-ZA was found to be well predicted by a pseudo-second-order kinetic model. The examined rate controlling model indicated that a multi stage mechanism of adsorption took place. Freundlich isothermal model explained the adsorption isotherms better as compared to Langmuir model for zeolitized CFA.

In addition to CFA-ZA, synthetic zeolite LTA and its gold-iron modified sample along with raw clinoptilolite sample and gold modified clinoptilolite were examined toward mercury removal.

Chapter 3 presented the experimental methods, results and discussion on this subject. It was determined that zeolite LTA removal efficiency increased by increasing adsorbent concentration from 1g/L reaching to optimized value at 10 g/L and decreasing afterwards. This strange behaviour was concluded to be consequence of free competitive sodium ions in the structure of zeolite LTA. Adsorption rate significantly increased after bimetallic modification of zeolite LTA for the same adsorbent concentration where the higher removal efficiency close to 100% achieved.

The best removal efficiency of 92% for natural clinoptilolte achieved at very high adsorbent concentration of 80 g/L. However ion-exchange modification of this zeolite with very small amount of gold sufficiently decreased the required adsorbent mass and

increased its efficiency towards mercury removal particularly in adsorbent concentrations below50 g/L.

The EDX and XRD analysis ensured that gold and iron modified the surface of parent zeolites. XRD also confirmed that crystalline structures of both zeolites were appropriately established after modification.

The pseudo second order kinetic model accurately described the adsorption kinetics. The adsorption mechanism was found to be chemisorption and the rate-limiting step was mainly surface adsorption for all raw and modified samples. Both the Langmuir and Freundlich isotherms showed good agreement with experimental data, indicating both chemisorption and physisorption counterpart in the adsorption process.

Overall, the promising results of this work suggest exploring the industrial capabilities of the proposed zeolites.

4.2 Future prospects and Recommendations

The future possibilities include:

- Granulize the raw and modified zeolitic mercury adsorbents to allow the practical application of these zeolites
- Design a proper continuous adsorption column and apply the selected zeolitic adsorbents to this system using real wastewater
- Examine the gold particle properties particularly particle size using TEM and evaluate the influence of gold particle size on its adsorbent properties.
- Investigate innovative methods to regenerate the used zeolitic adsorbents and recover the adsorbed mercury.

5 Appendices

5.1 Appendix A: Supplemental Material of Chapter 2

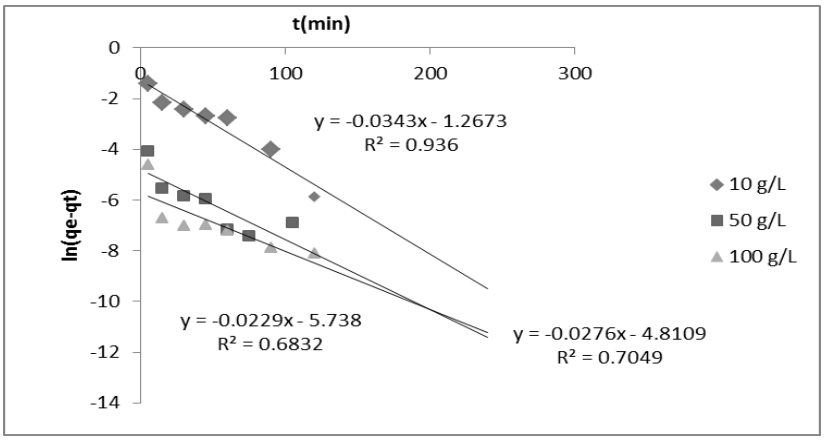

Figure S1. Application of the pseudo-first-order model (Eq.(3)) to the experimental dataof Figure 2-6. (experimental conditions: Hg(II) 10 mg/L, Adsorbent CFA-ZA 10g/ L, 50 g/L and 100 g/L, pH ≈ 2.5 at room temperature).

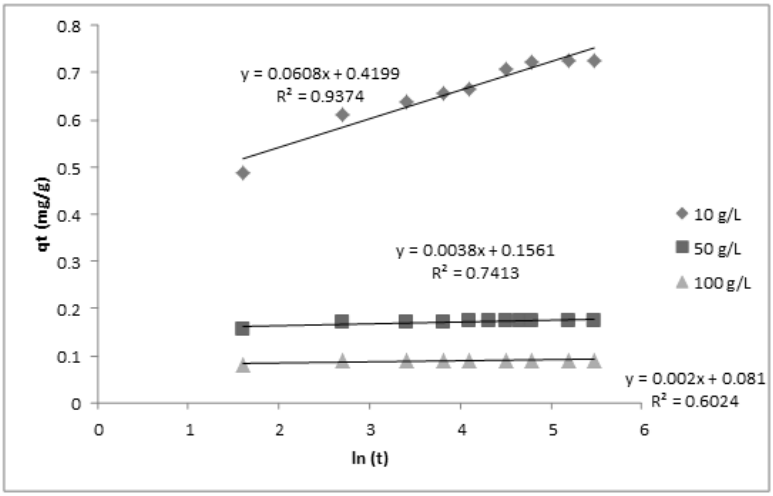

Figure S2. Application of the Elovich model (Eq.(5)) to the experimental data of Figure 2-8. (experimental conditions: Hg(II) 10 mg/L, Adsorbent CFA-ZA 10g/ L, 50 g/L and 100 g/L, initial pH ≈ 2.5 at room temperature).

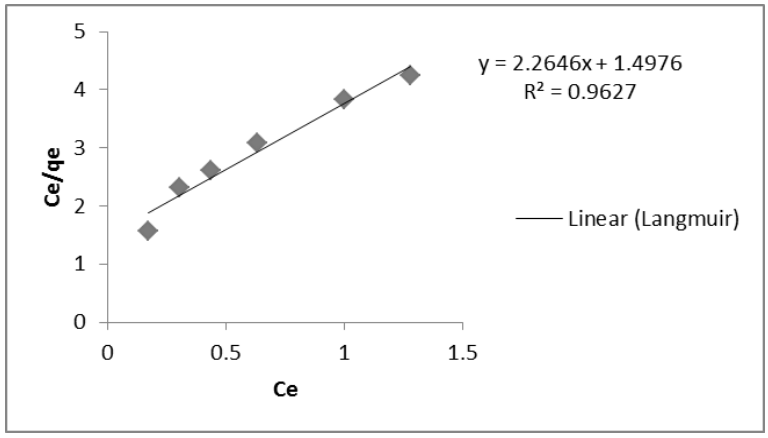

Figure S3. Langmuir isotherm for adsorption of Hg (II) onto CFA-ZA (experimental conditions: Hg(II) 10 mg/L, Adsorbent CFA-ZA dose in the rangee of 0.1, 0.2, 0.3 ,0.5 0.65,0.8,1 g , pH ≈ 2.5 at room temperature).

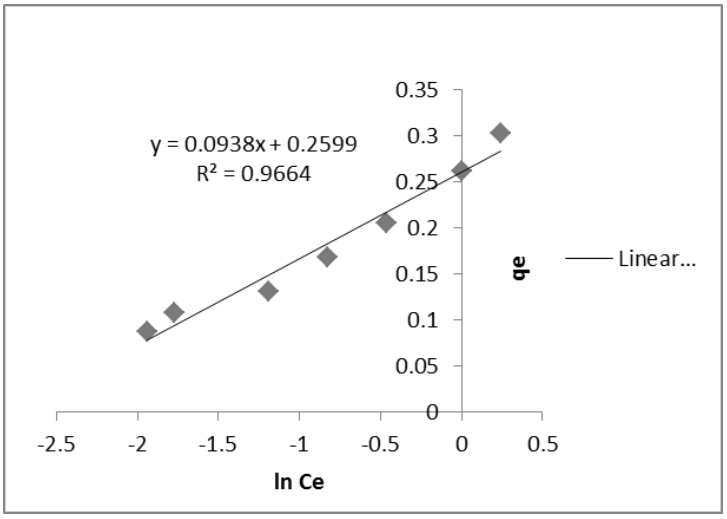

Figure S4. Temkin isotherm for adsorption of Hg (II) onto CFA-ZA (experimental conditions: Hg(II) 10 mg/L, Adsorbent CFA-ZA dose in the rangee of 0.1, 0.2, 0.3 ,0.5 0.65,0.8,1 g , pH ≈ 2.5 at room temperature).

5.2 Appendix B: Supplemental Material of Chapter 3

Adsorption Isotherms

B1. Langmuir Isotherm

The main assumption of Langmuir isotherm is monolayer adsorption on a uniform surface with homogenouse sites. As presented in Table 2 the linear form of this model described as

$$C_e/q_e = 1/(q_m K_L) + C_e/q_m$$

where K_L is the Langmuir constant related to the energy of adsorption and q_m is the maximum adsorption capacity (mg g^{-1}). The value of model parameters q_m and K_L for all examined adsorbents calculated from the linear plots of C_e/q_e versus C_e.

B.2 Freundlich Isotherm

The Freundlich isotherm assumed that adsorbate adsorbs onto the heterogeneous surface of an adsorbent. As illustrated in Table 2 the linear form of Freundlich equation is expressed as:

$$\text{Ln } q_e = \ln K_F + (1/n_f) \ln C_e$$

By plotting ln qe vs ln C_e the model parameters were determined for all adsorbents.

B.3 Temkin Isotherm

The main assumption of this model is the linearly decreasing of adsorption energy with surface coverage due to adsorbent–adsorbate interactions. The following equation describes the linear form of Temkin adsorption isotherm

$$q_e = k_1 \ln K_2 + k_1 \ln C_e$$

Where k_1 (l/g) is associated with heat of adsorption and k_2 (dimensionless) is Temkin constant and can be obtained from the linear plot of $\ln(C_e)$ vs q_e.

Table S1. Elemental analysis of the mine in BC Mine wastewater measured using ICP-AES technique.

Trace Metals	**Ag, As, Be, Cd, Co, Hg, Mo, Pb, Sb, Se, Sn, Ti,**	**Zn, V, Ti, P, Cr, Cu, Ba**	**Al, Mn**	**Ni**	**P**	**Sr**	**Fe**	**B**	**Si**	**Ca**	**Mg**	**K**	**Na**
Conc. (mg/L)	**< 0.01**	**0.02**	**0.03**	**0.06**	**0.25**	**0.7**	**0.55**	**3.4**	**12.17**	**43.65**	**107.96**	**222.45**	**610.43**

Table S2. Chemical composition of Bromley natural clinoptilolite sample and Chinese Zeolite LTA(from XRF analysis)

Element	MRLa	Canadian Bromley.	LTA
SiO_2	0.2	66.70	34.17
TiO_2	0.04	0.20	0.02
Al_2O_3	0.1	11.21	29.79
Fe_2O_3	0.04	1.76	0.02
MnO	0.06	0.02	0.04
MgO	0.11	0.49	< 0.01
CaO	0.03	1.65	0.01
K_2O	0.06	3.72	0.54
Na_2O	0.08	1.16	17.46
P_2O_5	0.01	0.03	0.01
Cr_2O_3	0.01	<0.01	< 0.01

BaO	0.02	4.34	< 0.01
SrO	0.02	0.12	< 0.01
L.O.I.[b]	0.01	8.22	18.14
Total	--	99.61	100.17
Si/Al	--	5.04	1.01

a = MRL : Method Reporting Limit

b= L.O.I: Loss on Ignition

Figure S1. End over end shaker and oven used for batch experiments.

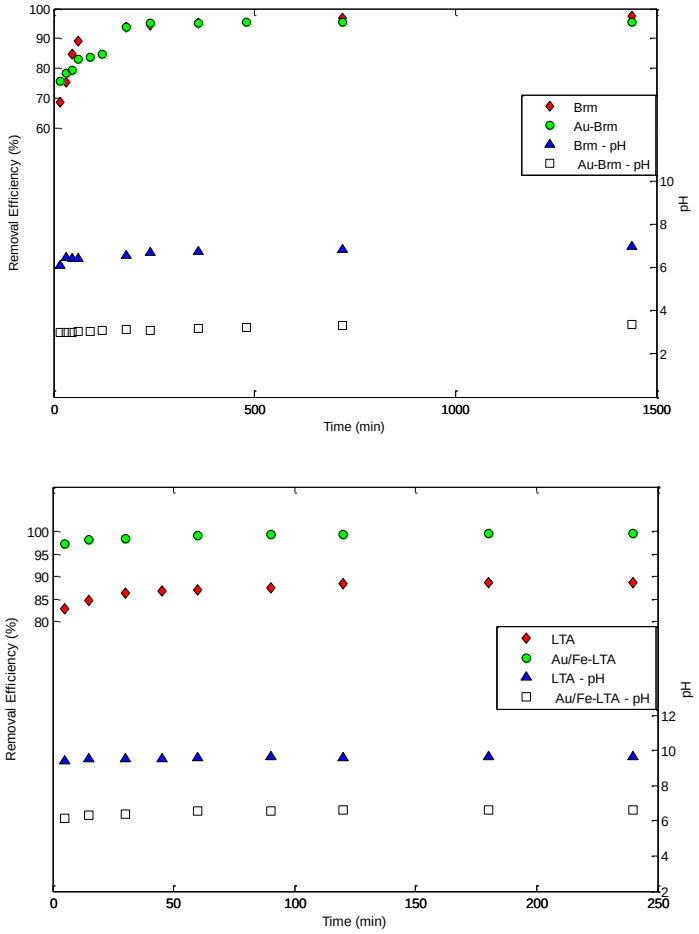

Figure S2. Removal efficincy of (a) Brm (70 g/L), Au-Brm(50 g/L) and (b) LTA, Au/Fe-LTA (10 g/L) towards Hg(II) compared with change in pH of Hg(II) solution as a function of time (experimental conditions: Hg(II) 10 mg/L, initial pH≈2.5 at room temperature).

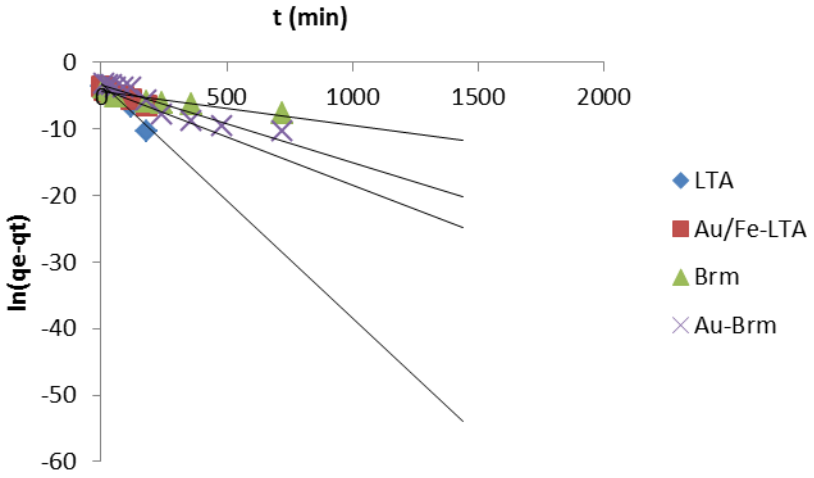

Figure S3. Application of the pseudo-first-order model (Eq.(4)) to the experimental data of Figure 3-8. (experimental conditions: Hg(II) 10 mg/L, Adsorbent Brm, Au-Brm and (b) LTA, Au/Fe-LTA, pH ≈ 2.5 at room temperature).

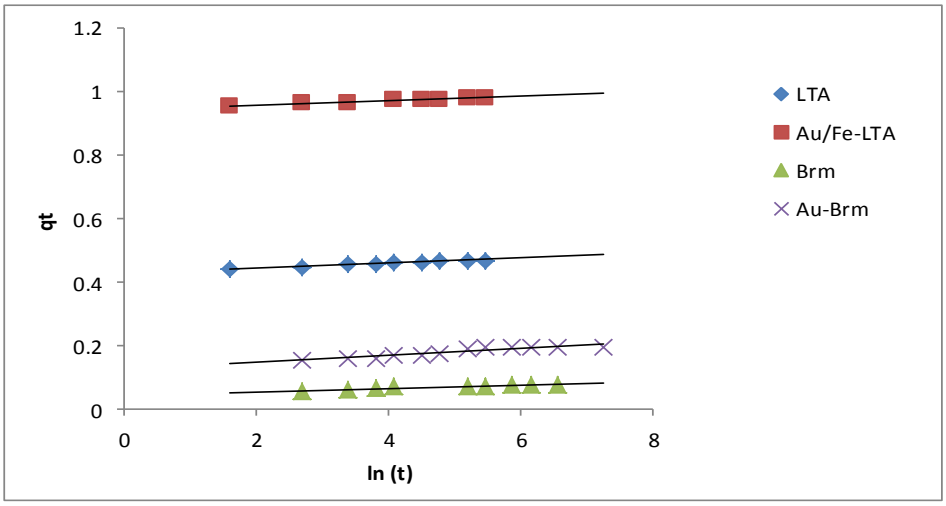

Figure S4. Application of the Elovich model (Eq.(7)) to the experimental data of Figure 8. (experimental conditions: Hg(II) 10 mg/L, Adsorbent Brm , Au-Brm and (b) LTA, Au/Fe-LTA , pH ≈ 2.5 at room temperature).

CV

Education

- M.Sc student in Chemical Engineering, Western University, (May 2014, August 2015).

- M.Eng student in Biomaterials and Biochemical Engineering, Western University (September 2013- April 2014).

- Master's degree in Conservation science; GPA: 3.6/4.0 (A+), The University of Tehran, Tehran, Iran.

Thesis: Consolidation of Pasargardae World Heritage Site black limestone using two synthetic Nano-composites.

Graduation: October 2009

- Bachelor of Science: Applied Chemistry, Tehran Azad University, Tehran, Iran. Graduation: May 2001

Specific skills

- TGA
- BET
- ICP-AES
- Surface analysis techniques:
  - Scanning Electron Microscopy (SEM),
  - X-ray diffraction (XRD),
  - X-ray Fluorescence (XRF),

- Spectroscopy techniques:
  - Fourier Transform Infrared (FT-IR),
  - Optical Microscopy,
  - UV-Vis absorption spectroscopy,

- Chromatography techniques:

- Gas chromatography (GC),

- Conservation techniques:

- Accelerated aging for stone and paper.

Research Experience

- Master of Chemical Engineering thesis in "Mercury removal from industrial wastewater using natural, synthesize and modified zeolites", (May 2014, August 2015).

- Collaboration in "Monitoring of stone corrosion in historical-cultural sites" research project, The Art University of Tehran (2007-2009),

- Collaboration in "The conservation of wall paintings of Karim-khan fort" project, Shiraz, Iran (2007).

- Preparation of the proposal for "The conservation of the entrance of Divan-khaneh (historic jurisdiction building)", Shiraz, Iran (2006).

Publications

✓ **Book Chapters**

- M. Kanani, M. Attari, Think-Tank Management, Fanavaran Development Center, 2009 (In Persian).

✓ **Journals**

- M.Attari et.al, "Mercury Removal from Aqueous Solution by Zeolitized Coal Fly Ash: Equilibrium and Kinetic Studies," Journal of "Chemosphere" : Under review

- M.Attari et.al, "Mercury Removal from Industrial Wastewater Using Gold/Iron-Modified Natural and Synthetic Zeolites," Journal of Hazardous Material : Submitted

- M. Attari, Z. Sarikhani, Z. Khezri, "The Role of Monitoring in Conservation of Stone Cultural-Historical Sites," The Art's Manifest Tech. Jour., In Press, (In Persian).

- M. Attari, "The Prospect of employing Nanotechnology in Conservation of Cultural Heritage – A Multidisciplinary Approach," Tech. Jour. of Research and Restoration, no. 4, 2008 (In Persian).

- M. Attari, “Cultural Heritage and Conservation Science – A Multidisciplinary Research” Daneshgar Tech. Jour. of Iran’s Scientific Research Center, no. 30, Oct. 2008 (In Persian).

- M. Attari, “Sivand, A Dam Against History,” Daneshgar - The Tech. Jour. of Iran’s Scientific Research Center, no. 23, May 2007 (In Persian).

- ✓ **Conferences**

- Z. Khezri, M. Attari, "Asbad Windmill, The Forgotten Industrial Heritage of the Ancient Asia", Icomos International Conference, Thailand, Oct. 2013 (Accepted).

- M. Attari, G. M. Mohamad-Sadeghi, R. Vahidzadeh, M. H. Talebian, “Acrylic/Silanes/Nanoclay-based Nano-composite to Consolidate the Black Limestone of Pasargad World Heritage Site,” Int. Conf. on Nanotechnology, Fundamentals and Applications, Ottawa, Aug. 2010.

- M. Attari, “Synthesis of Two Nano-composite Samples, used in Consolidation of Historic Stones”, Stu. Conf. on Nano-technology, Mashhad, Iran, Nov. 2010 (In Persian).

- M. Attari, “Stone corrosion in Pasargadae”, Int. Workshop on Conservation and Restoration of Pasargad World Heritage Site, Pasargad, Iran, Mar. 2009 (In Persian).

- M. Attari, “Synthesis of Acrylic, Silanes, and Nanoclay composites to Consolidate the Black Limestone of Pasargad,” Proc. of the 9’th Conf. on Conservation and Restoration of Cultural-Historical Objects, Tehran, Iran, Nov. 2009 (In Persian).

Internship Experience

- Paper and manuscript conservation, The Library and Document Center of Iran’s Parliament, Tehran, Iran, Nov. 2009 - May 2010.

- Conservation and restoration of paper records and manuscripts, Iran’s Cultural Heritage Research Institute, Tehran, Iran, 2006.3

- Fibre Identification, Iran’s Cultural Heritage Conservation and Restoration Research Institute, Tehran, Iran, 2006.

Work Experience

- Volunteer conservator at Museum of Ontario Archaeology, London, summer 2013.

- The Head of the Board of Directors, Tarahan Ideh Barsav Inc., since March 2010.

- Collaboration in the design of a traditional teahouse at Persepolis World Heritage site, since June 2010.

- Senior Expert in paper records and manuscript conservation, The Library and Document Center of Iran's Parliament, Tehran, Iran, May 2010 – Sep. 2011.

Awards

- Distinguished Student, Conservation Science Program, The University of Tehran, Iran, 2009.